Characterization of the Tanana River at Nenana, Alaska, to Determine the Important Factors Affecting Site Selection, Deployment, and Operation of Hydrokinetic Devices to Generate Power

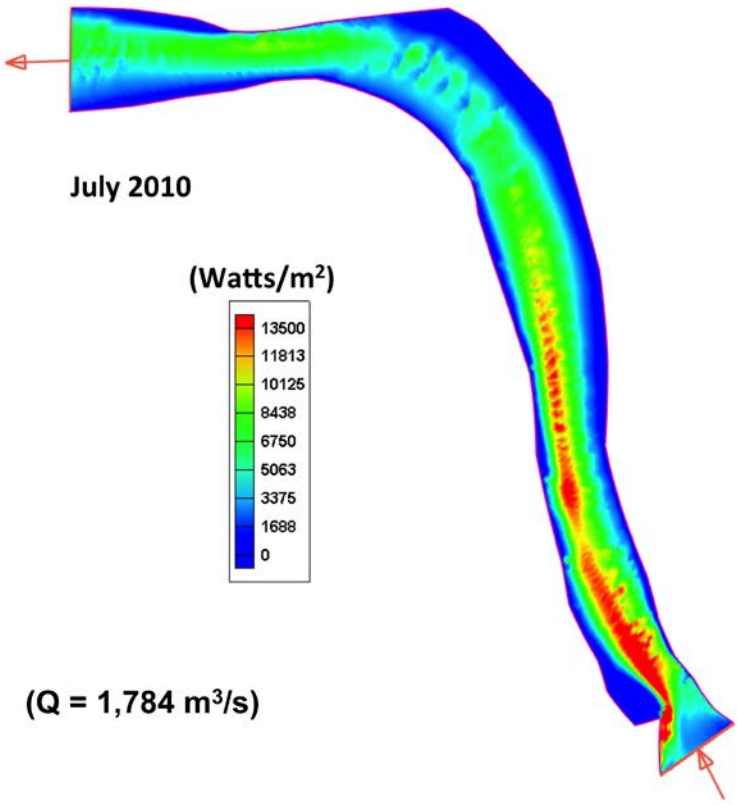

Prepared by

J. B. Johnson, H. Toniolo, A. C. Seitz, J. Schmid, P. Duvoy

Alaska Center for Energy and Power,
Alaska Hydrokinetic Energy Research Center

March 2013

ACEP
Alaska Center for Energy and Power

UAF
UNIVERSITY OF ALASKA FAIRBANKS

Cover figure modified from Duvoy and Toniolo 2012

To cite this report:

Johnson, J.B., Toniolo, H., Seitz, A.C., Schmid, J., and Duvoy, P. (2013). Characterization of the Tanana River at Nenana, Alaska, to Determine the Important Factors Affecting Site Selection, Deployment, and Operation of Hydrokinetic Devices to Generate Power. Alaska Center for Energy and Power, Alaska Hydrokinetic Energy Research Center, Fairbanks, AK, 130 pp.

For information about this report:

Jerome B. Johnson, Principal Investigator
Alaska Hydrokinetic Energy Research Center
Alaska Center for Power and Energy
P.O. Box 755910
University of Alaska Fairbanks
Fairbanks, AK 99775-5910

Preface

The Tanana River hydrokinetic characterization study started in 2009, when little was known about how river environments in Alaska would affect hydrokinetic power generating devices or how those devices might affect the state's river environments. Few hydrokinetic devices were beyond the concept/design stage, and a first attempt at demonstrating a hydrokinetic device at Ruby, Alaska, had just concluded. The primary focus of previous paper studies of hydrokinetic power generation in Alaska involved determining the locations of highest average river currents and hydrokinetic power densities without regard to other aspects of river environments. This project took a broader approach by examining a range of river conditions that include sediment transport and riverbed conditions, river current velocity and turbulence and their seasonal variation, woody debris, fish stocks, and wintertime flow. As the project progressed, it became apparent that many of the river environmental factors identified in our study had the potential to significantly affect the deployment and operation of hydrokinetic power generating devices. For example, both the Ruby demonstration project and another demonstration at Eagle, Alaska, were ended due to problems with debris. To adequately characterize the most important river environmental factors, it was necessary to go beyond the project's original scope of work to include river hydrodynamic modeling, more extensive fisheries measurements, and an expanded study of woody debris and its mitigation. The results from this expanded scope of work provide a solid basis for moving to the next stage of hydrokinetic technology development and testing needed for successful long-term deployment and operation of hydrokinetic devices in Alaska rivers.

Contents

List of Figures

List of Tables

Acknowledgments

Primary support for this study was provided by the Alaska Energy Authority through grant #2195437. Additional support was provided by the Alaska Power and Telephone Company, the Ocean Renewable Power Company, and the University of Alaska Fairbanks through the Alaska Center for Energy and Power, the School of Fisheries and Ocean Sciences, the Institute of Northern Engineering, and the College of Engineering and Mines. We thank the community of Nenana and the Nenana Native Council for their cooperation.

Abbreviations and Acronyms

ACEP	Alaska Center for Energy and Power
ADCP	acoustic Doppler current profiler
AEA	Alaska Energy Authority
AEA-REF	Alaska Energy Authority Renewable Energy Fund
AHERC	Alaska Hydrokinetic Energy Research Center
AKE	average kinetic energy
ATKE	average turbulent kinetic energy
CI	confidence interval
CPUE	catch per unit effort
DC-EETG	Denali Commission Emerging Technology Grant
DI	debris index
DOE	Department of Energy, U.S.
EETF	Emerging Energy Technology Fund
EPRI	Electric Power Research Institute, Inc.
FERC	Federal Energy Regulatory Commission
GAMs	generalized additive models
HKD	hydrokinetic power generating device
KE	total hydrokinetic energy
ORPC	Ocean Renewable Power Company
REF	Renewable Energy Fund
TKE	turbulent hydrokinetic energy
TRTS	Tanana River Test Site
UAF	University of Alaska Fairbanks
USGS	U.S. Geological Survey

Executive Summary

A three-year study (2009–2011) was conducted to characterize the Tanana River environment at Nenana, Alaska, as it relates to the deployment and operation of hydrokinetic power generating devices (HKDs) (Figure 1). An additional goal was to conduct baseline studies required to establish the Tanana River Test Site (TRTS) at Nenana to facilitate development and testing of HKD technology under realistic Alaska river conditions.

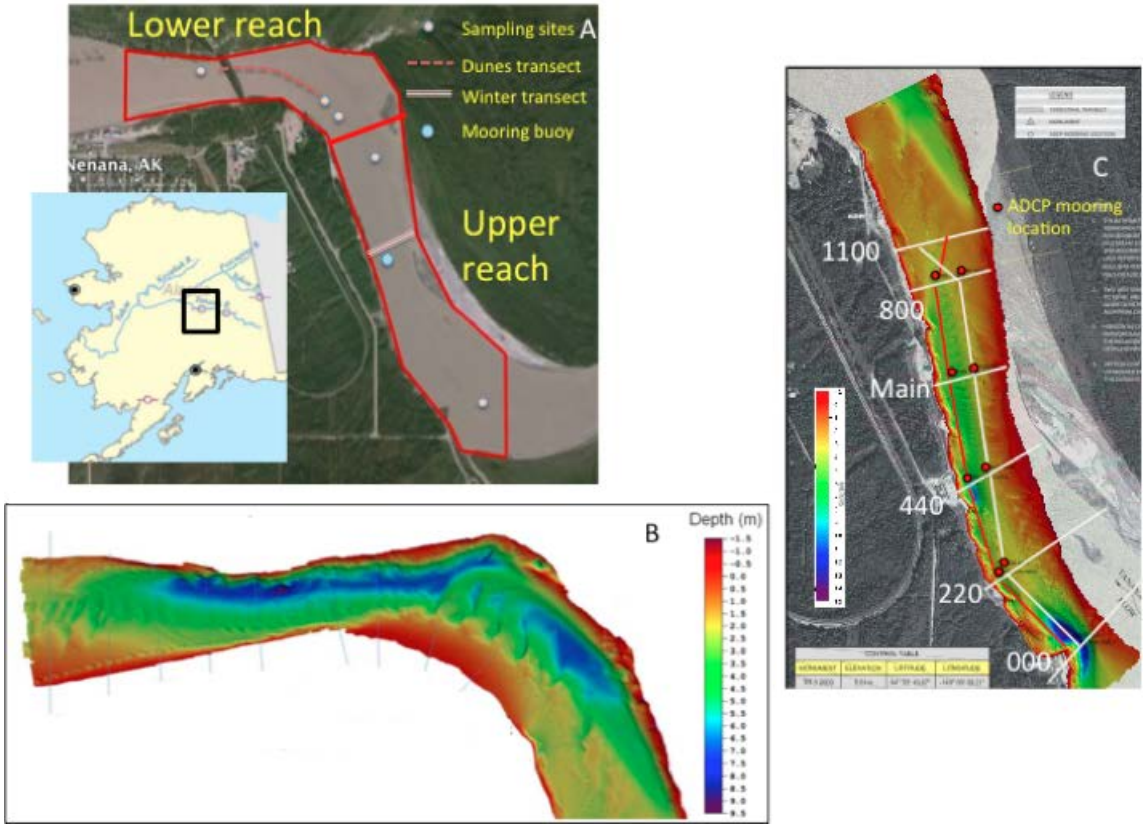

Figure 1. Tanana River Test Site location and sediment sampling station map. The mooring buoy is used to tether measurement or HKD test floating platforms (A); bathymetry and velocity transect locations for the lower reach (B); upper reach bathymetry, velocity measurement transect locations, and ADCP mooring turbulence measurement locations (C).

Measurements of river discharge, current velocity, and suspended and bed load sediment transport were made to determine the ice-free river hydro-sedimentological conditions. Additionally, longitudinal ADCP profiles were performed to describe the riverbed configuration. Power density was calculated and river turbulence was characterized from current velocity measurements. Fall and wintertime measurements of frazil ice and current velocity were conducted in 2009 and 2010. The fish baseline data were needed to compare with fish stocks when hydrokinetic testing is conducted at the TRTS. Bathymetry measurements of the TRTS upper reach were made in 2009 and 2010, and bathymetry measurements of the TRTS lower reach were made in 2010 (Figure 1B and C). A two-dimensional numerical model (CCHE2D) of both the upper river reach (2010) and the complete river reach (2011) was constructed using TRTS bathymetry and discharge measurements (Figure 2). The model was validated using current velocity measurement

data. A hydrokinetic calculator module (HYDROKAL) was developed to process CCHE2D output to estimate the instantaneous power density, maximum current velocity, and specific discharge in each river cross section. An HKD efficiency factor, used to account for turbine efficiency, allows HKD developers and users the ability to quickly estimate the amount of hydrokinetic energy that can be extracted at a given location in the river.

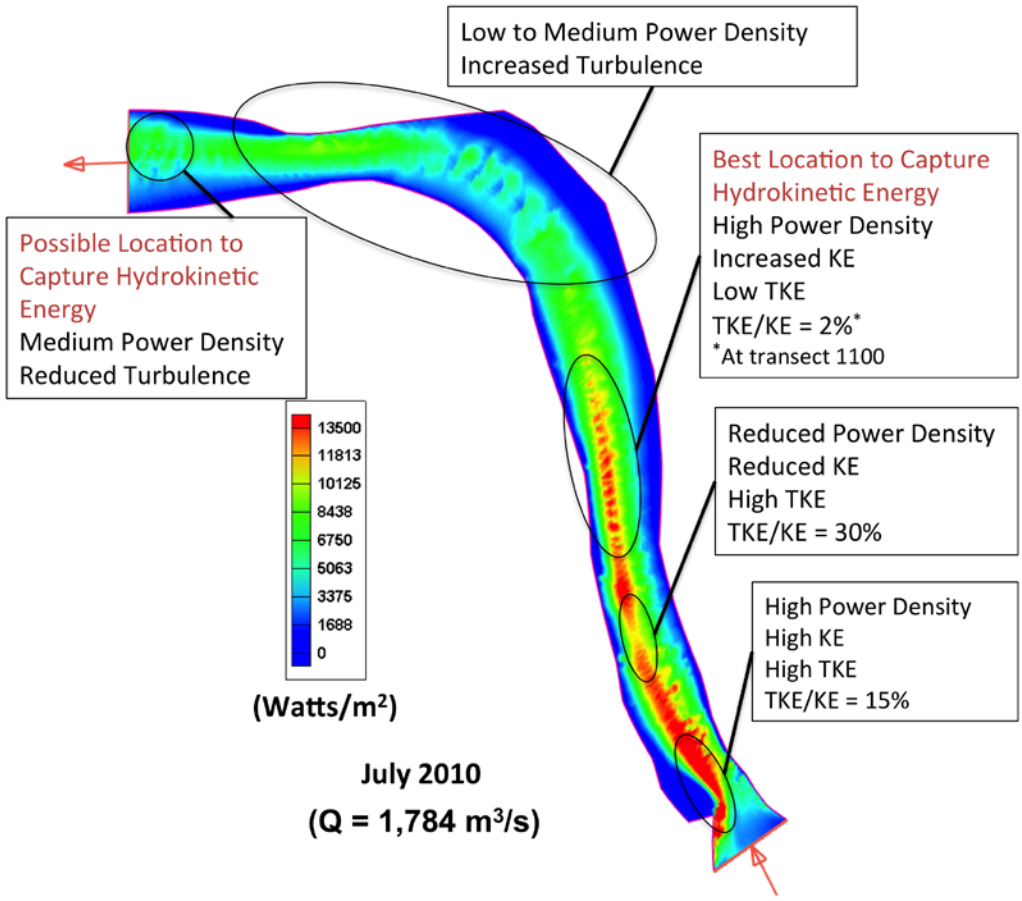

Figure 2. Power density as a function of location in the Tanana River Test Site river reach, with notations about turbulence and placement of HKDs. Figure modified from Duvoy and Toniolo 2012.

River Hydro-Sedimentological Conditions

Maximum measured current velocities at the TRTS ranged between less that 0.5 m/s in winter months to over 2.5 m/s during summer months and over 3 m/s during high-water events. Average monthly discharge ranged from a low of 496 m^3/s to a high of 1702 m^3/s during the open-water season (i.e., May to October), and from a low of 185 m^3/s to a high of 268 m^3/s during the winter months (i.e., November to April). The minimum discharge year during the period of record occurred in 1996, and the maximum average discharge occurred in 1967. During the summer months of July, August, and September, the average discharge was approximately 1423 m^3/s when considering years 1962 to 2010. In 1996, the discharge was only 1047 m^3/s for the same summer months, while in 1967, discharge increased to 1940 m^3/s (historical discharge data obtained from http://waterdata.usgs.gov/nwis/nwisman/?site_no=15515500).

River power-density magnitudes are proportional to the cube of the current velocity, producing the highest power densities in the thalweg near the upstream end of the upper reach (Figure 2). Power densities for August 2009 and July 2010 were 6500 W/m^2 and 13,500 W/m^2, respectively. The maximum wintertime power density in 2010 was about 256 W/m^2. The high discharge year (occurring in 1967) peak power density is estimated to be 27,800 W/m^2, the average discharge (based on a 48-year record) peak power density is estimated to be 12,800 W/m^2, and the low discharge year (corresponding to 1996) peak power density is estimated to be 6,800 W/m^2. Seasonally, discharge and power density increase from the middle to the end of April (when breakup occurs) to a peak sometime in July or August, and then decrease to normal winter low-discharge levels in early to mid-October when freeze-up occurs.

Current velocity-measurement transect lines, modeled current velocities, and locator markers P1, P2, and P3 are shown in Figure 3. Non-quantifiable estimates of the instantaneous power density for the three locator markers were made from modeled results using 2009 bathymetry to demonstrate how power density might change as a function of location throughout the open-water season (Figure 4). Due to the uncertainty of bathymetry changes with time in these estimations, these power density values are qualitative results.

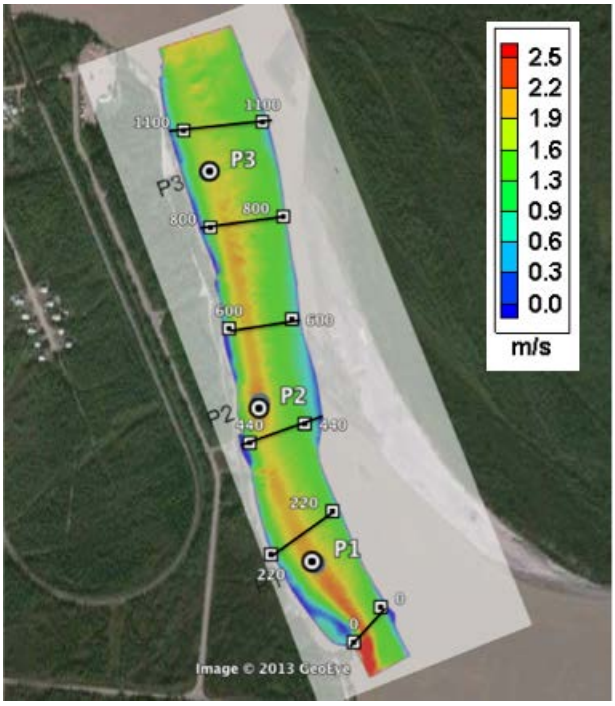

Figure 3. Current velocity plot for the upper TRTS reach, with the three locations used to estimate seasonal power densities shown in Figure 4.

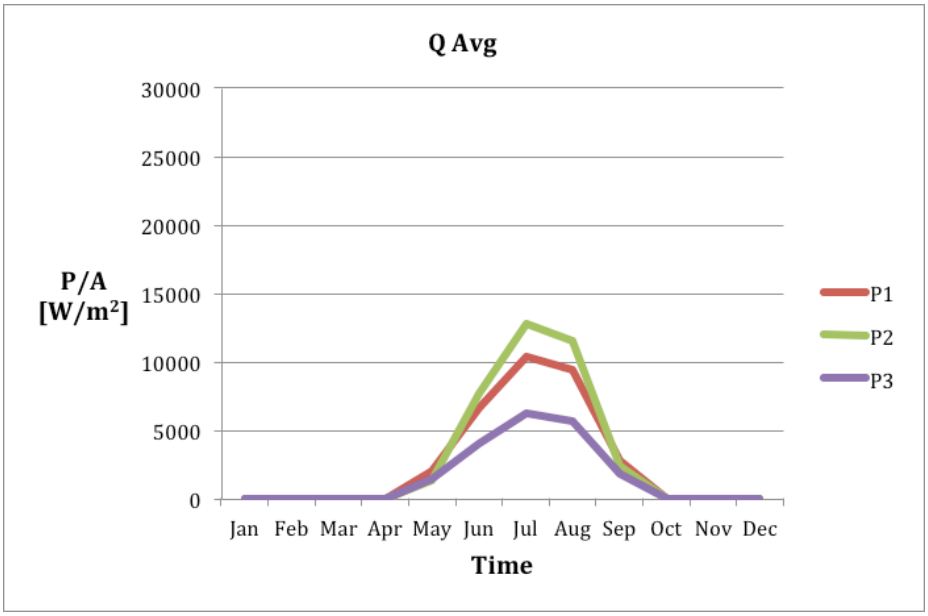

Figure 4. Instantaneous power density in W/m^2 for the three locations shown in Figure 3 for an average discharge year. Discharge data for the Tanana River near Nenana, Alaska, can be accessed from the USGS gauging station at the Tanana River near Nenana (http://waterdata.usgs.gov/nwis/nwisman/?site_no=15515500).

Riverbed dunes occur along the river bottom in the transition between the upper and lower reaches of the TRTS, as the river changes direction (Figure 1A). Average dune wavelengths ranged from 41 to 67 m, and average dune heights ranged from 0.6 to 1.2 m. Bed load grain-size distributions ranged from fine sand to medium gravel. Suspended and bed load sediment concentrations are nonlinear functions of discharge, ranging from 0.2 to 2.3 g/l for suspended sediment and ranging from around 1 g/l to 16 g/l for bed load sediment.

Extra turbulence in rivers is generated by changes in bathymetry or flow direction caused by river bends. Bathymetric depressions and changes in flow due to river bends are shown in Figure 1 and Figure 2. Optimal locations for siting HKDs, that is, locations that provide high power density and low turbulence, are shown in Figure 2. These locations correspond to a relatively straight reach of the river that exhibits little change in bathymetry and a nearly uniform river cross section.

Frazil ice forms in October when cold air temperatures supercool the water. During freeze-up, frazil adheres to isolated structures. Frazil accumulation thickness on isolated objects (e.g., cylinders) is limited by shear forces from water flowing around the objects (frazil accumulations of up to 150 mm were observed during freeze-up).

Debris Hazards and Mitigation Approaches

Any river that flows through wooded terrain has the potential to entrain and transport woody debris downstream, posing a risk of debris accumulation or impact against infrastructure that is in or on a river. As debris travels downriver, it can float on the surface, in a vertical orientation with its root ball scraping along the riverbed, or in a submerged state. Most floating debris follows the thalweg in straight sections of a river when the river stage is rising, but moves toward the riverbanks when the river stage is falling.

Submerged debris (including neutrally buoyant debris) is common in most rivers in Alaska. Submerged debris has been observed catching on HKD electrical cabling in the Yukon River at Eagle, Alaska, and it has been observed riding up the anchor chain of the mid-channel mooring buoy in the Tanana River at Nenana. During flood stage conditions, extensive amounts of surface and submerged debris can be transported in the river flow. In locations of high turbulence, subsurface debris can be carried to the river surface by water boils and then expelled, to immediately sink.

In 2010, debris accumulation and impacts were responsible for ending HKD demonstration projects on the Yukon River, Alaska, at Ruby and Eagle (Figure 5) and on the Mackenzie River, Northwest Territories, Canada, at Fort Simpson.

a **b**

Figure 5. Debris accumulation on the bow of the 5 kW New Energy EnCurrent turbine barge at Ruby, Alaska (Pelunis-Messier 2010) (a); debris accumulation in front of a 25 kW New Energy turbine barge at Eagle, Alaska (photo credit: Alaska Power & Telephone) (b).

Existing debris mitigation methods include:

1. Using debris diversion booms
2. Placing HKDs in locations where debris encounters have a low probability of occurrence
3. Using manual or mechanical debris removal methods
4. Designing HKDs to be debris tolerant
5. Furling HKDs (i.e., removing the HKD from the debris travel path)
6. Blocking or capturing debris with trash racks

The important factors affecting performance of a debris diversion boom include the angle between the boom pontoons, pontoon surface friction, current velocity, and the ratio of debris diameter to length. Reducing the separation angle between pontoons and reducing the surface friction of the pontoons improves the ability of a diversion boom to shed debris.

Fish Baseline Information about Juvenile and Larval Downstream Migration

The goal of the fish study was to provide baseline information about the downstream migration of juvenile and larval fish in the mainstream of the Tanana River near Nenana to understand spatial and temporal patterns (Figure 6). This information provides a means to determine periods when potential interactions between juvenile and larval fishes and a hydrokinetic turbine may occur.

Figure 6. The three most commonly captured fish species in the margins of the Tanana River in 2011. From top to bottom: whitefish, longnose sucker, chum salmon.

In the surface waters of the mid-channel, the location where a hydrokinetic device would likely be installed, at least six species were captured, with Chinook/coho salmon and chum salmon being the only commonly captured species, and whitefish, Arctic lamprey, and burbot being very infrequently captured. Most of the captured fishes were relatively small juveniles (<10 cm), including age-1 Chinook/coho and age-0 chum salmon smolts that were migrating to the Bering Sea. In the river margins, at least eleven species of fishes were captured, with whitefish being the most abundant, followed by longnose suckers, chum salmon, lake chub, larval lamprey, burbot, Arctic grayling, Chinook/coho salmon, slimy sculpin, Arctic lamprey, adult Alaskan brook lamprey, and northern pike.

Several species/taxa of fishes displayed temporal trends in abundance in the Tanana River. Longnose sucker abundance had a small peak in late May; whitefish abundance peaked in late June. Other species of fish displayed increasing or decreasing trends in catches throughout the sampling season, such as chum and Chinook/coho salmon, both of which generally decreased in abundance, and lake chub, which increased in abundance. In contrast to the species that exhibited seasonal patterns in catches, the remaining species did not display temporal patterns in catches.

This study has shown that, for a hydrokinetic device mounted in the surface of the mid-channel of the Tanana River, most potential interactions with fishes occur with Chinook salmon, coho salmon, and chum salmon smolts as they down-migrate to the ocean from May through July, particularly during periods of increasing discharge.

Current State of Knowledge for Fisheries Studies

The realized impacts of hydrokinetic devices on fishes in Alaska rivers are unknown at this time because no observational or modeling studies have been conducted on common fish species in Alaska. Results from studies conducted elsewhere suggest that realized impacts of hydrokinetic devices on fishes are

likely related to the species and size of fish passing through a spinning turbine. Four studies have been conducted in which fish were passed through a spinning turbine. Only one of these studies was conducted in an actual free-flowing river. This study (conducted in 2009 at the Hastings, Minnesota, Mississippi Lock and Dam No. 2 Hydroelectric Project), monitored the survival and injury of several freshwater fish species, including representatives from the perch, sunfish, sucker, catfish, and temperate bass families, that passed through a HGE (Hydro Green Energy) hydroelectric turbine (Normandeau Associates 2009). Of fish that passed through the turbine, the survival estimate for those between 114 and 710 mm in size was 99%, and no blade-strike injuries were observed. Additionally, the turbine design appeared to eliminate the possibility of pressure-related injuries. Based on the results of this study and the turbine design, the authors concluded that the HGE hydrokinetic unit "has little if any considerable impact on the fish populations in the vicinity of the Mississippi Lock and Dam No. 2 Hydroelectric project." (Normandeau Associates 2009, page ES-2).

Three additional studies on the impacts of hydrokinetic turbines on fishes have been conducted in laboratory flumes. The first study (conducted at Alden Research Laboratory, Inc.) observed injury and survival rates as well as behavioral reactions and avoidance by two species of fish—rainbow trout and largemouth bass—that were exposed to two hydrokinetic turbines (Lucid spherical turbine and Welka UPG) in a flume (EPRI 2011). The second study (conducted at Conte Anadromous Fish Research Laboratory) observed injury and survival rates as well as behavioral reactions and avoidance of two different species of fish—Atlantic salmon and American shad—that were exposed to EnCurrent turbines in a flume (referenced in EPRI 2011). In these studies, there was no evidence of blade-strike injuries or mortality associated with passing through the turbines.

The third flume study (conducted at Oak Ridge National Laboratory) observed how several species of fish larvae and juveniles, including members of the perch, sunfish, minnow, and temperate bass families, encountered different blade profiles of hydrokinetic devices at different approach velocities and how such encounters influenced survivorship (Schweizer et al. 2012). This was the only study that examined larval and juvenile fishes as small as 4 mm. The presence of a spinning turbine blade in the path of drifting larval and juvenile fishes increased mortality rates when compared with control fishes that did not experience a spinning turbine blade. The mortality rate of experimental fishes appeared to be inversely related to the development of the fish (size, age, and life stage) and the current velocity of the water. Mortality also appeared to be related to the shape of the leading edge of the turbine blade.

The river environment and fish community in Alaska are unlike those that have been represented in previous laboratory experiments. The largest and most powerful rivers in Alaska are relatively fast and glacially turbid, and the fish community in these rivers contains small larvae and juveniles from several species whose behavior around a turbine has not been observed. These fish are particularly important because they support culturally and economically valuable subsistence, sport, and commercial fisheries (Bradley 2012). Because of the distinctive characteristics of Alaska rivers and the importance of fishes in them, fish-turbine interaction studies need to be conducted for hydrokinetic deployments in Alaska.

Implications for Hydrokinetic Energy Production Devices

The goal of HKD developers and users is to generate electricity from the hydrokinetic power of river currents economically (i.e., to make a profit for developers and utilities and provide power to consumers

at an affordable cost). The interaction of an HKD with a river environment, which is the focus of this study, can affect hydrokinetic power generation economics. Those interactions include the following:

1. The power density and turbulence of the river current, which determine the available extractable energy and the shear forces that create fatigue stresses in HKD infrastructure.
2. Suspended and bed load sediment concentrations, which can affect the rate of abrasion on HKD components and the erosion and deposition of sediment around riverbed-mounted HKD infrastructure.
3. Surface and subsurface woody debris, which can accumulate on or damage HKD infrastructure.
4. Downstream migrating juvenile and larval fish and upstream migrating adult anadromous fish of commercial and cultural value. Concern about ensuring that fish stocks are not harmed by HKDs affects the degree of agency oversight and regulation, which add costs and delay timelines for HKD projects.

Selecting the best site for an HKD installation requires a characterization survey of the river to determine river power density and turbulence as a function of location and river discharge over as long a period of record as possible. This information is needed to determine where the combination of high specific power density and low turbulence occurs that optimizes HKD power extraction efficiency. Selection of the best site for an HKD installation also requires determining the river's suspended and bed load sediment concentrations as a function of discharge.

Most HKD site investigations include a multi-beam sonar bathymetric survey to determine riverbed conditions to aid in planning HKD installations. With bathymetry, it becomes possible to conduct hydrodynamic modeling to examine the flow and power density character of a river in detail. Two bathymetries within the same open-water season, along with suspended and bed load sediment concentration rating curves, are needed to calibrate the sediment transport model parameters to model the hydro-sedimentological character of a river. Hydro-sedimentological models enable estimation of changes in river bathymetry and, with three-dimensional models, the full characterization of the velocity field. Models may also allow the inclusion of HKD modules to evaluate their influence on the river flow.

All rivers carry woody debris to some extent, and HKD developers and users need to incorporate debris mitigation strategies if they are to avoid disruptions to their operations. Such strategies may involve placing HKDs in channeled waterways behind dams or other structures that prevent debris from entering the water channel, or designing HKDs that are debris tolerant or easily repaired or that incorporate a detect-and-protect scheme of debris mitigation that is only deployed when debris is detected. Work on debris-deflection technology at the TRTS demonstrates that surface debris can be deflected in most situations. No single debris mitigation system will work for all HKDs, and work remains to be done to find practical debris mitigation systems.

Alaska regulators responsible for balancing the risks and benefits both to HKD project proponents and to public trust fish resources need to know the potential for, and magnitudes of, interactions between fish and any proposed device. Until the permitting agencies have developed sufficient information to establish specific guidelines for HKD operations, there will be a need to gather device-specific information on the potential mechanisms for interactions (strike, pressure change, etc.) of the device with fish, site-specific information on which fish species and life stages may be present and susceptible to such interactions, and

information about whether or not fish in fact interact with the device in a way harmful to them. Establishment of test bed sites and the sharing of engineering characteristics can be important ways to spread the risks and costs of acquiring the needed information. Each new evaluation and deployment adds to the knowledge base, but HKD proponents can expect a cautious approach to continue for the next few years (J. Durst – Alaska Dept. of Fish and Game, personal communication).

Recommendations

1. Focus research and development related to HKD interactions with Alaska's river/ocean environments at a center for hydrokinetic energy research and development (such as exists in Europe). The center would provide facilities for testing, consulting services for HKD developers and users, and information on lessons learned from their work and the work of others. The center would have a test site and mobile test-and-measurement capability for use at the test site or for transport to other sites for conducting specialized studies.
2. Develop methods to detect and characterize debris, and develop technology and methods to mitigate debris-flow problems with HKDs.
3. Conduct measurements of two bathymetries, current velocity, and turbulence in a single open-water season to support development and testing of two-dimensional and three-dimensional hydro-sedimentological models, and to model debris/HKD infrastructure interactions.
4. Conduct collaborative studies that include HKD developers/users and relevant agencies to provide baseline information about adult fish upstream migration and how the migration paths of salmon are affected by hydrodynamic conditions, and information about HKD/fish interactions in Alaska. This information is needed to allow agencies to establish known procedures for HKD operators. Because of the distinctive characteristics of Alaska rivers and the importance of the fishes in them, agencies need data from fish/turbine interaction studies to set regulatory policies for hydrokinetic deployments in Alaska.
5. Conduct direct testing of HKD systems, measuring data to develop models of HKD economics to help developers and users assess economics.
6. Conduct turbulence studies to better understand how turbulence magnitude changes in a river as a function of river discharge, to predict its effect on HKDs and to examine its role in debris-transport pathways.

Introduction

Purpose and Background

This report describes the results of a three-year study to characterize the river environment of the Tanana River at Nenana, Alaska, as it relates to the deployment and operation of hydrokinetic power generating devices (HKDs). Our particular interest was in determining those aspects of the river environment that may affect the infrastructure deployment and operations of HKDs and the effects of HKD operation on the river environment. A goal was to establish the Tanana River Test Site (TRTS) at Nenana to facilitate development and testing of HKD technology in a realistic Alaska river setting and develop methods of evaluating river hydrokinetic conditions, HKD performance parameters, and the economics of HKD power (Figure 7). The study site was initially identified by the Ocean Renewable Power Company (ORPC), which subsequently obtained a Federal Energy Regulatory Commission (FERC) preliminary permit to operate at the site. The ORPC approached the University of Alaska Fairbanks (UAF) Alaska Center for Energy and Power (ACEP) about a collaboration to conduct HKD-related studies of the Tanana River at Nenana. This collaboration led to the creation of the Alaska Hydrokinetic Energy Research Center (AHERC) and the start of this project, which was supported by the Alaska Energy Authority's (AEA) Renewable Energy Fund.

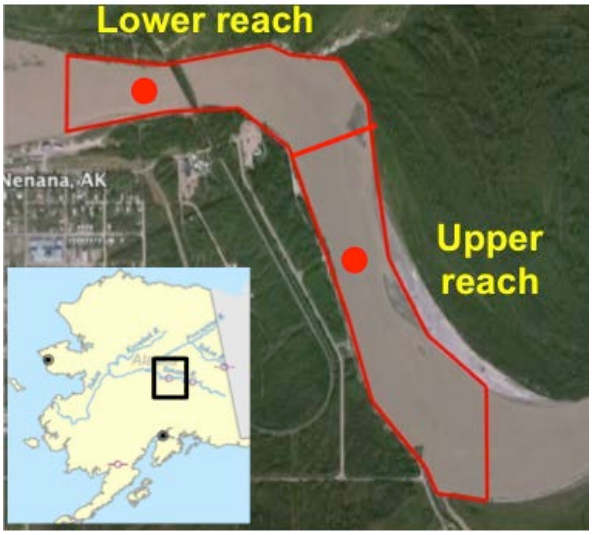

Figure 7. Tanana River Test Site at Nenana, Alaska. The solid markers indicate prospective HKD deployment locations.

Motivation

Alaskans are dealing with dramatically increasing energy costs that are significantly higher than those in the continental U.S. Throughout Alaska, the cost of energy (in 2011 U.S. dollars) ranges from $0.12/kWh to $1.00/kWh, with the lowest cost in Juneau, where locally available hydropower is used, and the highest cost in the village of Newtok. Rural Alaska communities are particularly affected by energy costs, paying more than three times the U.S. average, a hardship compounded by per capita incomes that are less than 75% of the U.S. average (Wilson et al. 2008). Alaska also has the highest per capita energy usage within the U.S. Comparably, in the rest of the U.S., the cost of electricity (in 2010 U.S. dollars) ranges from a

low of $0.065/kWh (Idaho) to a high of $0.25/kWh (Hawaii), with an average of $0.098/kWh (USEIA 2012; AEA 2012).

Along with high energy costs, Alaska has abundant renewable energy resources (AEA 2011), and it is committed to developing them. In 2011, legislation was enacted to establish a statewide energy policy with a goal of producing 50% of the state's electricity from renewable energy sources by 2025. The state funds renewable energy projects and emerging energy technologies through its Renewable Energy Fund (REF) and Emerging Energy Technology Fund (EETF). Available renewable energy sources include hydropower (power generated from the potential energy difference in water height), which presently produces about 24% of the state's electricity, wind, geothermal, and hydrokinetics (power generated from the kinetic energy of water current).

In many of Alaska's rural villages, those located along major rivers and experiencing some of the highest energy costs, there is great interest in displacing high-cost diesel-generated power with hydrokinetic generators. The FERC has issued several tidal preliminary permits and a river hydrokinetic preliminary permit to private developers interested in conducting hydrokinetic projects (Figure 8). In addition, state and federal funding sources have provided funds to advance hydrokinetic power in Alaska through demonstration projects, resource characterization studies, and technology development funding (Table 1). Hydrokinetic power is generated by placing an HKD in tidal, river, or ocean currents. It is estimated that Alaska contains 40% of the total U.S. river energy resource (Table 2) and 90% of the total U.S. tidal energy resource (Miller et al. 1986; Previsic 2008; Previsic and Bedard 2008; Polagye and Previsic 2006; Bedard et al. 2009).

Figure 8. Preliminary FERC permits for tidal and river hydrokinetic projects and a wave power project (FERC staff, Dec. 4, 2012).

Table 1. Summary of funded hydrokinetic projects and studies in Alaska as of 2011.

Project Description	Funding Source
Hydrokinetic resource study of Alaska rivers (University of Alaska Anchorage)	AEA-REF
Tanana River characterization study at Nenana (Alaska Hydrokinetic Energy Research Center)	AEA-REF
Igiugig power generation project (Alaska Energy Authority)	AEA-REF
Eagle demonstration project (Alaska Power and Telephone)	DC-EETG
Ruby demonstration project (Yukon River Intertribal Watershed Council)	AEA-REF
National hydrokinetic resource study (Electric Power Research Institute)	DOE
Cook Inlet Beluga whale study (Ocean Renewable Power Company)	DOE
Sediment abrasion study (Ocean Renewable Power Company	DOE
Delta Junction demonstration project (Whitestone Power and Communications)	DOE

Table 2. Alaska site-specific river hydrokinetic resource summary (Previsic and Bedard 2008).

Site	Average Available Power (kW)
Tanana River	
Nenana	694
Whitestone (Big Delta)	762
Yukon	
Pilot	1,675
Eagle	4,601
Taku	
Juneau	482
Kvichak	
Igiugig	719
Total	8,933

The estimated costs of energy from hydrokinetic sources, using Electric Power Research Institute, Inc. (EPRI) study results converted to 2010 U.S. dollars, range from $0.11/kWh at Knik Arm (near Anchorage) from tidal resources, up to $0.68/kWh at Igiugig and Eagle from river hydrokinetic resources (Polagye and Previsic 2006; Previsic 2008). While the average energy cost in Alaska is significantly higher than in the continental U.S., hydrokinetic power might be competitive with competing Alaska power generation sources, as estimated from EPRI studies (Table 3).

Table 3. Estimated economics of hydrokinetic power production at selected locations in Alaska updated to 2010 dollars (Previsic and Bedard 2008; Polagye and Previsic 2006).

Location	Estimated Renewable Cost/kWh	Estimated Current Cost/kWh
Igiugig (Kvichak River)	$0.69	$0.73
Eagle (Yukon River)	$0.68	$0.47
Whitestone (Delta River)	$0.19	$0.14
Knik Arm (Cook Inlet – tidal)	$0.11	$0.14

The focus of most studies of hydrokinetic power generation in Alaska has been on technology development or characterization of available power resources in a general way. An example of this is using available data from U.S. Geological Survey (USGS) or other gauging stations and estimated or measured river cross-section average velocities to determine available power densities and an idealized power extraction factor to determine usable power. A close correlation is then assumed between the cost of energy and the river's power density, whereby higher power densities indicate a lower cost of energy (Previsic and Bedard 2008). This approach is highly idealized, and it does not take into account the effect of the river environment on the performance of HKD technology under realistic Alaska river conditions. Many rivers in Alaska are glacier fed and have high concentrations of suspended and bed load sediment, instances where sheet and frazil ice can affect HKD infrastructure, current velocities that are not uniform across a river's cross section, turbulence, and debris flows. In addition to the aspects of a river's environment that can affect HKD operations and performance, there is a need to understand the effects of HKD operations on a river's environment including changes in flow patterns, wake turbulence, local sediment deposition or scour, and influence on fish stocks.

At the beginning of this study (2009), it was commonly assumed that river debris would not be a significant problem and that HKDs mounted on a river bottom beneath the winter surface ice would be able to generate power year-round. Field measurements conducted during this study have demonstrated that wintertime current velocities drop drastically compared with summertime flows, making it highly unlikely that economic power generation can occur during winter months. All HKD demonstration projects on the Yukon River in Alaska at Ruby (2008–2010) and Eagle (2010) and on the Mackenzie River in Northwest Territories, Canada, at Fort Simpson (2010 and 2011) were terminated because of significant problems with debris that clogged or damaged the HKD infrastructure and created hazardous operating conditions (Johnson and Pride 2010; Tyler 2011; NUL 2012). Turbines have been observed to perform below their rated capacity for a given river current velocity, which is most likely due to the effects of river turbulence. One of the authors (Johnson) observed a noise level change in the 25 kW New Energy hydrokinetic turbine at Eagle, which is associated with torque or power generation of the turbine, as large vortex swirls moved through generating blades. In addition to the problems just described, the

Fort Simpson 25 kW turbine deployment suffered problems related to low electrical output, extended downtime due to debris strikes, and the logistics of installing and removing the turbine from the river (NUL 2012). These were common issues with the Eagle turbine deployment as well.

So far, the performance difficulties of HKDs in the Yukon and Mackenzie Rivers have not been the result of malfunctioning technology, but rather the result of problems related to deploying, retrieving, and operating HKDs in the river environment. The goal of this study is to provide information and methods to HKD developers and users by identifying and characterizing river environments that can affect HKD operations. Such information is needed to help guide development of HKD technology that is designed to overcome challenges to HKD river operations and facilitate the development of HKD use in Alaska. As such, we have examined the Tanana River's hydrodynamics (current velocity, power density, turbulence, suspended and bed load sediment transport, and discharge), winter ice conditions, fish stocks, and debris.

Hydrokinetic Power Generation Basics

The use of hydrokinetic devices to convert the kinetic energy of river currents into useful mechanical energy has a long history (e.g., the waterwheel). Modern HKDs, however, are a recent invention and come in a variety of technology designs. Three different HKD designs are shown in Figure 9: a propeller type, a cross-flow hydrofoil type, and a vortex induced vibration type. As recently as 2009, HKDs were considered pre-commercial (Khan et al. 2009). Presently, there are no commercial HKD installations in Alaska. Hydro Green Energy operates a commercial hydrokinetic power project on the Mississippi River at Hastings, Minnesota, just downstream of a hydropower dam (www.henergy.com). This is a protected river environment, as the dam blocks debris and sediment, and the stream channel is straight with controlled flow from the dam. The first commercial HKD tidal installation, currently operating in the U.S., is the ORPC Beta TidGen™ (Figure 9b), installed on the bottom of Cobscook Bay near Lubec, Maine (Woodard 2012, www.orpc.co).

Figure 9. Hydrokinetic power generating devices. (a) Verdant axial flow turbine [http://verdantpower.com/]; (b) Ocean Renewable Power Company's Beta TidGen™ Turbine Generator Unit, the precursor to ORPC's commercial-scale TidGen™ Power System [http://www.orpc.co/]; (c) Vortex Induced Vibrations for Aquatic Clean Energy (VIVACE) [http://www.vortexhydroenergy.com/].

To operate economically, HKDs require current velocities of between 1.5 m/s and about 3.5 m/s and a current velocity of at least 0.5 m/s to overcome the internal resistance of HKD components (Figure 10). The kinetic energy of a river or tidal flow is proportional to the cube of its current velocity, which results in a power output for HKDs also proportional to the cube of the current velocity. The cubic dependence

on HKD output power can be seen in the measured output energy for the ORPC Beta TidGen™ compared with design values, shown in Figure 10. A more extensive description of the state of HKD developments in Alaska and elsewhere can be found in Johnson and Pride (2010) and Johnson et al. (2011).

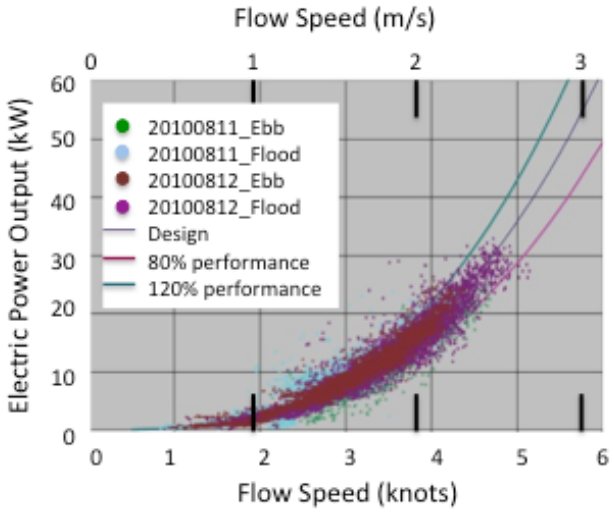

Figure 10. Electric energy output versus tidal flow speed for the ORPC Beta TidGen™ turbine (figure credit: ORPC, http://www.orpc.co/).

Report Structure

This report is structured to first present the measurements and analyses completed as part of our efforts to characterize the Tanana River at Nenana, including its hydrodynamic conditions, fish stocks, and debris, and the potential impact of these characteristics on HKD operations. The section on hydrodynamics encompasses a wide variety of river flow properties and processes, including river current velocities and turbulence, power densities, bed load and suspended sediment transport, discharge, riverbed dune formation, and ice formation processes. Since the primary purpose of this work was to develop information and methods useful to HKD developers and users, we have included a section on the impacts of the river environment on HKD operations, using results from our other studies.

This study has produced significant data and results that have been published as our findings warranted so that information would be available to the HKD community in a timely manner, rather than delayed until a final report. The first page of each primary publications is included in Appendix A and copies of the publications are included in electronic form as Appendix C.

Hydro-Sedimentological Conditions

Introduction

An understanding of the hydro-sedimentological conditions of a specific river reach is necessary for determining where to best locate a hydrokinetic power generating device (HKD), how well an HKD will perform, the effect that the river will have on HKD operations, and the impact of an HKD turbine on the river environment. It is critical to know the river's baseline conditions to evaluate changes in river dynamics resulting from the installation and operation of a turbine, since river dynamics respond immediately to objects placed in the current. River dynamics and bathymetric conditions along the river channel determine the suitability of a specific reach of river for deployment and operation of in-stream hydrokinetic turbines, individually or in arrays.

Local hydrokinetic power variations, total extractable power, and available space for positioning turbines are defined by the bathymetry and instantaneous power density as a function of location along the length and width of a river reach. The total recoverable power for a turbine is a function of total extractable river hydrokinetic power, described by the efficiency with which a given turbine device acquires the available energy, and the spacing between turbines needed to avoid wake turbulence effects from turbines placed upstream.

River turbulence produces shear and off-directional stresses and stress gradients on deployed HKDs, reducing their effectiveness and increasing stress fatigue on turbine structural components. While all rivers exhibit turbulent flow, the magnitude and scale of turbulent parameters are affected by discharge, bathymetry, changes in river channel configuration (e.g., straight channels, river bends, etc.), and the geometry and size of objects placed in the river. It is important to understand where in a river reach that turbulence is enhanced or decreased in order to evaluate its effect on HKD operating efficiency and the magnitude of imposed shear stresses on HKD components. These factors influence where to site an HKD, as well as the design parameters, expected operating life, and maintenance costs of an HKD.

High turbulent areas along specific regions in channels may indicate the instability of the river's thalweg and its migration. Such regions can occur just upstream of a river bend, where the main river flow could be transitioning from one side of the river to the other as the flow moves into the river bend. Such migration may cause the thalweg to move away from an installed turbine, thus decreasing the percentage of the total available power from the river that can be converted to electricity.

Suspended sediment transport can affect HKD operations through abrasion of components, while bed load sediment transport can impact foundation or anchoring systems. Thus, understanding suspended and bed load sediment transport and bed form characteristics is crucial for the design of HKD infrastructure.

Too much measurement detail about a river's hydro-sedimentological condition incurs higher startup costs for HKD developers and operators, and too little detail may result in future increased HKD operating costs and decreased revenue. In the following sections, we summarize the measurements, analysis results, interpretation of data, and modeling efforts for the Tanana River Test Site (TRTS) at Nenana to answer questions about siting HKDs. While focused on the TRTS, the methods and modeling approaches used in this study are generally applicable to other river reaches in Alaska being considered as

a potential location of an HKD. Additional details on specific aspects of this work can be found in the published papers describing our work (see Appendix A).

Methods

Our approach to characterizing the Tanana River combined extensive field measurements along with two-dimensional (2D) hydrodynamic modeling and analysis. We measured river current velocity, suspended and bed load sediment transport, bathymetry, and riverbed dunes. Current velocity measurements were made using an acoustic Doppler current profiler (ADCP). Turbulence parameters over small volumes of water can be calculated from measurements done using acoustic Doppler velocimeters (ADV) by performing point measurements (Oberg et al. 2002). The level of detail in turbulence provided by ADV measurements was not needed for the turbulence study conducted in this project, which focused on estimating macroturbulence over the full water column, rather that examining fine-scale turbulence at a point.

Current velocity measurements were made along geo-referenced transects during 2009 and 2010 (Figure 11 and Figure 12), and measurements of suspended and bed load transport and riverbed profiles were made at locations shown in Figure 13. Current velocity measurements were used to determine river discharge, specific hydrokinetic power, and turbulence. Sediment transport measurements were used to define sediment rating curves for both suspended and bed load sediment as a function of river discharge.

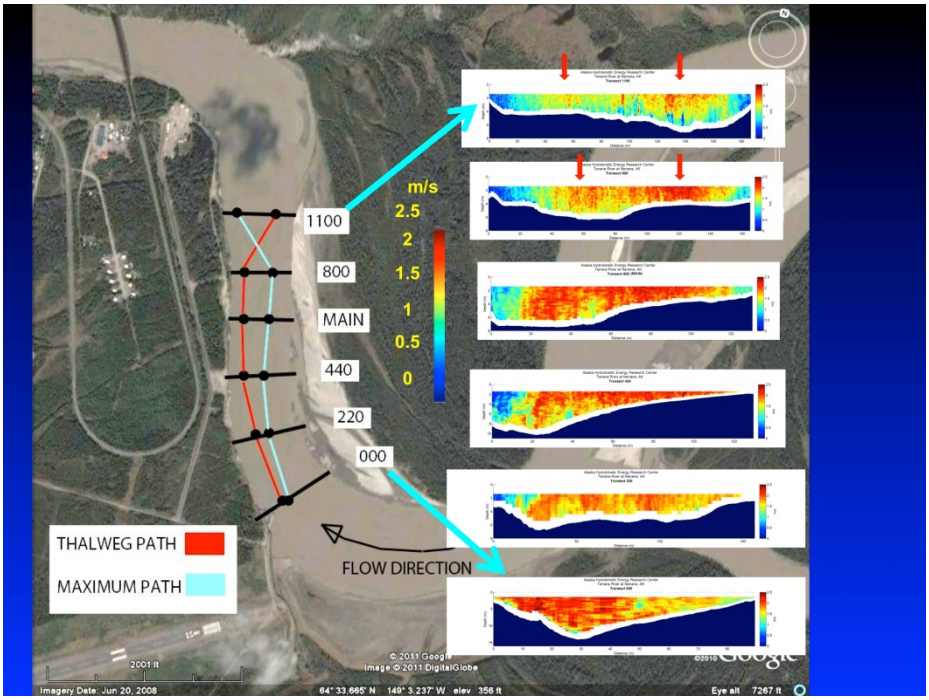

Figure 11. Aerial view of the study reach. (Lines indicate river transects where velocity measurements were made during August 2009. Thalweg and maximum flow paths and their relative velocities are shown.) Modified from Walsh et al. 2012.

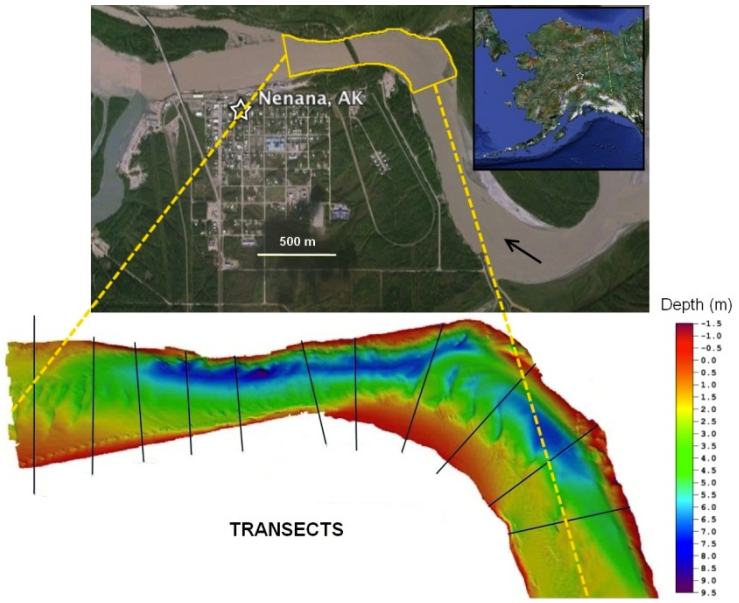

Figure 12. Bathymetry and ADCP transect lines acquired by TerraSond, Inc. during August 2010. Flow direction is from right to left.

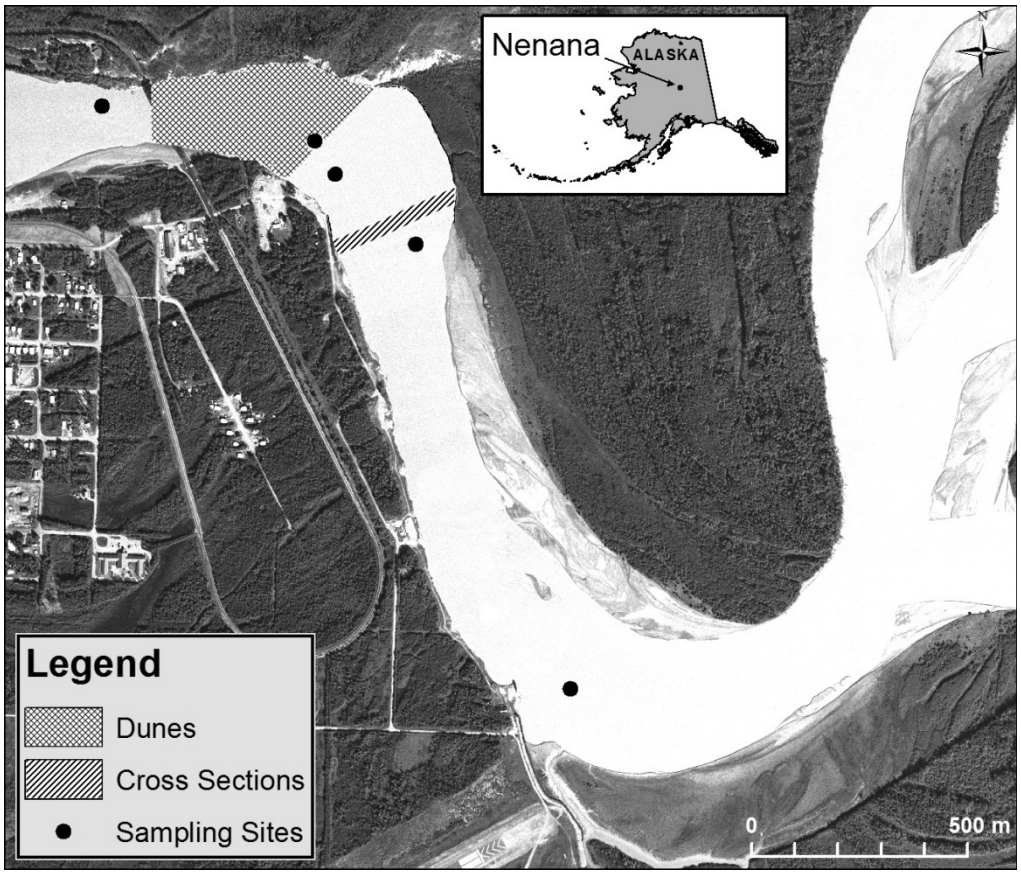

Figure 13. Location of suspended and bed load sediment sampling sites (solid circular markers) and the area where riverbed dune profiles were measured (crosshatched) (Toniolo 2013).

Velocity measurements used in turbulence analysis were made in the upper river reach by placing upward-looking ADCPs on the riverbed at specific locations along the thalweg and maximum flow paths, shown by the dots along the ADCP transect lines (Figure 11) (Toniolo et al. 2010). The ADCPs were configured to record data at a high frequency rate and minimal averaging, and left in position for about 15 minutes to determine the three-dimensional (3D) time variation of current velocity about a mean value. The velocity deviation about the mean current velocity was used to determine turbulence magnitude and direction. Measurements were made along both the thalweg and maximum positions to determine relative turbulence for each of these high-flow energy locations as a means of examining river channel stability, for example, thalweg migration and meandering.

In an ongoing study, macroturbulence in the lower river reach is being analyzed using ADCP transect measurements taken from surface measurements to characterize flow conditions along a given river cross section. The results from the macroturbulence study will be reported in a future publication. The transect method of determining turbulence has several operational advantages over the riverbed-mounted upward-looking ADCP method. Measurements using the transect method can be made quickly with lower risk of equipment damage or loss than when deploying ADCPs on the riverbed (TerraSond lost an ADCP during our riverbed ADCP turbulence measurement effort). In addition, data obtained from the transect method provide a sense of turbulence over a complete river cross section rather than at a point location. The primary disadvantage of the transect method is that it provides a quasi-instantaneous picture of river condition, which can change in a short time. Thus, a variation (or error) associated with mean flow conditions, estimated from multiple transects, can be expected. The amount of error is related to both the time it takes to complete a transect and the rapidity of turbulence change. Efforts to estimate errors in determining turbulence using the transect method are in-progress.

To develop a continuous view of current velocity of the river reach, a 2D river hydrodynamic model, CCHE2D (http://www.ncche.olemiss.edu/software), was used to describe the TRTS hydrodynamics (Toniolo et al. 2010). Accurate model simulations require that the river reach bathymetry be measured in detail, which was done by TerraSond, Inc. The bathymetry of the upper reach of the river study site was measured during August 23–28, 2009, and the bathymetry of both the upper and the lower reach of the river study site was measured in early August 2010. The 2010 bathymetry of the combined upper and lower study site sections is shown in Figure 14. The 2D hydrodynamic model was calibrated against water slope at the river reach, bed roughness adjustments of the model, and current velocity measurements made on the same day as the bathymetry measurements.

A hydrokinetic calculator module (HYDROKAL) was developed to process CCHE2D river hydrodynamic simulations for estimating the instantaneous power density, maximum current velocity, and specific discharge locations in each river cross section. The tool includes a user-defined HKD efficiency factor to account for turbine efficiency, allowing HKD developers and users the ability to quickly estimate the amount of hydrokinetic energy that can be extracted at a given location in the river (Duvoy and Toniolo 2012). HYDROKAL is available to download as supplementary material from http://www.sciencedirect.com/science/article/pii/S009830041100207X.

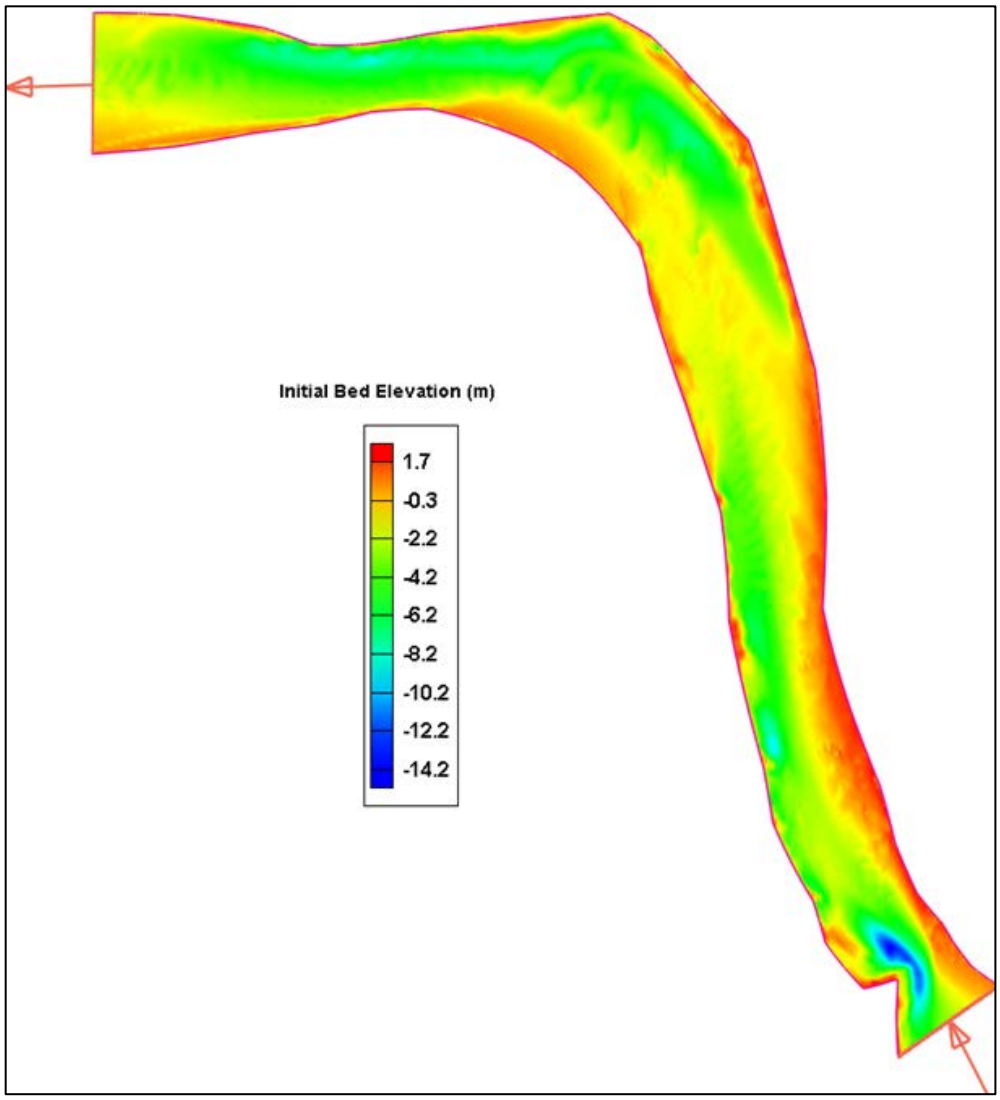

Figure 14. The 2010 bathymetry profile of the complete river reach (Duvoy and Toniolo 2012; reprinted by permission of Elsevier). Refer to Figure 11 to reference the bathymetry to the river's study site reach.

Fall and wintertime river conditions were measured during 2009 and 2010 to determine ice thickness and river current velocities under the ice and to develop a qualitative characterization of frazil ice conditions. Frazil ice forms in open sections of fast-flowing rivers at cold temperatures, when the water can supercool; that is, when water temperature drops below the freezing point. Normally, frazil ice discs are about 0.1–5 mm in diameter and 25–100 µm thick (Schaefer 1950). During their active growth period, frazil ice particles readily adhere to objects that they contact (Ashton 1986). Engineering structures can become coated with frazil ice, causing problems with their operations. Figure 15 illustrates frazil ice adhesion to several different types of tubing from a frazil ice growth test conducted on the Tanana River.

Figure 15. Frazil ice growth on three different materials. From right to left: Teflon®, 316 SS, and mild steel (Oct. 22, 2010, air temperature = -11°C; 12 hr 40 min of submersion). Frazil growth perpendicular to the current was limited by river shear that eroded the frazil causing the growth to proceed upstream and downstream.

Measurements of ice thickness, water depth, and velocity at approximately 0.5 m (20 in.) intervals were taken over a course of a year (Figure 16). Measurements were taken in April and December 2009 and January, February, and April 2010. The measurement locations were a series of 25 cm (10 in.) holes drilled along a transect near the Main transect (Figure 11) of a reconnaissance survey for hydroelectric turbine sites reported by TerraSond (2008). The location of each hole was marked and stored in the memory of a Garmin eTrex handheld GPS (see Appendix B, Table B-4 for transect hole locations). Velocity measurements were made with a Marsh-McBirney model 2000 Flo-mate portable flowmeter.

Figure 16.Tanana River under-ice current velocity measurements. UAF photo by T. Paris.

Results

Discharge and Specific Power

Maximum measured current velocities at the TRTS ranged between less than 0.5 m/s in winter to over 2.5 m/s during summer months and over 3 m/s during high-water events (Toniolo et al. 2010; Langley 2006). River dynamics (current velocity, turbulence) are primarily a function of river discharge for any given reach of river. Discharge data for the Tanana River near Nenana can be accessed from the USGS gauging station at the Tanana River near Nenana (http://waterdata.usgs.gov/nwis/nwisman/?site_no=15515500). The seasonal variation of discharge provides insight into the seasonal variations in river dynamics during summer, fall, winter, and spring, which are crucial for understanding the river regime. By using the measured seasonal discharge as input into the 2D hydrodynamics model for the TRTS, it is possible to estimate the seasonal variation of river current velocity and specific power. Although results will be limited by restrictions imposed by the interaction of sediment and flow in a river, the model calibrated by the team was only hydrodynamic, not hydro-sedimentologic.

For a given river, the kinetic instantaneous power density in Watts of a parcel of water per unit area (specific power) is proportional to the cube of the velocity of the water flowing through the channel's cross section given by

$$P/A = (1/2)\cdot\rho\cdot v3 \quad (1)$$

where P is power, A is the area over which the power is calculated, ρ is the density of water, and v is velocity (Couch and Bryden 2004; Hau 2006; Khan et al. 2008).

The average, maximum, and minimum monthly discharge for the Tanana River at Nenana for 1962–2010 is shown in Table 4 and plotted in Figure 17. The average monthly discharge ranged from a low of 496 m^3/s to a high of 1702 m^3/s during the open-water season (i.e., May to October), and from a low of 185 m^3/s to a high of 268 m^3/s during the winter months (i.e., November to April). The minimum discharge year occurred in 1996, and the maximum average discharge year occurred in 1967. During the summer months of July, August, and September, the average discharge was approximately 1423 m^3/s when considering years 1962 to 2010. In 1996, during the same summer months, the discharge was only 1047 m^3/s, while in 1967, the discharge increased to 1940 m^3/s.

Table 4. Minimum, average, and maximum monthly discharge for years 1962–2010 in m^3/s.

YEAR	Jan	Feb	Mar	Apr	May	Jun	Jul	Aug	Sep	Oct	Nov	Dec
MIN 1996	196	186	181	263	747	870	1272	1175	693	338	224	187
MAX-1967	142	142	142	176	1056	1666	1911	2781	1128	471	216	195
AVG 1962–2010	193	187	185	250	883	1334	1702	1611	957	496	268	212

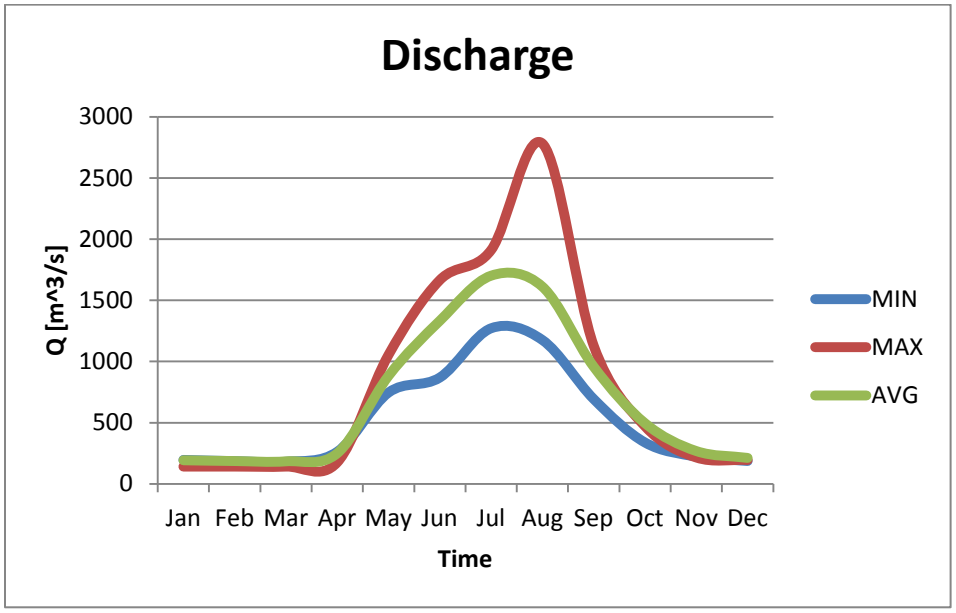

Figure 17. Minimum, average, and maximum monthly discharge for years 1962–2010 in m^3/s.

Current Velocity and Power

The calibrated 2D hydrodynamic model of the TRTS river reach was used to assess current velocities and discharge, and the HYDROKAL tool was used to estimate instantaneous power density and to compute maximum values of velocity and specific discharge, providing insight on the stability of the river reach. The model was calibrated by estimating the roughness coefficient. Model parameters included the initial water surface elevation for the entire domain, total simulation period, and time step increments. A parabolic eddy viscosity model was chosen for the turbulence model. Default values for Coriolis force, acceleration of gravity, von Kármán constant, and kinematic viscosity were selected. The current velocity, specific discharge, and instantaneous specific power density for the upper TRTS river reach based on the 2009 bathymetry and current velocity measurements are shown in Figure 18, Figure 19, and Figure 20. A

comparison of point velocity measurements with calculated velocities using the 2D model is shown in Figure 21.

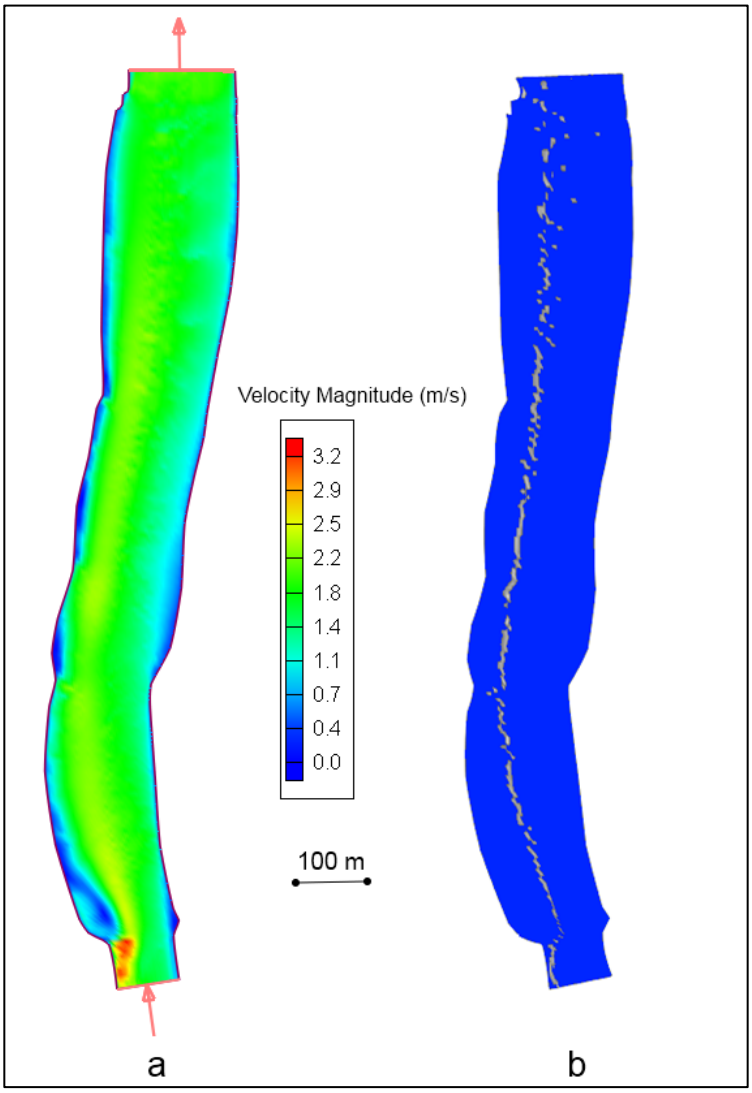

Figure 18. Velocity magnitude (a) and location of maximum velocity at each river cross section (b) (Toniolo et al. 2010; reprinted by permission of SAGE).

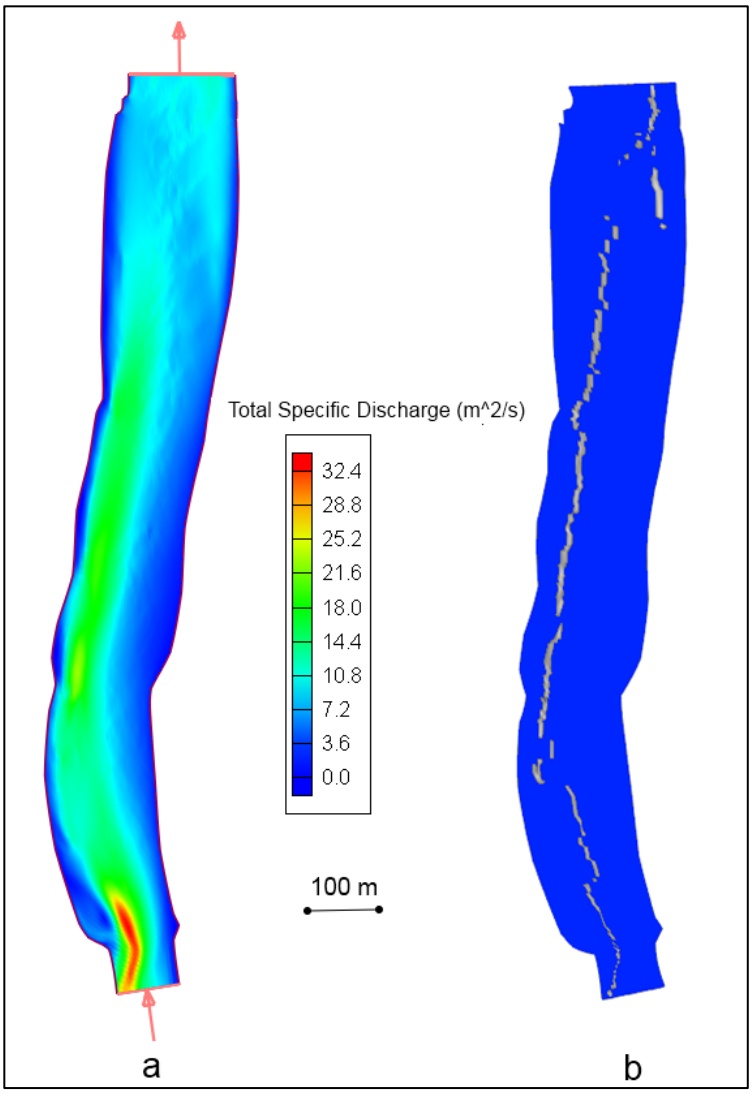

Figure 19. Specific discharge (a) and location of maximum specific discharge at each river cross section (b) (Toniolo et al. 2010; reprinted by permission of SAGE).

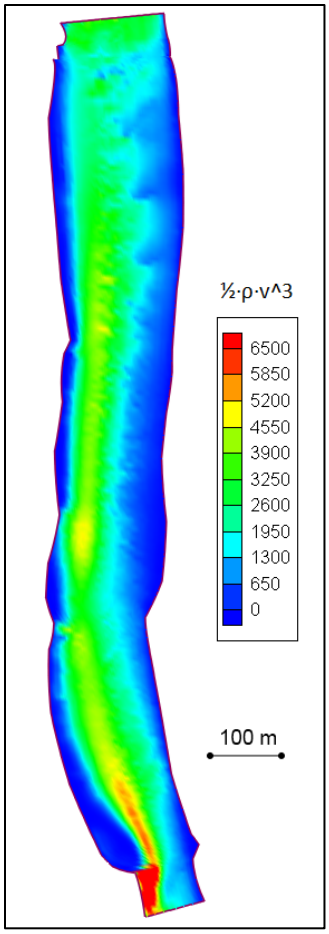

Figure 20. Instantaneous specific power density plot in W/m^2 (Toniolo et al. 2010; reprinted by permission of SAGE).

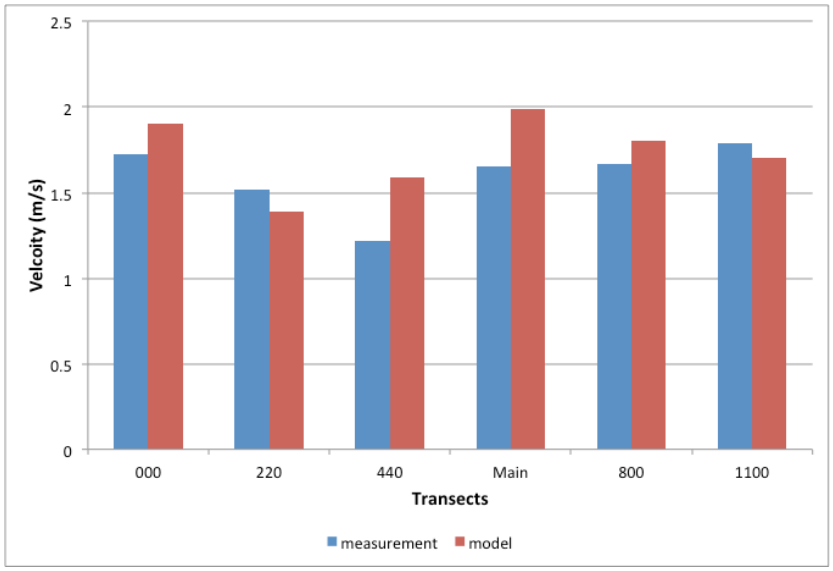

Figure 21. Comparison of measured current velocities with 2D model calculated velocities for the thalweg flow path (Toniolo et al. 2010; reprinted by permission of SAGE).

Differences between the model calculated and the measured current velocities averaged throughout the measurement region were about 3% (Toniolo et al. 2010), which is reasonable for a 2D hydrodynamic model. The model generally reproduces velocity measurements in the river reach. Significant factors affecting numerical model accuracy are the precision of river reach bathymetry measurements, the quality of the mesh where the domain is discretized, and the choice of the turbulence closure model for the calculation of the turbulent eddy viscosity. The bathymetry for the TRTS upper river reach was detailed, but with some uncertainty because of difficulty with definitively being able to locate some parts of the riverbed with the multi-beam sonar. Initially, the difficulty of locating the riverbed with the sonar was attributed to the river's high sediment load; however, a more likely explanation is that large amounts of mulch-like small-scale debris observed flowing in the lower third of the river (see the Debris chapter of this report, Figure 44a) interfered with acoustic returns from the sonar at some locations.

Non-dimensional profiles for measured current velocities indicate similarity for the flow in maximum path locations along the study reach (Figure 11), with the exception of the profile located immediately downstream of the river bend (transect 000). The flow condition in the thalweg does not present similarity for any of the other transects, indicating a highly variable hydrodynamic condition along the thalweg. Average transect-measured velocities around the thalweg are around 1.5 m/s, with maximum values of about 1.9 m/s (Toniolo et al. 2010).

River current velocities and specific discharge are highest upstream along the thalweg. Downstream of the reach, the river flow transitions from the left bank to the right bank of the river (Toniolo et al. 2010). (Refer to Figure 11 to place the upper reach in context with the overall river morphology.) This transition of flow from the left bank to the right bank can be seen in the shift of the maximum specific discharge shown in Figure 19b, which indicates instability of the channel in that area.

The instantaneous specific power in the river reach, shown in Figure 20, has its highest magnitudes in the thalweg path and near the upstream end of the reach. The distribution of specific power densities for the entire river reach in 2010, as shown in Figure 22, is similar to the specific power in the river reach during 2009, which indicates that the highest power densities are in the upper part of the river reach concentrated in the thalweg. The magnitude of power density diffuses and becomes unsteady around the bend (through the transition of flow from the left bank upstream of the bend to the right bank downstream of the bend). Power densities again concentrate against the right bank downstream from the river bend.

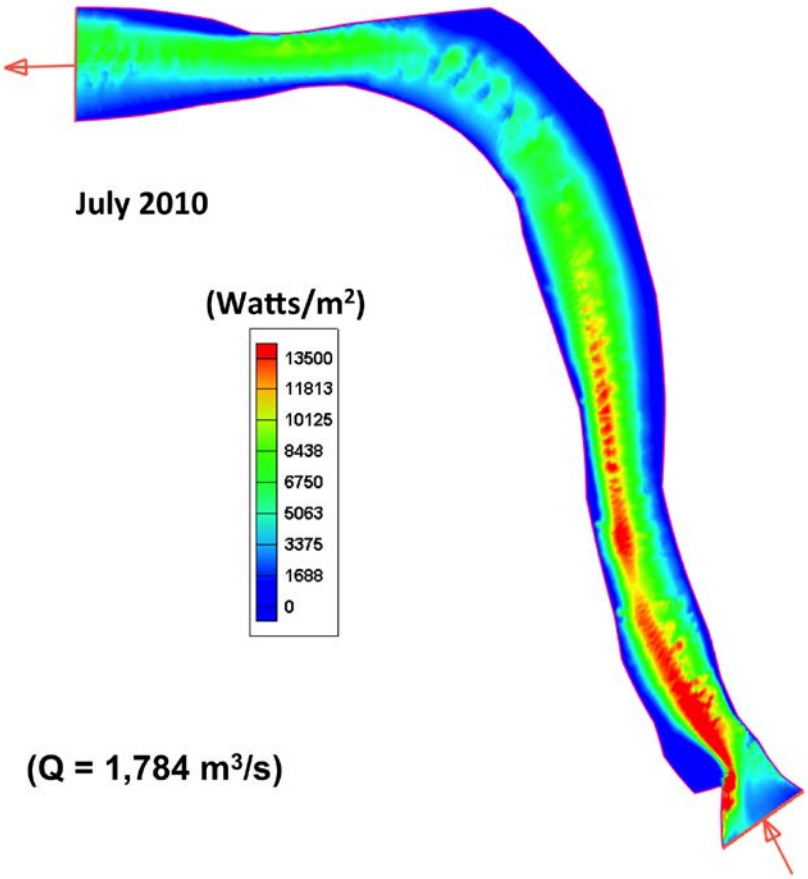

Figure 22. Instantaneous specific power density (W/m^2) for the complete TRTS river reach (Duvoy and Toniolo 2012; reprinted by permission of Elsevier).

Variations in Specific Power as a Function of River Location, Season, and Annual Discharge

Hydrodynamic modeling is the only feasible method for estimating, as a function of location, season, and discharge year, the specific power density at any point in a river reach being considered as a place to deploy an HKD. A discharge year is defined as the overall discharge throughout a year (e.g., minimum, average, maximum – see Figure 17). The two-dimensional CCHE2D hydrodynamic model of the TRTS river reach is used to calculate river current velocities for the river reach over periods when discharge data are available. The HYDROKAL tool is then used to process the CCHE2D river hydrodynamic simulations to estimate the instantaneous power density for the discharge conditions of interest at selected locations in the river reach. HYDROKAL can also be used to determine the location and magnitude of the maximum current velocity and specific discharge in each river cross section.

Three locations in the upper TRTS river reach, where CCHE2D simulations were run for the discharge conditions shown in Figure 17, are shown in Figure 23; the HYDROKAL tool was applied to determine the instantaneous power density. The instantaneous power for the three locations for the maximum discharge year (Figure 24), the average discharge year (Figure 25), and the minimum discharge year (Figure 26) are determined from modeled results using the 2009 bathymetry, as there are no bathymetries available for other years. Therefore, due to the uncertainty of bathymetry changes with time in these estimations, these power density values are qualitative results. The results indicate that location P2 has the

highest power density, followed by P1 and P2 for all three discharge years. The results also indicate that power density can vary significantly from one discharge year to another. For example, the peak power density at P2 during the maximum discharge year is more than 100 times larger than the peak power density during the average discharge year, and the peak power density during the minimum discharge year is less than half of the average discharge year's power density.

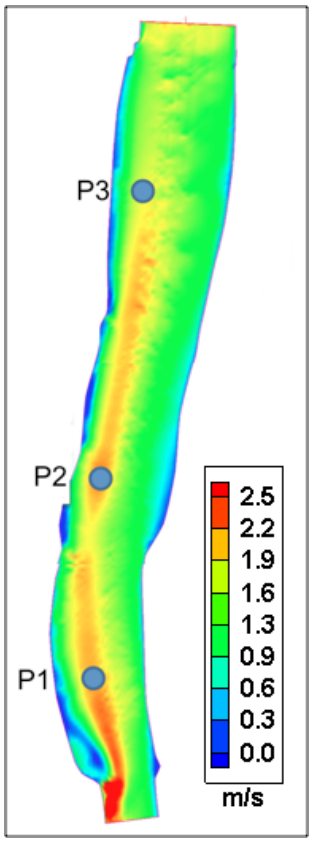

Figure 23. Location of Point 1, Point 2, and Point 3 over a velocity magnitude plot of the upper TRTS river reach.

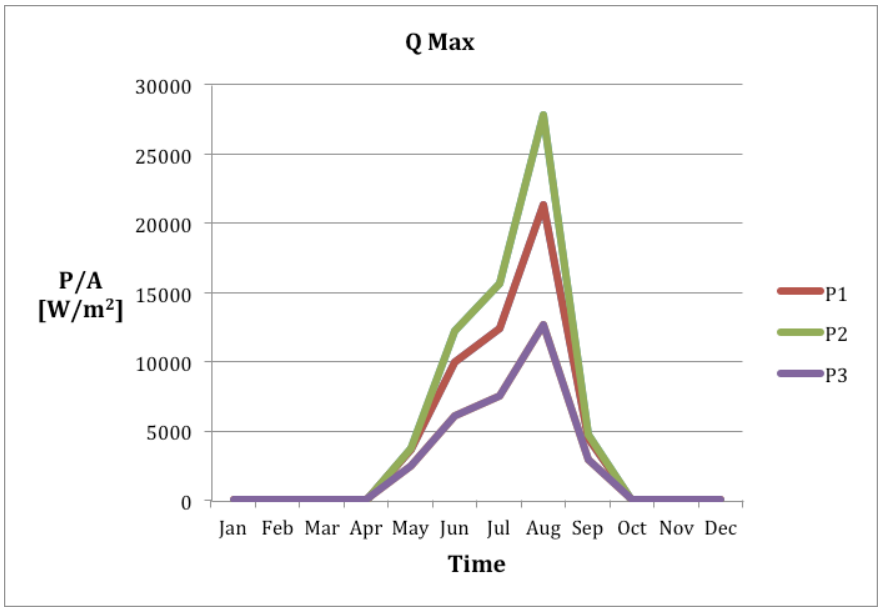

Figure 24. Instantaneous power density in W/m^2 for the three locations shown in Figure 23 and the maximum discharge year shown in Figure 17.

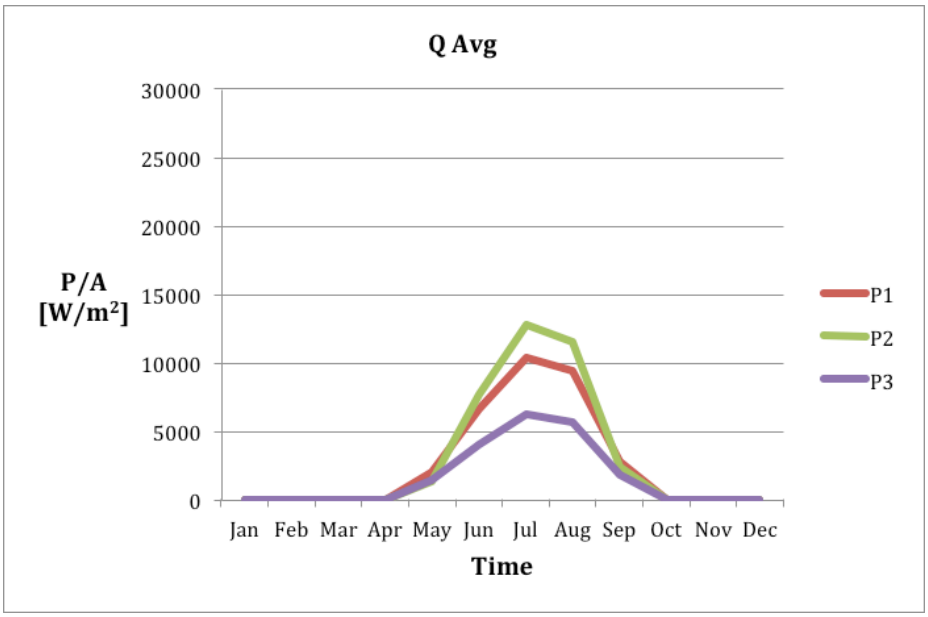

Figure 25. Instantaneous power density in W/m^2 for the three locations shown in Figure 23 and the average discharge year shown in Figure 17.

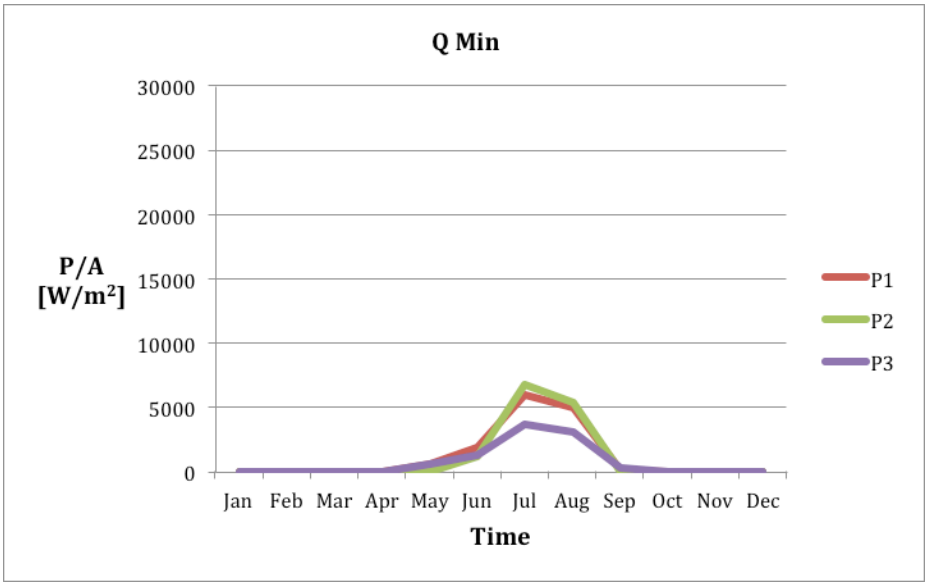

Figure 26. Instantaneous power density in W/m^2 for the three locations shown in Figure 23 and the minimum discharge year shown in Figure 17.

Power density indicates the amount of available hydrokinetic energy that is present at a location in a river reach, but it does not indicate the vector components of the power, which determine the available extractable energy. The CCHE2D model cannot determine the vector components because it is a depth-integrated 2D model with governing 2D equations that are obtained by depth integrating the original 3D equations (Zhang 2006). Hydrokinetic devices are designed to extract power from a river's main flow direction. Consequently, as the magnitude of turbulence at a river location increases, the efficiency of HKD conversion of hydrokinetic energy into electricity decreases because the amount of energy directed in the main flow direction decreases. In addition, energy not directed in the main flow direction can impose stresses on the HKD infrastructure in ways it is not designed for, leading to HKD fatigue that increases maintenance and reduces operational life. Thus, it is important to understand how the total kinetic energy is partitioned between turbulence and the main flow river velocities.

Turbulence

Specific power density provides the first order of information needed to help determine potential locations for HKD deployments. To further refine which locations are most suitable for deploying HKDs, it is important to know the magnitude of turbulence within high power density flows. Ideally, regions with high total kinetic energy and low turbulent kinetic energy should provide the best locations for HKD operations. The total kinetic energy (KE) and turbulent kinetic energy (TKE) for the thalweg and maximum flow paths in the upper TRTS reach are shown in Figure 27 through Figure 29. Both the KE and the TKE at the 000 transect are high due to the combined effects of turbulence from the river-flow direction changes caused by the river bend just upstream, the sudden change in cross-sectional area caused by the presence of a deep hole, and a constriction caused by a projection from the river's left bank (Figure 27). Between transects 000 and 440, KE and TKE rapidly decrease as the flow spreads out after the constriction at 000. Near transect 440, KE is near its minimum, while TKE has increased significantly due to a deep hole that exists just upstream from 440 (Figure 28). From 440 to 800, KE increases while TKE decreases to very low magnitudes relative to the rest of the river reach. This occurs because from

400 to 800 the river reach is relatively straight with constant flow direction and riverbed cross-sectional areas, such that from Main to near 1100, the KE remains relatively high and constant and the TKE remains relatively low (Figure 29) (Walsh et al. 2012).

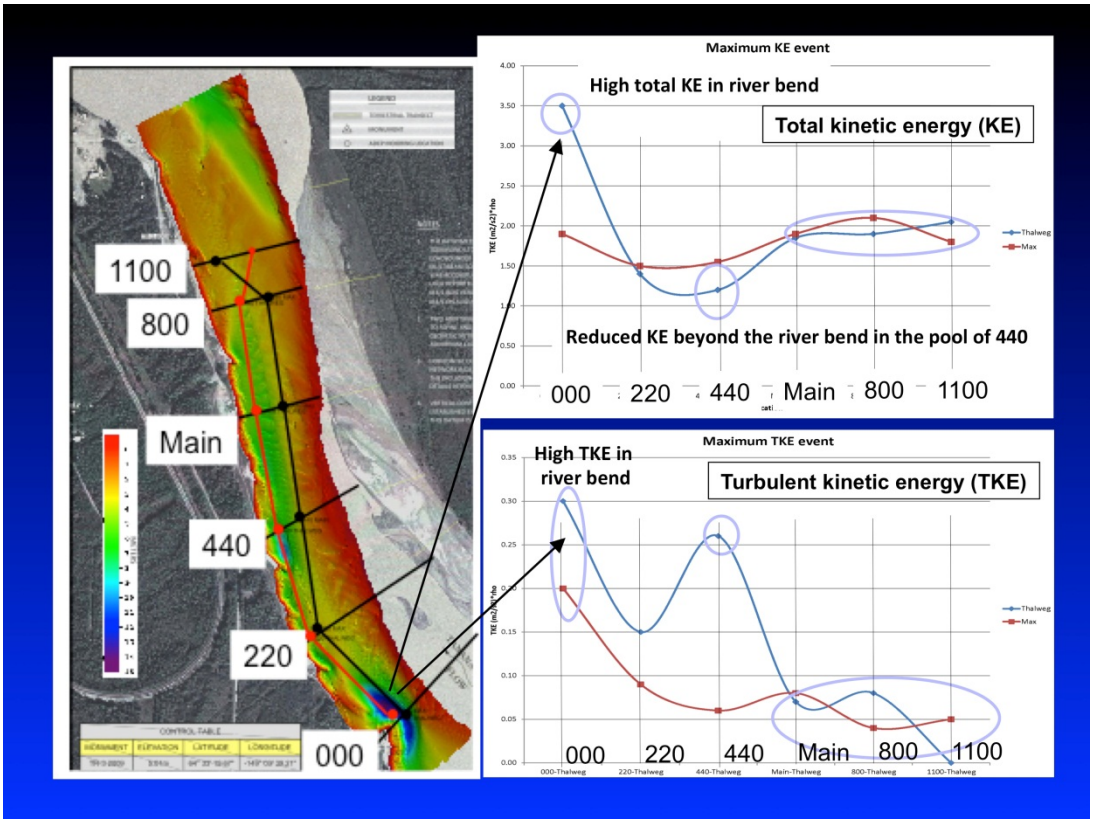

Figure 27. Total hydrokinetic energy (upper) and turbulent hydrokinetic energy (lower) at transect 000 (arrows) for the thalweg and maximum flow paths (KE and TKE plots by Walsh et al. 2012; reprinted by permission of SAGE).

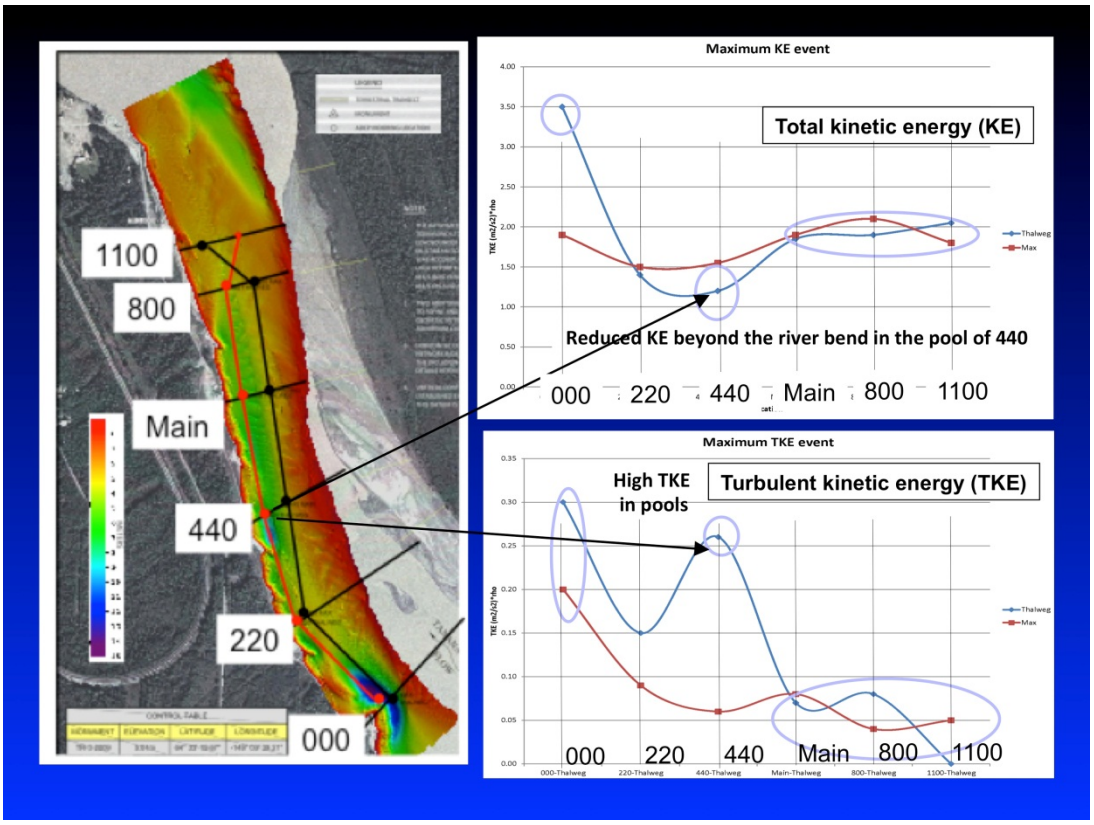

Figure 28. Total hydrokinetic energy (upper) and turbulent hydrokinetic energy (lower) at transect 440 (arrows) for the thalweg and maximum flow paths (KE and TKE plots by Walsh et al. 2012; reprinted by permission of SAGE).

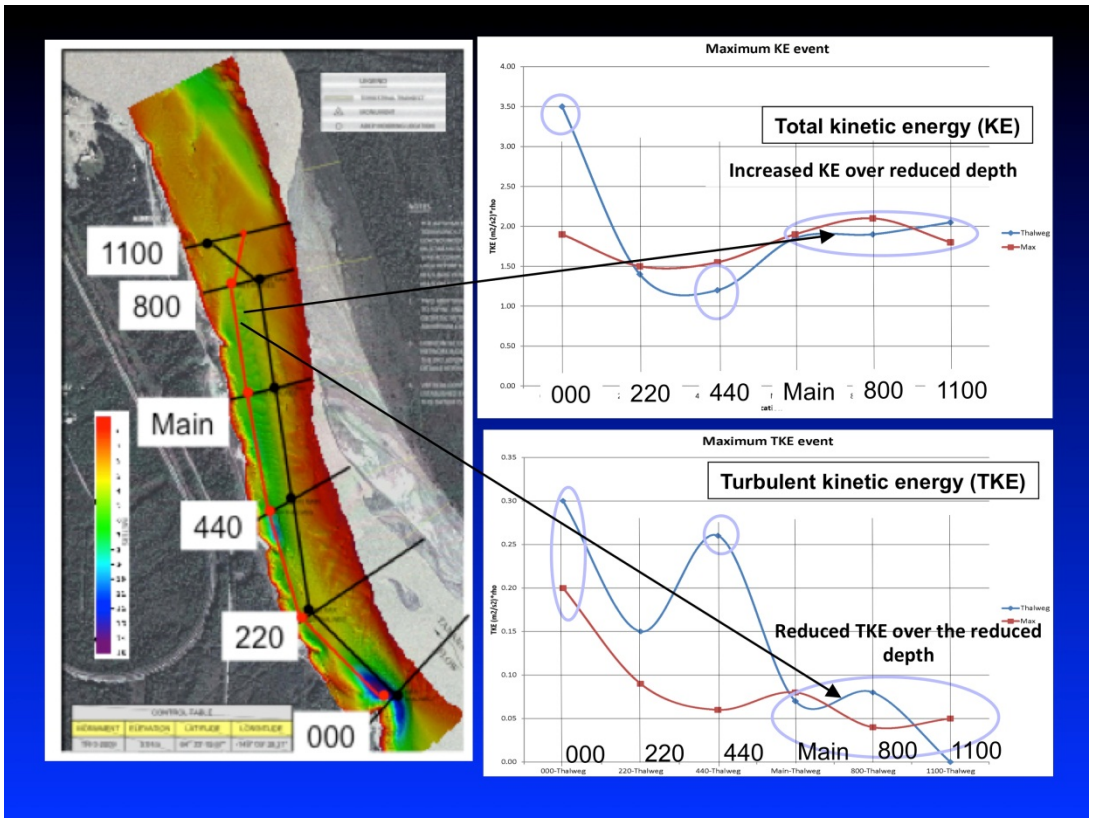

Figure 29. Total hydrokinetic energy (upper) and turbulent hydrokinetic energy (lower) at transect (Main – 1100) (arrows) for the thalweg and maximum flow paths (KE and TKE plots by Walsh et al. 2012; reprinted by permission of SAGE).

As seen in Figure 27 through Figure 29, turbulence magnitude can vary significantly throughout a river reach, even in sections that appear from the surface to be fairly straight. In addition to the well-known concerns about placing HKDs in turbulent locations (e.g., reduced HKD conversion efficiency from kinetic to electrical power and increased stresses that act on HDK infrastructure), there should be concern about debris flows that transition turbulent areas. During extremely high water events, such as the September 2012 high-water event on the Tanana River, neutrally buoyant and submerged debris can become entrained into eddies and boils that bring submerged debris to the surface or move it in unexpected directions (J. Holmgren, personal communication, 2012). Walsh et al. (2012) has identified locations in the TRTS and river morphology features that produce increased turbulence magnitude. However, information about how turbulence magnitude changes as a function of river discharge and current velocity does not exist at present, and this information will be needed to inform HKD designs and establish deployment and operating procedures.

Sediment Transport and Dune Characteristics

Engineering design of HKD infrastructure, such as anchoring systems, bottom-founded support structures, abrasion of HKD blades, and bearings require knowledge of suspended and bed load sediment transport and bed form characteristics (e.g., dunes). Most large rivers in Alaska carry heavy sediment loads during their open-water period, and understanding how this sediment load affects HKD infrastructure directly or through changes in river morphology is important. At the TRTS, it was observed

that significant changes in sediment deposition and erosion occur as river discharge changes during the open-water season (A.C. Seitz, personal communication).

To better understand the nature of sediment transport and bed forms at the TRTS, measurements of both bed load and suspended sediment were made at different locations (Figure 13) during periods of different river discharge magnitudes during the 2009 and 2010 field seasons. Grain-size distributions of bed load sediment consist of three distinct types: (I) nearly uniform fine sand, (II) bimodal distributions containing sand and gravel, and (III) medium gravel. Sediment transport rating curves were developed from both suspended and bed load transport measurements. Measurements of dunes were made at different discharge magnitudes during the 2010 field season to determine dune geometry (Figure 30) and the steepness ratio of the dune height (Δ) to its wavelength (λ) as a function of discharge (Figure 31) (Toniolo 2013).

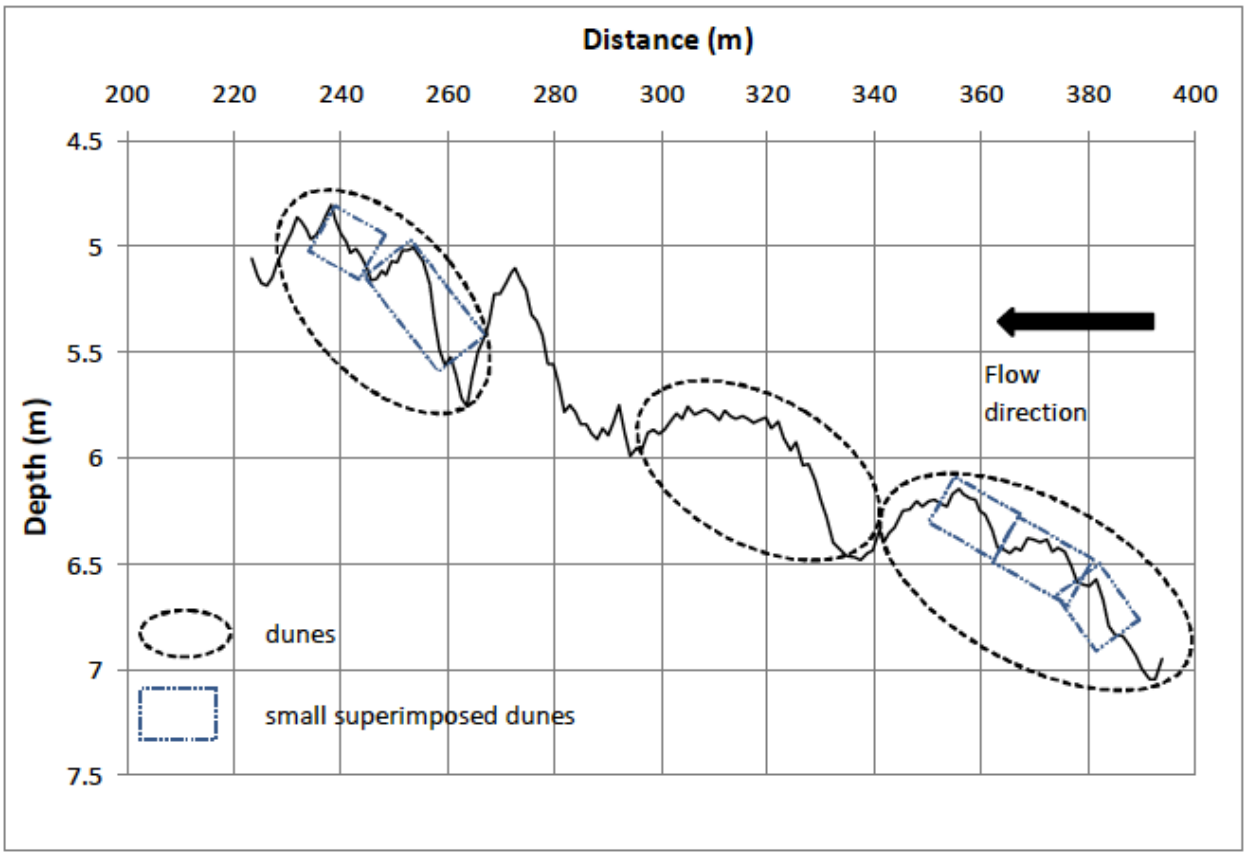

Figure 30. Riverbed forms as a function of depth and distance (Toniolo 2013; reprinted by permission of Journal of Natural Resources).

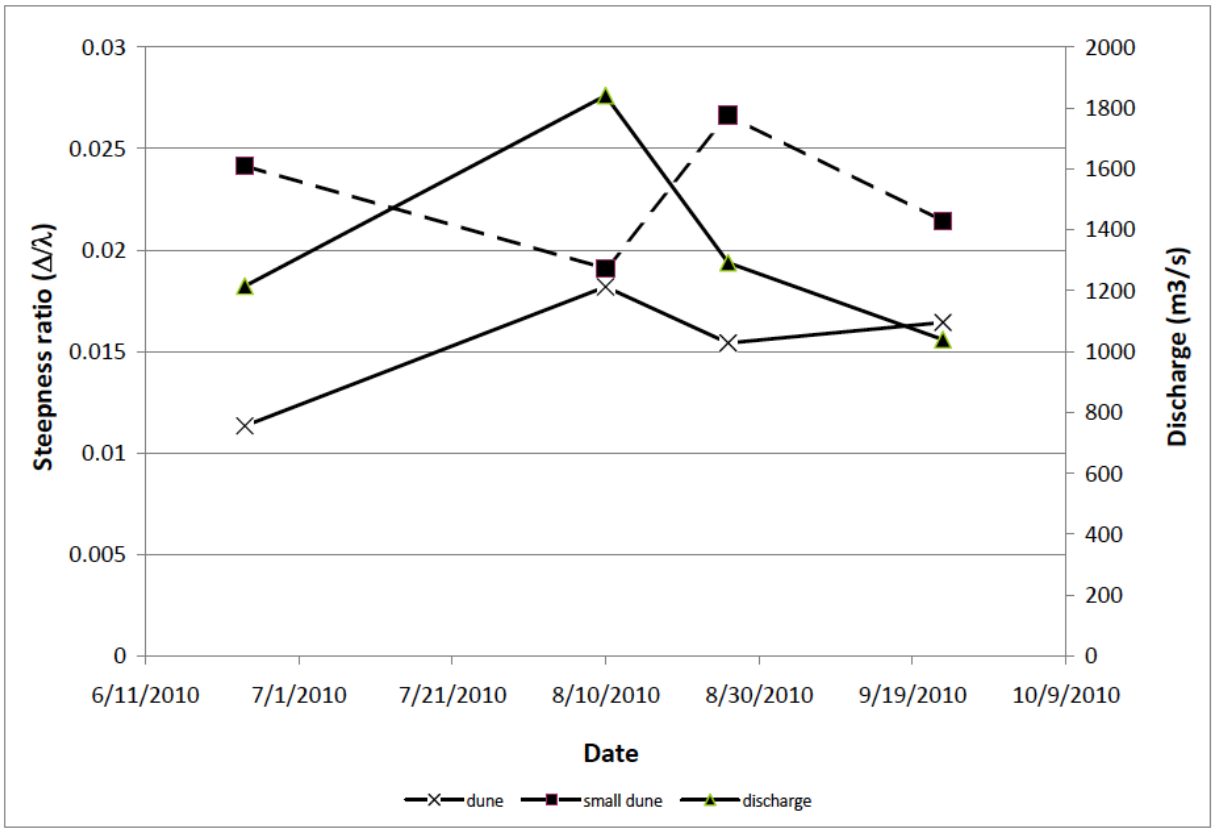

Figure 31. Dune steepness ratio related to river discharge, where Δ is the dune height and λ is the dune wavelength (Toniolo 2013; reprinted by permission of Journal of Natural Resources).

The sediment rating curves shown in Figure 32 indicate that both suspended and bed load sediment concentrations increase nonlinearly with increasing discharge. This result is not surprising, since the ability of a river to carry sediment is related to its shear stress, which increases with the force exerted by water on the bed. Sediment transport concentrations vary significantly with discharge, which means that as the discharge changes, the riverbed geometry will also change. In general, decreasing discharge results in a high rate of sediment deposition, while increasing discharge produces significant erosion resulting in large changes to riverbed geometry seasonally as discharge decreases drastically at the end of summer and then increases in the spring after ice-out. Large flood events will have significant impacts as well.

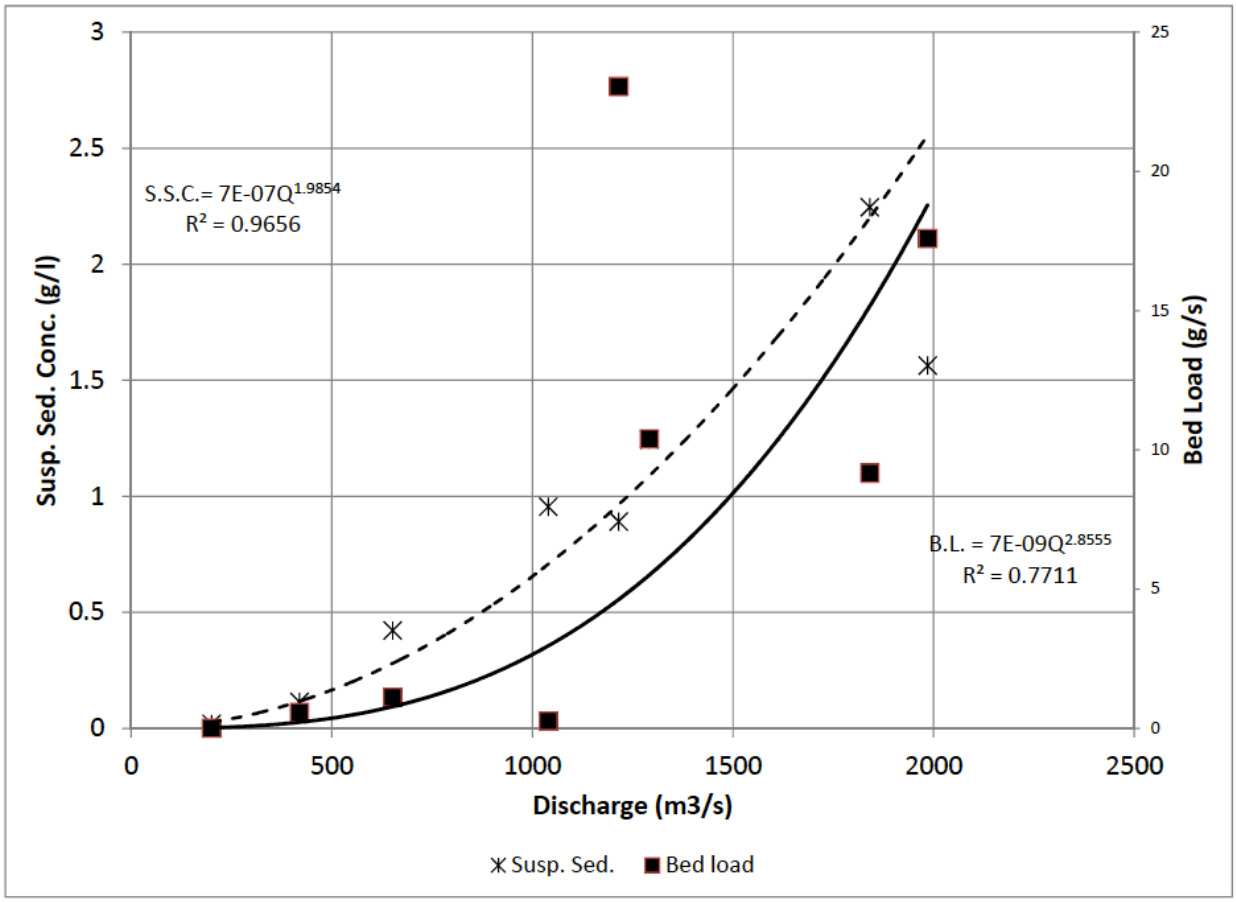

Figure 32. Sediment rating curves. Trend lines represent power curve fits to the data. Dashed and solid lines correspond to suspended-sediment concentration and bed load sediment concentration, respectively (Toniolo 2013; reprinted by permission of Journal of Natural Resources).

Toniolo (2013) found that riverbed sediment in the TRTS river reach consists of fine gravels and sands in a bimodal distribution. The mobility of this sediment along the riverbed produces dunes whose character depends to some degree on discharge. Wavelengths of the large dunes ranged from 41 to 67 m, while wavelengths for the smaller dunes superimposed on the large dunes had wavelengths of from 13 to 16 m (Figure 30). Results from Toniolo (2013) show that small superimposed dunes are always steeper than dunes, that dune wavelength predominantly increases with increasing discharge, and that steepness increases moderately with increasing discharge (Figure 31).

The influence of sediment transport on river hydrodynamics can be simulated using 2D hydrodynamic models, such as the CCHE2D model used in this work, to describe current velocities. To accurately include sediment transport in a model requires at least two separate measures of bathymetry in a given open-water season taken at different river discharges. The two bathymetries at different river discharges capture the riverbed geometry changes that occur as a result of sediment deposition or erosion. The changes in geometry and the discharge differences between the two measurements are used to calibrate and test the accuracy of the hydro-sedimentological model. The importance of sediment transport on a river's discharge-dependent morphology and the potential impact of sediment transport on HKD

infrastructure points to the need for developing accurate ways to simulate both the hydrodynamics and the sediment transport of river flow.

Wintertime Conditions

The three major considerations for using HKDs in Alaska are the effects of frazil ice during river freeze-up, the current velocity magnitudes during winter when the river is ice-covered, and the potential for ice to damage HKD infrastructure during spring breakup. Early assessments of river hydrokinetic energy indicated that the low-magnitude discharge of rivers in Alaska during winter nearly precludes producing power at economic levels during winter (Previsic and Bedard 2008). Our winter current velocity measurements at the TRTS support those early estimates of low hydrokinetic potential during winter (Figure 33). Maximum current velocity was measured at between 0.5 and 0.9 m/s, which is much too low to produce economic power from HKDs. The potential for HKD infrastructure being damaged by ice in spring is primarily a risk of ice jam formation, where ice pileups extend to the depth of HKD infrastructure. Ice jams generally form at the same locations due to constrictions or other features of a river, such that the risk of ice jam can be assessed from historical data and a survey of the river.

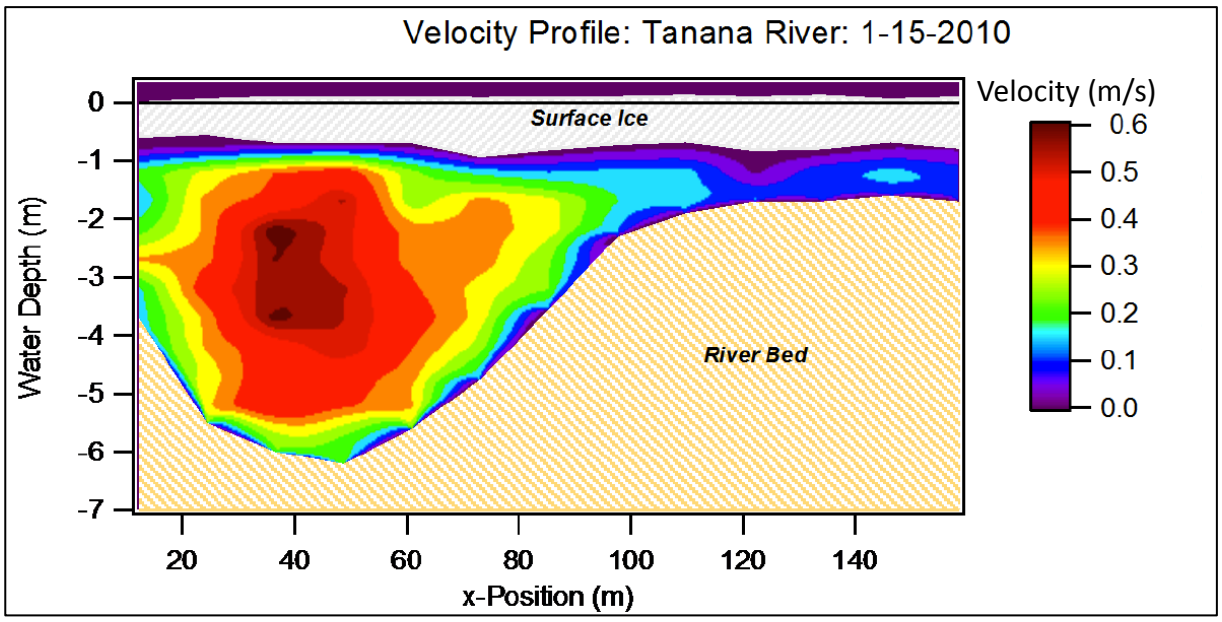

Figure 33. Current velocity across the Main transect (see Figure 11 for reference) for January 15, 2010.

The process of freeze-up in a river begins when water is supercooled due to cold air temperatures and turbulent mixing throughout the river water column. In these conditions, frazil ice begins to grow from nucleation particles (e.g., snow or frozen water droplets). Frazil ice can exist throughout the water column, growing as long as the water is supercooled (Hicks 2009; Osterkamp and Gosink 1983). During the growth phase, frazil ice particles are highly adhesive to any object that they contact (Figure 34). This results in frazil ice crystals coalescing into larger ice masses that eventually become sufficiently buoyant to overcome river turbulence and float to the surface of the river, forming slush that collects into ice pans (Figure 35). The concentration of ice pans eventually becomes sufficiently high, such that they interfere with each other at constrictions in the river channel, where they freeze in place creating an ice cover

(Hicks 2009) (Figure 36). At this point, the water temperature is no longer supercooled and active frazil growth ends.

Figure 34. Frazil ice adhesion on nylon line and steel framework after about 5 hours of submersion in the Tanana River at Nenana (Oct. 22, 2009, air temp. -5 to +4°C). Photo credit: J. Johnson.

Figure 35. Frazil slush ice pans on the Tanana River at Nenana (Oct. 23, 2009). Individual frazil pans ranged from about 0.5 to 1 m agglomerating into larger ice masses. Photo credit: J. Johnson.

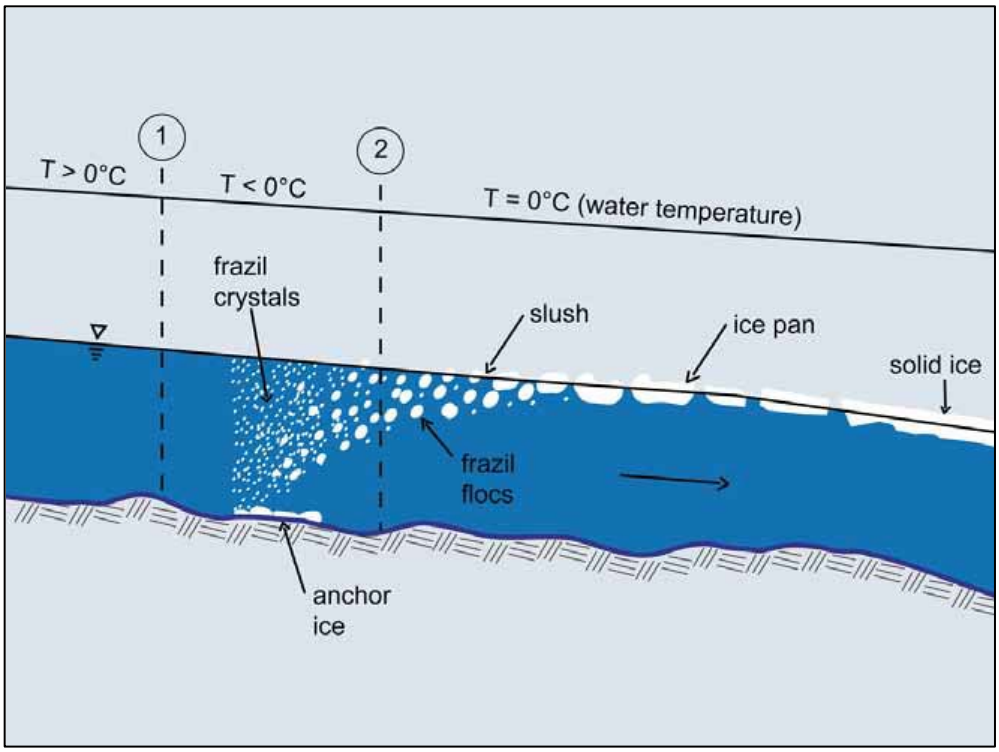

Figure 36. Evolution of frazil ice to a solid river ice sheet.

It is during the frazil ice growth phase that HKDs can be most affected by frazil as it adheres to a variety of surfaces (Figure 15), including rocks on the riverbed (anchor ice, Figure 36) (Schaefer 1950). Water intake grates can become completely covered with ice as frazil grows out from the grates or adheres to debris or twigs caught on a grate (Figure 34). The extent that frazil adhesion can grow perpendicular to a current is limited by shear forces acting on the ice as water flows past (Figure 15). As frazil grew perpendicular to the river current from one of the test rods, shear forces from the flow water produced stress on the frazil, causing it to erode into a hydrodynamically efficient shape where frazil extends upstream and downstream to a greater extent than perpendicular to the current (Figure 37 and Table 5).

Frazil ice accumulation on engineering structures is controlled primarily by either mechanical or thermal means (Daly 1991). Hydrophobic coatings can reduce the adhesion strength between frazil ice and an object's surface, making it easier to mechanically dislodge ice (e.g., by vibration or manual scraping or impact). Thermal methods are used to prevent frazil ice adhesion, melting ice once it has bonded on an object by using electrical heaters attached to the object to be protected or by flowing water that is slightly above the freezing temperature over the object. Efforts to control and manage frazil ice around water intakes has an extensive history of use, and much literature exists that can benefit developers and users that plan to overwinter HKDs (e.g., Daly 1991).

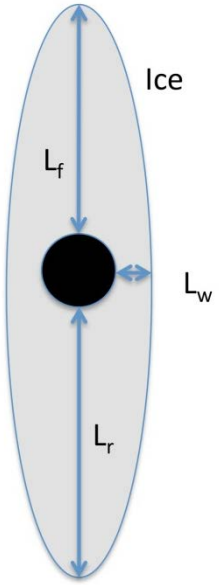

Figure 37. Schematic of frazil ice growth on cylinders of different materials. Refer to Figure 15 for experiment setup and Table 5 for frazil accumulation dimension with time.

Table 5. Frazil ice accumulation on cylinders of different materials

Top of sample (at junction of sample and ABS holder)	Growth time (hr:min)	Air temp (°C)	Teflon® Deposited frazil thickness (mm)			316 Stainless Steel Deposited frazil thickness (mm)			Mild Steel Deposited frazil thickness (mm)		
10/21/10 9:45 PM	start		L_f	L_r	L_w	L_f	L_r	L_w	L_f	L_r	L_w
10/22/10 3:00 AM	5:15	-11	none	none	none	n/d	n/d	n/d	35	20	25
10/22/10 10:25 AM	12:40		76	52	42	55	45	29	95	72	95
Middle of sample											
10/21/10 9:45 PM	start		L_f	L_r	L_w	L_f	L_r	L_w	L_f	L_r	L_w
10/22/10 3:00 AM	5:15	-11	none	none	none	none	none	none	none	none	none
10/22/10 10:25 AM	12:40		lost	lost	lost	66	46	35	66	53	25
Lower end of sample											
10/21/10 9:45 PM	start		L_f	L_r	L_w	L_f	L_r	L_w	L_f	L_r	L_w
10/22/10 3:00 AM	5:15	-11	none	none	none	35	n/d	25	35	20	25
10/22/10 10:25 AM	12:40		lost	lost	lost	90	47	43	150	150	150

Notes: Refer to Figure B-5 (Appendix B – Equipment and Operation Notes) for description of frazil collection material sample configuration
"none" means the sample was observed and no deposition was noted
"n/d" means no data; no observation was recorded
"lost" indicates that a large part of the frazil deposited on the Teflon® sample broke off and fell into the river before a measurement could be made

Discussion

Evaluating TRTS open-water hydrodynamic conditions that are important for HKD operations was done by first measuring current velocities at selected transects and bathymetry of the TRTS river reach. Current velocity transects were then used to calculate the river discharge, and the measured bathymetry was used to construct a numerical bathymetry grid for 2D hydrodynamic model simulations. The river discharge calculated for the same day as the bathymetry measurements was used to construct and initialize the 2D hydrodynamic model. Velocities from ADCP point measurements were compared to model velocities to determine the accuracy of model simulations.

Model simulations were used to determine river velocities and specific discharge throughout the computational domain, and the HYDROKAL tool was used to determine the instantaneous power density throughout the river reach. The 2D hydrodynamic model and the HYDROKAL tool, in conjunction with seasonal discharge from the USGS gauging station at Nenana, were used to produce a qualitative calculation of the seasonal variation of power density.

While critical for determining the viability of extracting energy from a river, specific power density is not the only factor that developers and users need to take into account when deciding where to place an HKD. It is important to select a site with relatively high specific hydrokinetic power density and relatively low turbulence. Thus, developing methods to assess where turbulence is most likely to occur and to determine the magnitude of the turbulence is an important part of the river's hydrokinetic assessment, as turbulence can affect hydrokinetic river power-conversion efficiency and produce off-axis stresses on an HKD.

Fall and wintertime current velocity measurements are important for determining the viability of operating an HKD during winter. Knowledge of frazil ice conditions is important for determining the effect of frazil ice accumulation on HKD infrastructure during winter deployments, whether or not the HKD operates during winter (e.g., it may be easier to leave an HKD in place during the winter to avoid problems of deployment and redeployment underwater).

Suspended sediment transport can affect HKD operations through abrasion of components (e.g., blades, bearings, foundation support struts) and by deposition or erosion around a deployed HKD due to changes in velocity or HKD wake turbulence. Bed load sediment transport will affect riverbed conditions related to scour and deposition and to abrasion of foundation or anchoring components.

The combined effects of current velocity (power density), turbulence, sediment, and ice need to be considered during HKD design, deployment, and operation to determine the potential amount of hydrokinetic energy that can be extracted from a river, the HKD design parameters, and an estimation of operation and maintenance costs. Ultimately, these factors will play a significant role in determining the economics of using HKDs in rivers. The data and simulations results presented in this report provide useful information that will aid HKD developers and users in making informed decisions about the development and use of hydrokinetic devices in rivers.

Summary and Conclusions

The hydro-sedimentological conditions of a reach of the Tanana River at Nenana was characterized to determine the important factors that may affect the deployment and operation of HKDs in river environments and to establish the TRTS. Measurements of current velocity, bed load and suspended

sediment transport, bathymetry and estimations of turbulence were made during the open-water season. A 2D hydrodynamic model of the reach was developed using bathymetry data from 2009 for the upper TRTS river reach and bathymetry from 2010 for both the upper and lower reaches of the TRTS. The model, which was validated using the 2009 current measurements and the 2010 water slope, was applied to determine instantaneous specific current velocity throughout the TRTS. A hydrokinetic calculator module (HYDROKAL) was developed to process output from the 2D river hydrodynamic simulations for estimating the instantaneous power density, the locations of maximum current velocity, and the specific discharge in each river cross section. The tool includes a user-defined HKD efficiency factor that accounts for turbine efficiency to allow HKD developers and users the ability to quickly estimate the amount of hydrokinetic energy that can be extracted at a given location in the river

Wintertime measurements of current velocity were made to determine the amount of power available to HKDs during winter months. Observations of frazil ice growth on metal frameworks and on cylinders of stainless steel, Teflon®, and mild steel were made during fall to determine what effect frazil ice might have on submerged HKD infrastructure.

The bathymetric surveys indicate a major riverbed depression located in the upstream end of the TRTS, just at the exit of the upstream river bend, and another riverbed depression located approximately in the 440 transect of the upper reach of the TRTS. Dunes, a type of riverbed form, were identified along the river bottom at the transition between the upper and lower reaches of the TRTS, as the river enters the lower bend just before the railroad bridge. A well-defined thalweg, located on the left side of the channel, is present in most of the upstream reach. Near the end of this area, the thalweg moves to the right side of the channel as the current flow enters the lower river bend. The thalweg maintains its right-side location along the downstream (lower) reach.

Average dune wavelengths ranged from 41 to 67 m, and average dune heights ranged from 0.6 to 1.2 m. Small and superimposed dunes with characteristic dimensions close to 15 m (wavelength) and 0.3 m (height) were also found along the riverbed. Grain-size distributions of sediment moving close to the riverbed consist of three distinctive types: (I) nearly uniform fine sand, (II) bimodal distributions containing sand and gravel, and (III) medium gravel. Additionally, preliminary sediment rating curves developed for the reach indicate that both suspended and bed load sediment concentration are nonlinear functions of discharge. Suspended sediment concentrations ranged from around 0.2 g/l at 500 m^3/s discharge to 2.3 g/l at 1800 m^3/s discharge. Bed load sediment concentrations ranged from around 1 g/l at 500 m^3/s discharge to 16 g/l at 2000 m^3/s discharge.

Non-dimensional profiles of velocity measurements on maximum flow path locations were nearly similar, which indirectly shows a condition of hydrodynamic equilibrium along current velocity measurement transects. However, hydrodynamic similarity was not observed in profiles representing the velocity measurements done on thalweg locations. Thus, changes in thalweg position, especially downstream of the 800 transect can be expected. Maximum transect-measured velocities near the water surface along the thalweg reached around 1.9 m/s.

Turbulence analysis indicates that the highest turbulence magnitudes are associated with the river bends (both the upper and lower river bends), a channel constriction, and bathymetric depressions near the upper bend at transect 000. The turbulent kinetic energy at transect 000 was about 9% of the total kinetic energy. A bathymetric depression at transect 440 in the upper reach is also highly turbulent with turbulent

kinetic energy constituting about 20% of the total energy. These results indicate that the best possible sub-reach to harvest energy from the river is the area between the 440 and 800 transects, in the upper reach, where the turbulent energy is only about 4% of the total kinetic energy, and around the transect located most downstream in the lower reach (Figure 12). The reaches of river with relatively low turbulent kinetic energy are characterized by being relatively straight and having a relatively constant cross section, which allow turbulent magnitudes to decrease and more of the river's kinetic energy to align with the main current flow direction.

Results from CCHE2D, a 2D hydrodynamic model, provide a complete and continuous description of the velocity field along the computational domain. CCHE2D was successfully validated using discrete velocity measurements and measured water slope. Due to high sediment transport conditions, the hydro-sedimentological model was not implemented.

Instantaneous power density was calculated using the HYDROKAL software, which was fully developed by the UAF team. Power density values were around 6500 W/m^2 for the 2009 simulation (average discharge condition) and 13,500 W/m^2 for the 2010 simulation (high-discharge condition). In addition, HYDROKAL identified the locations of maximum velocity and specific discharge in each river cross section defined in the numerical domain. A plot of these maximum values indicates a stable thalweg from the upstream river bend to the 800 transect.

A rough and qualitative assessment of seasonal power variation was made using existing historical data collected in the area by the USGS. Three river conditions were used in the calculations: (a) high discharge (corresponding to 1967), (b) average discharge, and (c) low discharge (corresponding to 1996). Instantaneous power density values were approximately 27,800 W/m^2, 12,800 W/m^2, and 6,800 W/m^2 for high, average, and low conditions, respectively.

Current flows in wintertime are substantially lower than during the open-water season due to the lack of available liquid water and the overlying ice cover. Under-ice maximum velocities measured during the winter of 2009 and 2010 were in the range of 0.5 to 0.8 m/s, which corresponds to a maximum obtainable power density of 256 W/m^2. This measurement clearly illustrates the broad range of seasonal variation that impacts the obtainable hydrokinetic power at this reach of the Tanana River.

Frazil ice forms in open-water rivers during periods of cold that supercool the water, and exists throughout the water column, actively adhering to objects submerged in a river. Frazil ice can block water intakes, but reaches a steady-state profile on isolated cylinders, because the shear from water flow limits the thickness of frazil that can adhere to a cylindrical object. Frazil ice stops its growth and is no longer adhesive once the river becomes ice covered and the river water reaches freezing temperature.

Exportable/Extractable Conclusions and Recommendations for Hydrodynamic Studies at Other Sites

The following list contains key findings related to resource assessment and hydrokinetic siting that may be applicable to other study sites:

- Related to resource assessment:

- ✓ Perform at least 2D hydrodynamic numerical simulations using high-resolution bathymetric surveys. It was recently reported (Toniolo 2012) that 1D resource assessment could significantly underestimate the available resource.
- ✓ In environments with high sediment loads, complete at least two consecutive bathymetric surveys during the same open-water season to calibrate a hydro-sedimentological model.

- Related to hydrokinetic siting:
  - ✓ Locate turbines in areas where the channel is relatively straight.
  - ✓ Avoid the presence of bed depressions or constriction immediately upstream of the deployment site. A sufficient separation distance is needed to allow turbulence to dissipate.
  - ✓ Try to deploy the device in areas where the total cross-sectional area is comparatively small (relatively high velocity value).
  - ✓ Do not locate the deployment site downstream of secondary channels (Toniolo 2012) or immediately downstream of river bends.

Characterizing the Fish Community in the Tanana River to Assess Potential Interactions with Hydrokinetic Devices

Introduction

Fishes play an important role in Alaska's commerce, food supply, recreation, and culture. Because of the importance of fishes in Alaska, a crucial aspect of the development of hydrokinetic devices in the Tanana River near Nenana is understanding the river's fishery resources in this location and how hydrokinetic devices may impact them. For any effects to occur, there must be an interaction between the hydrokinetic device and fish, such as when the turbine and fish use the same part of the river at the same time (Cada et al. 2007). To assess the potential of this interaction in the Tanana River at Nenana, it is necessary to know the species composition and the relative abundance of the fish community as well as the spatial and temporal patterns of distribution of fishes in the river channel.

Fisheries scientists have an incomplete understanding of fish communities in Alaska, specifically how fishes use river channels in large, glacially influenced systems such as the Tanana River. Therefore, two research goals—a literature review and a baseline field study—were identified and accomplished to improve available information:

- A comprehensive literature review was conducted and published to detail existing information and knowledge gaps about the fish community in the Tanana River basin and potential interactions of fishes with hydrokinetic devices (Seitz et al. 2011).
- A baseline field study was conducted to characterize the juvenile fish community and its habitat use in the Tanana River near Nenana (Bradley 2012).

Literature Review

During autumn 2010, a comprehensive literature review was conducted to detail existing information about the fish community in the Tanana River basin and to identify knowledge gaps that could be used to inform the design of field studies in 2011. This review was conducted on a variety of literature sources including peer-reviewed journal articles, student theses, and agency reports. A summary of the literature review is provided here. Full details are available in a peer-reviewed manuscript published in an international fisheries journal (Seitz et al. 2011).

Existing Information about Tanana River Fishes

Seventeen known fish species, both anadromous and resident, use the Tanana River drainage (Table 6). Of all the fish species that inhabit the Tanana River, the most important species to local fisheries are anadromous populations of Chinook *(Oncorhynchus tshawytscha),* chum *(O. keta),* and coho *(O. kisutch)* salmon (Seitz et al. 2011). Adult salmon use the main channel of the river as a migratory corridor when traveling to upstream spawning grounds during two periods. The summer season (July to mid-August) is dominated by runs of Chinook and summer chum salmon that spawn in runoff tributaries. The fall season (mid-August to October) includes runs of genetically distinct fall chum and coho salmon (Borba 2007; Cappiello and Bromaghin 1997). Fall chum salmon spawn from mid-October through November in several upper main stem and tributary areas; the coho salmon spawning distribution is limited to only clearwater tributaries (Ott et al. 1998). The peak of the coho salmon run occurs in Nenana in mid-

September (Borba 2007). Main stem chum salmon spawning sites are located in deeper portions of the channel, where groundwater upwelling through the gravel substrate helps to stabilize incubation temperatures and maintain levels of dissolved oxygen during the frigid winter (Cappiello and Bromaghin 1997). In large, swift rivers, up-migrating chum and coho salmon conserve energy by swimming close to shore and low in the water column where water velocities are slowest (Ransom et al. 1998; Daum and Osborne 1998). Chinooks, being generally larger and stronger fish, follow the same migration routes, but farther from shore in faster currents (D. Helmer, personal communication, 2010).

Table 6. Approximate timing of movement of selected fishes in the Tanana River (from Seitz et al. 2011).

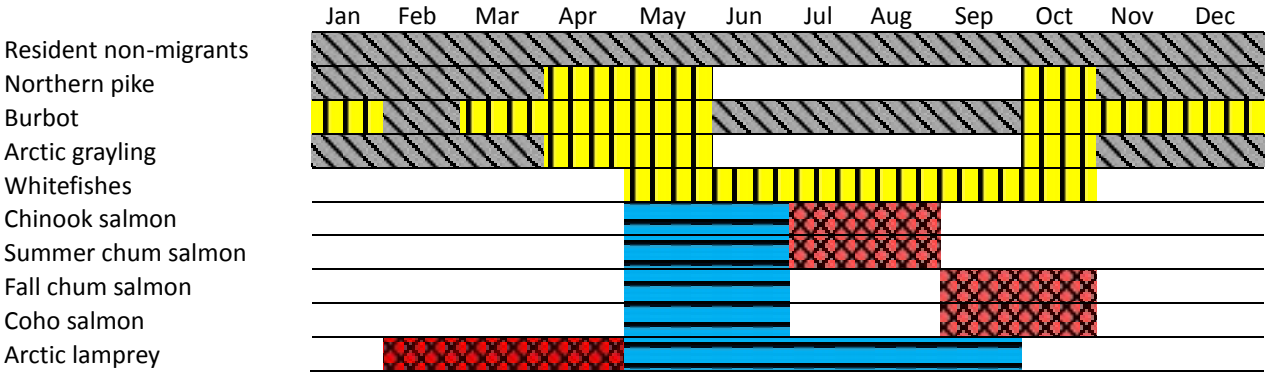

Note: Gray represents residency with limited movement; yellow represents movement of resident fishes; red indicates upstream movement of anadromous adults to spawning areas; blue represents downstream movement of anadromous juveniles to rearing areas. Resident non-migrant species include lake chub, longnose sucker, and slimy sculpin. Whitefishes include humpback whitefish, round whitefish, least cisco, broad whitefish and inconnu.

Age zero chum salmon smolts (juvenile salmon migrating to the ocean) begin their downriver migration soon after emergence from the riverbed during breakup, and their density in the mainstem of the Tanana River is greatest during the months of May and June (Hemming and Morris 1999; Durst 2001). In clearwater rivers, chum salmon smolts travel at night and in large schools to avoid predation (Koenig 2002), but the long migrations of Tanana River chum salmon may require daytime travel as well. There is evidence that smolt predation is reduced by the turbidity of glacial waters (Gregory and Levings 1998), and this may provide enough protection from visual predators to allow the smolts to travel during daylight hours (Koenig 2002; Gregory and Levings 1998). Migrating chum salmon smolts must feed during their long migration (Durst 2001), but as small young-of-the-year fish, their ability to maneuver in the fast currents of the river mainstem is not well understood. Chum salmon smolts are abundant in the river margins during their migration (Ott et al. 1998), but it is not known if they use this portion of the river channel exclusively for feeding, or traveling as well, nor is it known whether they use the middle of the river channel for migration.

Both Chinook and coho salmon rear in freshwater, where they feed and grow for one to several years before migrating to the ocean. Therefore, as larger fish, their ability to maneuver laterally and vertically throughout the mainstem river channel is probably better than the maneuverability of chum salmon smolts. Juvenile coho salmon are found in the river margins in significant numbers during their out-migration (Ott et al. 1998), with peak abundance occurring in mid-May (Hemming and Morris 1999). In contrast, sampling with minnow traps and shallow-water seines has been unsuccessful at capturing juvenile Chinook salmon in the margins of the Tanana River (Mecum 1984; Ott et al. 1998). It has been

speculated that this method is a sampling artifact resulting from the possibility that out-migrating Chinook salmon use higher velocity and deeper water in the center part of the channel, which is difficult to sample with traditional methods (Ott et al. 1998).

Five coregonine species have been documented in the Tanana River including inconnu *(Stenodus leucichthys)*, round whitefish *(Prosopium cylindraceum)*, humpback whitefish *(Coregonus pidschian)*, least cisco *(C. sardinella)*, and broad whitefish *(C. nasus)* (Brown et al. 2007; Seitz et al. 2011). All are locally important to subsistence users for human and canine consumption, and the largest, inconnu (sheefish), supports a local sport fishery as well. Coregonine fishes can exhibit a wide variety of life-history traits including both freshwater resident and anadromous behavior (Brown et al. 2007). It is thought that adult coregonines typically make upriver migrations in the summer and early fall to deposit eggs in the gravel bottoms of lakes and clear streams in late fall (Alt 1987). In the Tanana River, whitefishes concentrate in the mainstem and lakes in the fall, both of which are thought to be spawning areas (Seitz et al. 2011). After incubating until spring, the eggs hatch and the fry emerge from the gravel. Age-0 coregonines then migrate to downriver feeding and rearing locations, where they remain until reaching sexual maturity (Seitz et al. 2011), but timing of this down-migration has not been documented in the Tanana River, nor has lateral and vertical distribution within the river channel.

Arctic grayling occur throughout the tributaries of the Tanana River and are popular sport fish. This species often displays extensive migrations between spawning, overwintering, and feeding areas, depending on age and time of year (West et al. 1992; Seitz et al. 2011). In the Yukon River basin, including the Tanana River, Arctic grayling spawn in tributaries in the spring soon after ice-out and then migrate to summer feeding areas, which may involve down-migration of adults in the mainstem of the Tanana River (Seitz et al. 2011). Juvenile Arctic grayling are known to follow the adults during their migration to and from spawning locations, which probably serves as a mechanism for imprinting on migration routes (Seitz et al. 2011). During the summer months, juveniles tend to inhabit lower ends of clearwater tributaries, while larger adults inhabit the headwaters (Seitz et al. 2011). Migration timing and habitat utilization of the Tanana River mainstem by juvenile Arctic grayling have not been documented.

In addition to salmonids, a variety of freshwater resident species occur in the Tanana River. Lake chub (*Cousius plumbeus)*, longnose sucker (*Catostomus catostomus)*, and slimy sculpin (*Cottus cognatus)* are widely abundant resident species in the Tanana River. They are of no commercial, sport, or subsistence value, but represent important forage species for other fishes, as well as birds and mammals (Seitz et al. 2011). River margin sampling studies using minnow traps, seines, and electroshocking in the Tanana River have consistently found these three species to be the most common fishes (Mecum 1984; Ott et al. 1998). Both lake chubs and longnose suckers make migrations up small streams to spawn in the spring (Scott and Crossman 1973). In contrast to lake chubs and longnose suckers, slimy sculpins do not undertake migrations because they are relatively poor swimmers. It is not known whether lake chub, longnose suckers, or slimy sculpin use the swifter center portions of the Tanana River during any stage of their life history.

Burbot (*Lota lota*) are a benthic, piscivorous fish whose distribution ranges widely across Alaska, where they occur in a variety of lakes and rivers in the Tanana River drainage (McPhail and Paragamian 2000). They are popular as sport fish and important to subsistence users. It is thought that in large, glacial rivers,

burbot migrate and spawn in the main river channel during winter and are mainly sedentary during the remainder of the year (Breeser et al. 1988).

Northern pike (*Esox lucius*) are a top level predator and are typically found in slow moving water with aquatic vegetation (Muhlfeld et al. 2008), as found in Minto Flats in the Tanana River drainage. This species is one of the most esteemed indigenous sport fish species in Interior Alaska, from where up to 90% of the state's annual northern pike harvest comes (Burkholder and Bernard 1994). Radio-tagged northern pike in Minto Flats show extensive seasonal movements; some overwinter in the Tanana River mainstem (Burkholder and Bernard 1994). Migration timing and habitat utilization of the Tanana River mainstem by juvenile burbot and northern pike have not been documented.

Two species of lampreys are relatively common throughout the Tanana River drainage, but their ecology is poorly understood. Lampreys are benthic inhabitants when in freshwater and have only been captured close to the bottom in the margins of the river mainstem (Mecum 1984). The two species exhibit distinct life-history strategies. The Arctic lamprey (*Lethenteron camtschaticum*) is an anadromous parasitic lamprey found throughout the Tanana River (Mecklenberg et al. 2002). The Alaskan brook lamprey (*Lethenteron alaskense*) is strictly a freshwater, non-parasitic fish, and has been documented in a few tributaries of the Tanana River (Vladykov and Kott 1978; Mecklenberg et al. 2002). Both forms spawn in the mainstem of the Tanana River in medium water velocities over gravel substrate between late May and early July (Roberge et al. 2002). Lamprey eggs hatch in a few weeks and larva of both species, called ammocoetes, move immediately to river margins, where they burrow in soft substrates and filter feed on organic detritus for a few years (Sutton and Bowen 1994). After the ammocoete stage, Arctic lampreys migrate to the ocean and metamorphose into juveniles where they become parasitic, while Alaskan brook lampreys metamorphose into adults and remain in freshwater. The downstream migration of Arctic lamprey ammocoetes, which has been documented in the Russian Far East as occurring in July and August, is mainly nocturnal and strongly correlated with high discharge events (Kirillova et al. 2011).

Knowledge Gaps

Although a few studies have described the juvenile and larval fish community in the river margins of a few locations in the Tanana River (Mecum 1984; Ott et al. 1998; Hemming and Morris 1999; Durst 2001), the life-history patterns and habitat selection of fishes in this river are not fully understood, particularly for sub-adult fishes. This is partly because no studies conducted have sampled juvenile fishes in the middle of the river channel due to the system's size, complexity, high turbidity, and large woody debris during most of the ice-free season, which limits research and observation. Additionally, there has not been a comprehensive study conducted in the Tanana River at Nenana describing the temporal and spatial patterns in down-migration of juvenile fishes. Findings from previous research on the same fish species in small clearwater river systems are likely not transferable to Tanana River fishes because of the river's turbid characteristics. Complicating matters further, knowledge of fish distribution in large turbid rivers is sparse, as very few studies have attempted sampling of the mid-channel in large U.S. rivers (Mains and Smith 1964; Todd 1966; Tyler 1979; Dauble et al. 1989), let alone in a turbid glacial river in Alaska (Gissberg and Benning 1965). As a result, fisheries scientists have a poor understanding of how fish, particularly juveniles, distribute themselves in large glacial river channels such as the Tanana River. This scarcity of information makes it difficult to predict the potential impacts of a hydrokinetic device placed in a particular part of a river channel.

At the onset of this project, we hypothesized that adult fish in the Tanana River will have minimal interaction with a turbine because they are relatively large and competent swimmers with well-developed sensory systems that likely will sense a spinning device. In contrast, down-migrating juvenile fishes are small and relatively weak swimmers with less-developed sensory systems, and they may use the highest velocity area of the river channel to conserve energy during downstream migration. This location is exactly where hydrokinetic devices are typically deployed; therefore, it is imperative that river channel and habitat use by these juvenile fishes is studied. The potential impacts of a hydrokinetic device will probably be relatively small if down-migrating juvenile fishes mostly use river margins rather than the middle of the channel. Conversely, potential impacts may be more substantial if juvenile fishes use the middle of the river as a down-migration corridor, as they may pass through the turbine. Thus, we designed and conducted a field study in 2011 to rectify some of these gaps in knowledge of juvenile fishes in the Tanana River.

Field Study in 2011 Near Nenana, Alaska

Introduction

The goal of the field study was to provide baseline information about the downstream migration of juvenile and larval fishes in the mainstem of the Tanana River near Nenana, Alaska, to understand spatial and temporal patterns so that times of potential interactions between juvenile and larval fishes and a hydrokinetic turbine could be determined. To achieve this goal, the study objectives were as follows:

1. To characterize the juvenile and larval fishes communities in the mainstem of the Yukon and Tanana Rivers, including species composition and relative abundance.
2. To characterize the spatial and temporal patterns of the downstream juvenile and larval fishes migration and determine environmental associations with migration .

To accomplish these objectives, downstream migrating juvenile and larval fishes were sampled in the river margins and mid-channel of the Tanana River near Nenana. In addition to fish sampling, a suite of environmental variables was collected throughout the sampling season to explore possible associations of these environmental variables with temporal patterns of the downstream migrating juvenile and larval fishes. A summary of the field study is provided here; full details can be found in a recently published master of science thesis (Bradley 2012) and in an Alaska Department of Fish and Game Fisheries Resource Permit Completion Report (Bradley and Seitz 2011).

Methods

Fish sampling

Fish sampling was conducted in two distinct river habitats: the river margins and the river mid-channel (Figure 38). River margin habitats were characterized by water velocity less than 0.75 $m \cdot s^{-1}$, water depth less than 1.3 m, and within 30 m of the shoreline. Mid-channel habitats were characterized by water velocity greater than 1.2 $m \cdot s^{-1}$, water depth greater than 6 m, and not within 30 m of the shoreline. Sampling of the river margins was accomplished using fyke nets (Figure 39) with 1.2 m by 1.2 m frames, dual 9.1 m wings, and 1.27 cm mesh at locations on each riverbank in the Tanana River.

Sampling of the mid-channel in the Tanana River was accomplished using an inclined-plane trap (Figure 40) attached to a mooring buoy, near the deepest, fastest portion of the river. The inclined-plane trap

consisted of two major sections: the trap and the live-box (Todd 1994). The trap, composed of an inclined plane supported by a frame, had a front opening 1.1 m deep by 1.5 m wide, with an overall length of 2.4 m. The inclined plane was composed of v-shaped corrugated aluminum, perforated with 8 mm diameter holes (Todd 1994). When the inclined-plane trap was lowered into the current, the top 1.1 m of the water column was strained through it. Downstream migrant fishes were swept up the inclined plane and deposited into a protected solid-sided and floored live-box 1.2 m long, 0.9 m wide, and 0.6 m deep (Todd 1994).

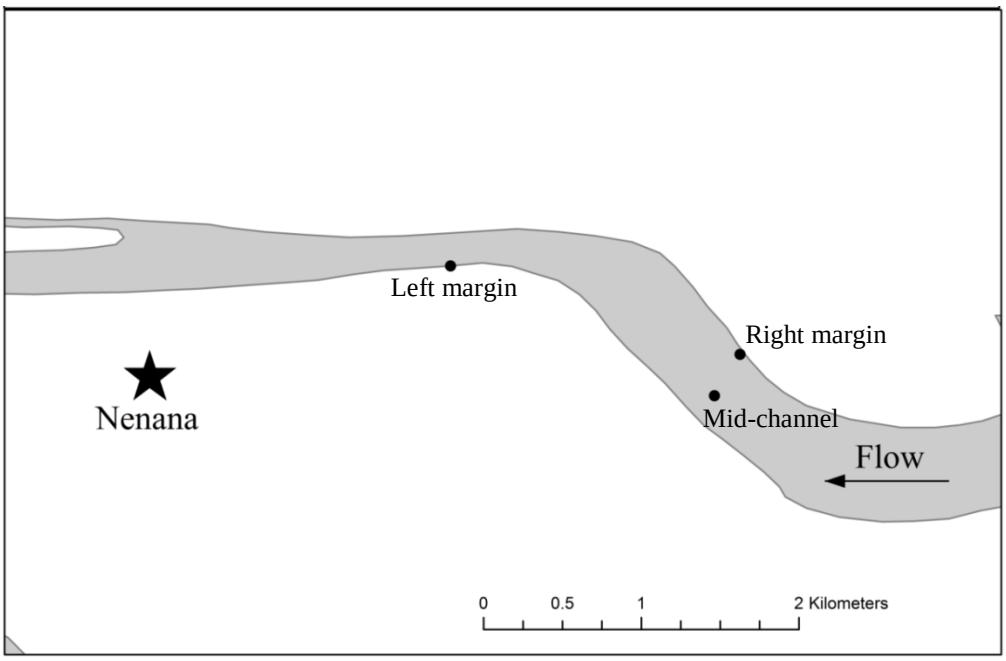

Figure 38. Sampling sites in the Tanana River near Nenana, Alaska.

Figure 39. Fyke net set on river margin of the Tanana River at Nenana, Alaska.

Figure 40. Inclined-plane trap used for sampling the top 1.1 m of the mid-channel of the Tanana River at Nenana, Alaska.

Sampling of river margins in the Tanana River began on 12 May 2011 and continued through 28 August 2011, and was conducted by concurrently deploying fyke nets at both river margin locations. Sampling times were evenly stratified over a 24-hour period. The target duration for fyke net sets was 30 minutes, and the sampling frequency goal was six fyke net sets per day. Sampling of the mid-channel with the inclined-plane trap in the Tanana River began 20 May 2011 and continued through 18 August 2011, and was conducted in conjunction with both set fyke nets. River debris collected in the inclined-plane trap reduces efficiency and increases fish mortality. As a result, the target sampling duration was limited to one hour per set, and the target number of sets per day was three.

All captured fish were visually identified to the lowest taxonomic level possible, measured to the nearest millimeter of fork length or total length (burbot, Arctic lamprey, Alaskan brook lamprey, and slimy sculpin), and released alive. Because of difficulty in identifying different species in the genera *Coregonus* and *Prosopium*, all were grouped into a general whitefishes category. Additionally, larval Arctic lamprey and Alaskan brook lamprey are morphologically and genetically indistinguishable, so all larval lampreys were grouped into a *Lethenteron* spp. category, while adult lampreys were identified to species. In the Tanana River, because of conflicting literature describing external features for distinguishing Chinook salmon and coho salmon, both species were grouped into a Chinook/coho salmon category (Dahlberg and Phinney 1967).

Environmental variables

The water temperature (°C) was measured with a YSI 85. A Debris Index (DI) was determined by visualizing a transect across the river, and counting the number of individual pieces of woody debris crossing that transect in a five-minute period. Additionally, water depth (m) at the frame, distance (m) between the two wings, and water velocity ($m \cdot s^{-1}$) at the frame was measured at 60% of depth from bottom with a Marsh McBirney Model 2000 Flo-Mate during each fyke net set. Water velocity ($m \cdot s^{-1}$) was measured with a Marsh McBirney Model 2000 Flo-Mate in front of the inclined-plane trap 0.64 m beneath the water surface for each set. Turbidity (cm) was measured daily in the middle of the river channel using a Secchi disk and river discharge ($m^3 \cdot s^{-1}$) data were obtained from the U.S. Geological Survey gauging station in Nenana (http://waterdata.usgs.gov/ak/nwis/uv?site_no=15515500). An attempt was made to measure each environmental variable for the duration of the study, but equipment availability prevented measurement during some periods.

Data analysis

Catch per unit effort (CPUE) of each fish species/taxa was calculated by dividing catch in each set by the volume of water sampled (water depth (m) × width of net (m) × water velocity ($m \cdot s^{-1}$) × 1,000). These CPUE (#fish·1,000 m^{-3}) values were used to compare relative abundances among species/taxa.

Generalized additive models (GAMs) were used to describe temporal patterns in catches and to determine associations of catches with environmental variables. Generalized additive models are non-parametric generalizations of generalized linear models and use additive instead of linear predictors (Hastie and Tibshirani 1990; Venables and Dichmont 2004). Two variations of GAMs were used to describe temporal patterns in catches on a seasonal scale and to determine associations of catches with environmental variables. All of the GAMs were only applied to species/taxa where sample size was > 150 fish, because catch data for species/taxa with a sample size < 150 fish contained too many zeros to elucidate any patterns.

Results from the GAMs were used to produce nonlinear smoothed trend lines ± 95% confidence intervals (CIs) of predicted number of fish per set, given the mean volume of water sampled, of each species/taxa over the sampling season. Species/taxa were determined to exhibit seasonal temporal patterns if the slope of the catch trend line was significantly different from zero ($\alpha = 0.05$ level). These temporal patterns in catches were either described as having peaks or increasing/decreasing trends, which was determined by examining the smoother trend line ± 95% CI. Peaks were qualitatively defined as a period of increasing catches, immediately followed by decreased catches. Increasing and decreasing trends occurred when the slope of the smoother trend line was either positive or negative.

To explore associations of catches with three environmental variables (water temperature, the Debris Index, and turbidity), an all subsets regression approach was used in the GAMs, and the most parsimonious nested model was chosen based on lowest Akaike Information Criterion (Akaike 1973). Once the best model was selected, a smoother trend line ± 95% CI was plotted to visually describe the effects of each environmental variable on catches.

To examine possible associations between catches and river discharge, a smoothed trend line ± 95% CI for each species/taxa from each location was overlaid on a plot of mean daily river discharge and visually assessed for co-occurrence of peaks/trends in catches and discharge. This approach was used based on the *a priori* assumption that increasing or decreasing trends in discharge, not the absolute value of discharge, would have the strongest association with catches.

Results

Catch composition

Three hundred eighty-four fyke net sets were made on the river margins from 12 May 2011 to 28 August 2011 ($4.2 \cdot day^{-1}$ ± 1.7, range 1–7) (Figure 41). The duration of each fyke net set (30 ± 3 minutes, range 24–60 minutes) was relatively consistent among sets. In the river margins, at least 11 species were captured, with whitefishes having the largest CPUE followed by longnose suckers, chum salmon, lake chub, *Lethenteron* spp., burbot, Arctic grayling, Chinook/coho salmon, slimy sculpin, Arctic lamprey, Alaskan brook lamprey, and northern pike (Table 7).

Seventy-three inclined-plane trap sets were made in the mid-channel of the Tanana River from 20 May 2011 to 18 August 2011 ($2 \cdot day^{-1}$ ± 0.7, range 1–3) (Figure 41). The duration of each inclined-plane trap set (63 ± 23 minutes, range 20–160 minutes) varied depending on the duration of concurrently set fyke nets. In late June, the inclined-plane trap required significant modification and repair and, as a result, was not operational again until late July. In the surface waters of the mid-channel, at least six species were captured, with Chinook/coho salmon and chum salmon having the largest CPUE, followed by whitefishes, Arctic lamprey, *Lethenteron* spp., and burbot (Table 7).

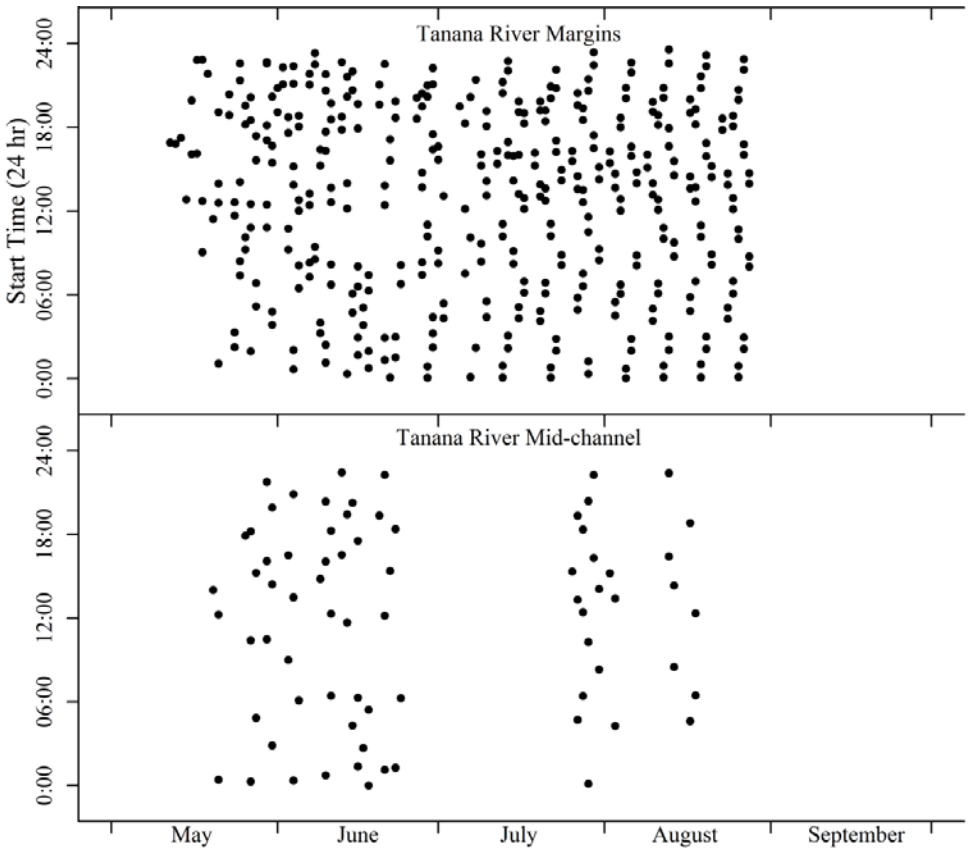

Figure 41. Start time for each fyke net set (top) and inclined-plane trap set in the Tanana River (bottom).

Table 7. CPUE (# fish•1,000 m-3) and mean fork/total length (mm) for each species/taxa captured in the Tanana River margins and mid-channel at Nenana, Alaska.

	Tanana River Margins		Tanana River Mid-channel	
Species	CPUE ± 1 SE	Mean length (mm) ± 1 SE (range)	CPUE ± 1 SE	Mean length (mm) ± 1 SE (range)
Chinook/coho salmon	0.032 ± 0.010	68.3 ± 2.5 (35–81)	0.533 ± 0.092	80.8 ± 0.5 (61–114)
Chum salmon	1.065 ± 0.154	36.3 ± 0.1 (27–48)	0.405 ± 0.073	41.8 ± 0.3 (32–54)
Whitefishes	3.682 ± 0.549	40.6 ± 0.7 (21–510)	0.017 ± 0.009	29.7 ± 1.6 (23–35)
Arctic grayling	0.056 ± 0.012	70.8 ± 6.9 (37–201)	0	0
Longnose suckers	1.485 ± 0.197	65.6 ± 1.6 (22–460)	0	0
Slimy sculpin	0.006 ± 0.003	55.5 ± 9.0 (40–81)	0	0
Lethenteron spp.	0.176 ± 0.028	114.4 ± 1.8 (42–170)	0.001 ± 0.001	162
Arctic lamprey	0.003 ± 0.002	327.5 ± 15.9 (305–350)	0.002 ± 0.002	365.0 ± 10.6 (350–380)
Alaskan brook lamprey	0.003 ± 0.002	132.5 ± 5.3 (125–140)	0	0
Lake chub	1.042 ± 0.120	53.0 ± 0.7 (24–152)	0	0
Burbot	0.070 ± 0.021	301.9 ± 21.8 (60–450)	0.001 ± 0.001	155
Northern pike	0.001 ± 0.001	600	0	0

Temporal patterns

Several species/taxa of fishes displayed a significant seasonal peak in catches in the Tanana River (Figure 42) including longnose suckers, which had a small peak in catches in the right margin in late May ($P < 0.0001$), and whitefishes, which peaked in both the right and left margins in late June ($P < 0.0001$). Several species of fish also displayed increasing or decreasing trends in catches, such as chum salmon in the left margin ($P < 0.0001$), Chinook/coho salmon in the mid-channel ($P < 0.0001$), longnose suckers in the left margin ($P = 0.0001$), and lake chub in the right margin ($P = 0.0002$).

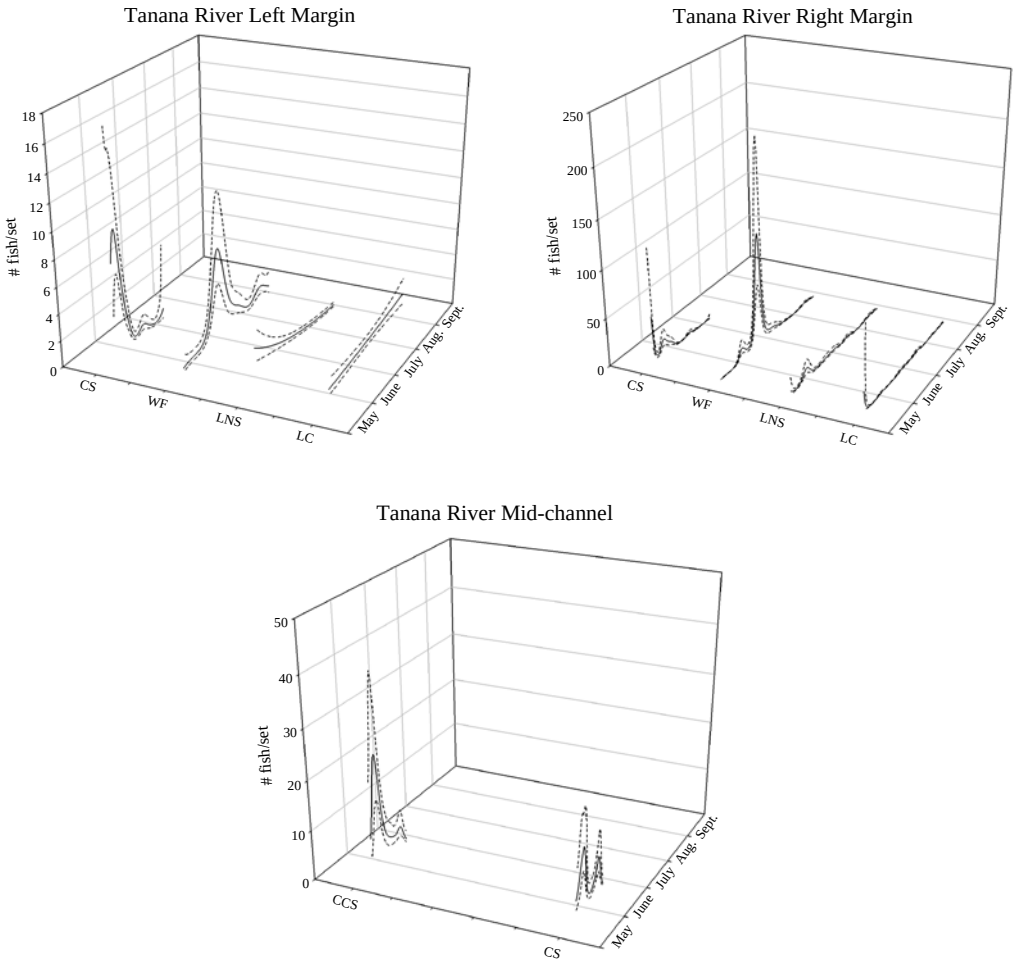

Figure 42. GAMs smoother trend line (solid line) encompassed by a 95% confidence interval (dashed line) describing trends in catches for each species/taxa—longnose suckers (LNS), whitefishes (WF), chum salmon (CS), lake chubs (LC), and Chinook/coho salmon (CCS)—in each location in the Tanana River.

In contrast to the previously described species/taxa that exhibited either peaks or trends in downstream migration abundance, chum salmon in the mid-channel exhibited both during the sampling season. Catches of chum salmon in the mid-channel initially decreased ($P = 0.0002$) in late May through early June, then showed a peak in mid-June (Figure 42).

In contrast to the species/taxa that exhibited seasonal and/or diel temporal patterns, the remaining species/taxa captured in the margins (Chinook/coho salmon, Arctic grayling, slimy sculpin, *Lethenteron* spp., Arctic lamprey, Alaskan brook lamprey, burbot, and northern pike) and mid-channel (whitefishes, Arctic grayling, Arctic lamprey, *Lethenteron* spp., and burbot) did not display temporal patterns in catches, as their frequency of occurrence was too small to identify seasonal or diel trends or peaks in migration.

Spatial patterns

Catches of Chinook/coho salmon primarily occurred in the mid-channel, while chum salmon occurred in both the mid-channel and river margins (Table 7). The remainder of the species primarily occurred in the river margins.

Environmental correlates

The Tanana River discharge exhibited an increasing trend until early/mid-July, then a decreasing trend through the end of the sampling season (Figure 43). Mean daily water temperature showed an increasing trend through May in the Tanana River, after which it generally ranged from 13 to 17°C, until the temperature steadily decreased starting in late July in the Tanana River (Figure 43). Turbidity in the Tanana River was relatively high when measurements began in mid-May, immediately decreased for one week, then increased until late May and remained high through the remainder of the sampling season. The daily mean of the Debris Index exhibited multiple distinct peaks throughout the summer (Figure 43), with highest debris counts occurring in May.

Catches of fish were associated with environmental variables in this study. Decreased catches of whitefishes ($P = 0.0004$) and increased catches of longnose suckers ($P = 0.0031$) were associated with the Debris Index. Decreased catches of chum salmon ($P = 0.0042$), whitefishes ($P = 0.0005$), longnose suckers ($P = 0.0315$) and lake chub ($P < 0.0188$) were associated with increased water temperatures. Decreased catches of whitefishes ($P = 0.0064$) and longnose suckers ($P < 0.0486$) were associated with decreased turbidity. Qualitative visual assessment of seasonal patterns in catches indicates that chum salmon, whitefishes, Chinook/coho salmon, and longnose suckers were associated with increasing river discharge.

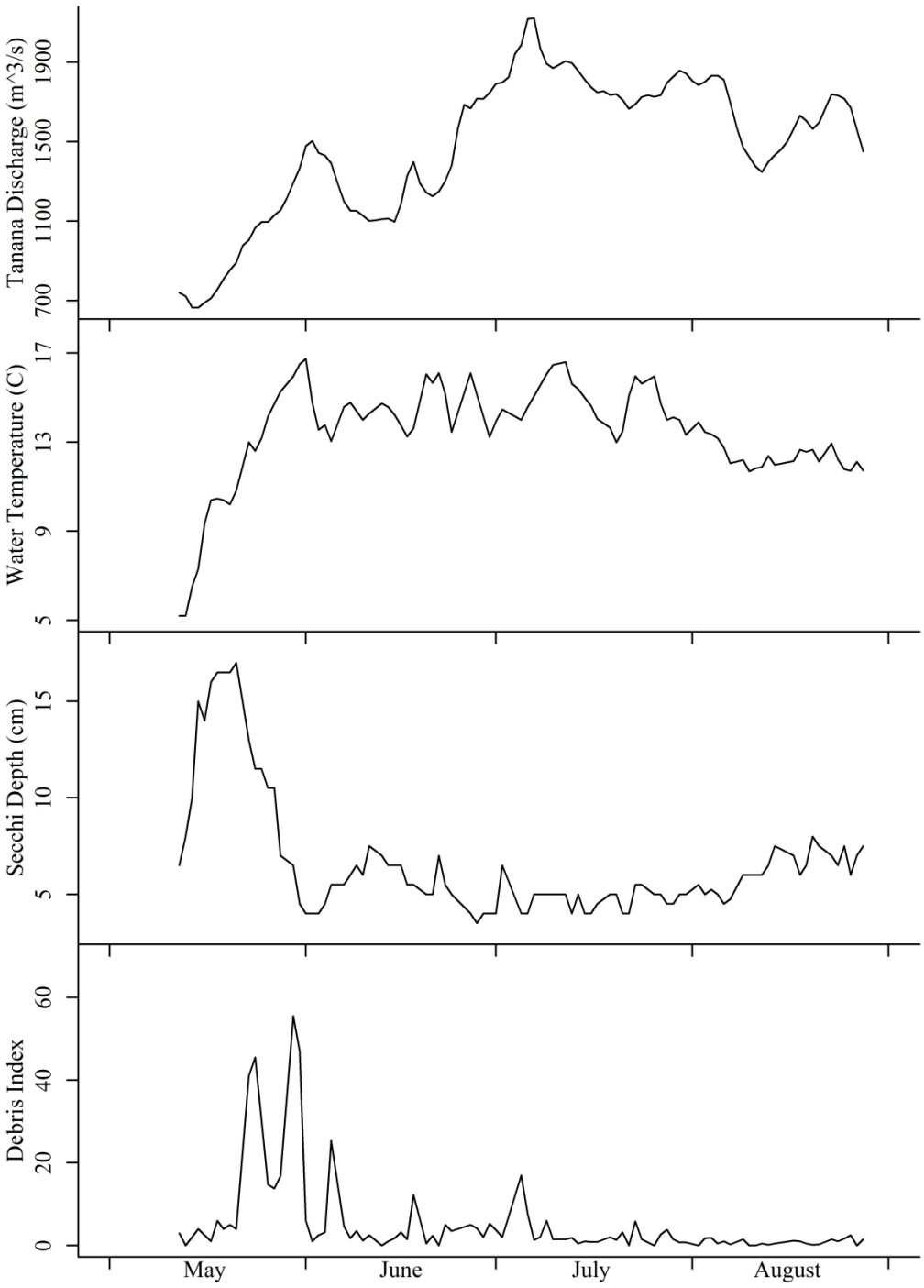

Figure 43. Discharge (m3•s-1) × 100, daily mean water temperature (°C), Secchi depth (cm), and daily mean of the Debris Index of the Tanana River at Nenana, Alaska.

Discussion

Catch composition

Size, time of capture, and published accounts of life histories may be used to infer age and migratory destinations of these juvenile fishes. All of the chum salmon were age-0 smolts migrating to the Bering Sea, as this species does not rear in freshwater, but rather migrates to the ocean soon after emergence from spawning gravel (Scott and Crossman 1973). The vast majority of Chinook and coho salmon were age-1 and age-2 smolts, respectively (Pearse 1974; Evenson 2002) migrating to the Bering Sea. The relatively small catch of age-0 Chinook/coho salmon fry suggest that some individuals of these species move downriver to overwinter in non-natal streams, as has been documented in the Yukon River (Daum and Flannery 2011).

While some whitefishes were age 1+, the vast majority were age-0. Age-0 whitefishes began appearing in catches in early June and, unfortunately, without morphological or genetic confirmation, it is nearly impossible to definitively identify species (Shestakov 1991; Bradford et al. 2008). However, when possible, round whitefish were informally distinguished from whitefishes belonging to the genus *Coregonus*, based on presence of parr marks, and this species made up a minimum of 70% of catches of whitefishes. In contrast, other studies in the Tanana River (Mecum 1984; Ott et al. 1998) had relatively few numbers of round whitefish compared with other whitefishes. This contradiction is likely because other studies in the Tanana River focused on residence and feeding in mainstem and backwater areas by capturing whitefishes with baited minnow traps, thereby not capturing the significant, but brief, downstream migration of age-0 whitefishes in late June documented in this study.

The minimal catches of age-0 Arctic grayling in the Tanana River indicate that this river does not serve as primary summer rearing habitat (Ott et al. 1998), and either the fall downstream migration of fry occurred after sampling ceased, or this section of the Tanana River may not serve as a migration route for fry moving to overwintering habitat.

Although age-0 and age-1+ of other species were captured, distinguishing the ages of these other species was less obvious. Based on known length-age relationships for longnose suckers in Alaska, it is probable that 94% of the longnose suckers captured in the Tanana River were age-0 and age-1 (Pierce 1977; Mecum 1984). Reasons for their occurring in the Tanana River mainstem are different depending on age and time of year, but it is likely the juveniles captured in this study use the mainstem as a migration corridor to access highly productive backwater areas (Mecum 1984; Ott et al. 1998).

Relatively high catches of lake chub in this study corroborate a previous research finding that lake chub are the most commonly captured species in the Tanana River drainage, particularly in backwater habitats (Mecum 1984; Ott et al. 1998).

The vast majority of lampreys captured were ammocoetes with the exception of a few adult Arctic lamprey and two gravid Alaskan brook lamprey. Arctic lamprey ammocoetes have been described as having a nocturnal downstream migration, tightly associated with high discharge events in Russia (Kirillova et al. 2011); however, catch rates were too small in this study to document any such patterns. Additionally, the ammocoetes captured in this study may not have been migrating, but rather actively or passively moving between feeding habitats.

Northern pike, burbot, and slimy sculpin were captured in relatively few numbers, probably because of relatively sedentary behavior and/or a preference for other habitats. Northern pike are typically found in areas with aquatic vegetation and less turbid waters, such as Minto Flats in the Tanana River drainage, which may explain the low capture rates in this study. Burbot are known to occur in a variety of habitats in Interior Alaska, including large glacial rivers, but are relatively sedentary except for movements from November to March, which are associated with winter spawning (Breeser et al. 1988). This habit likely explains their low capture rates in the present study, though burbot may also occur in habitats not sampled, such as the bottom of the mid-channel. Additionally, slimy sculpin are typically more abundant in clear headwater streams (Craig and Wells 1976).

Temporal patterns and environmental correlates

The association between river discharge and peaks in catches of chum salmon, whitefishes, longnose suckers, and Chinook/coho salmon suggests that these fish are either physically displaced from tributaries and backwater areas during high water (Wolter and Sukhodolov 2008) or use increasing discharge as a cue to initiate downstream migration (Lucas and Baras 2001; Achord et al. 2007). For each of these species/taxa, catches appear to be associated with only one high discharge event, suggesting that a majority of the fish migrated downstream in one pulse. As a result, fewer juveniles remained in the tributaries later in the year, and the association between catches and high discharge events was reduced (Whalen et al. 1999). Multiple studies have documented a similar pattern for chum salmon smolts in the Yukon River (Gissberg and Benning 1965), Tanana River drainage (Francisco 1977; Peterson 1997), and elsewhere in Alaska (Burril et al. 2009). Additionally, similar patterns have been documented for Chinook salmon smolts in the Chena River (Peterson 1997) and whitefishes in other locations (Shestakov 1991).

In addition to increasing discharge, increasing water temperature may also act as a cue to initiate downstream migration. For example, as water temperatures increased in the spring, catches of chum salmon and lake chub increased. It is likely that chum salmon emerged from the river gravel and initiated downstream migration with the initial spring increase in water temperature, which coincided with increasing discharge, suggesting that chum salmon smolts may be both physically displaced by high discharge and use increasing water temperature as a cue for downstream migration. The period of high catches of lake chub coincided with increasing water temperatures in mid-May, which may be a response to changing water temperatures in tributaries and backwater habitats. Ripe and spawning lake chub have been reported in a small Tanana River tributary in mid-July (Ott et al. 1998), so the high catches of lake chub in mid-May may have been a result of movement from overwintering habitat to summer rearing/spawning habitat, possibly cued by increasing water temperature.

Spatial patterns

Most species/taxa captured in this study primarily used either the river margins or the mid-channel, but not both. Chinook and coho salmon were the only species to mainly use the mid-channel. Similar patterns have been documented for Chinook salmon in the Columbia River (Dauble et al. 1989). The remaining species/taxa were mostly captured in the river margins. Tributary and backwater habitat use has been documented for many of these species/taxa (Mecum 1984; Ott et al. 1998; Durst 2001; Daum and Flannery 2011). The margins of the Tanana River mainstem probably serve as important migratory corridors between these habitats.

In contrast to the previously described species/taxa, chum salmon smolts were captured in both the river margins and mid-channel. Other studies have documented a similar pattern with chum salmon in the Yukon River (Gissberg and Benning 1965) and Fraser River in British Columbia (Todd 1966). Because chum salmon smolts feed during their long migration to the ocean (Durst 2001), it is possible that they use the margins for feeding and the mid-channel for traveling.

Implications

For a surface-mounted hydrokinetic device in the mid-channel of the Tanana River, most potential interactions will occur with Chinook salmon, coho salmon, and chum salmon smolts as they migrate downstream to the ocean from May through July, particularly during periods of increasing discharge. Unfortunately, because Chinook salmon and coho salmon were not distinguished, it is unknown if Chinook salmon or coho salmon would have higher potential for interactions. This study was limited to downstream migrating juvenile fishes, so the potential for interactions of adult fishes moving upstream and hydrokinetic devices remains unknown. Should hydrokinetic technology be implemented in Alaska's turbid rivers, future research should be conducted to determine if interactions between hydrokinetic devices and fishes do occur, and if so, what physical impacts they may have on fishes. Preliminary investigations in a laboratory flume indicate that salmonids large enough (> 120 mm) to maneuver in swift currents avoid spinning hydrokinetic turbines, resulting in survival rates > 99% (EPRI 2011), while non-salmonid larval fishes (< 25 mm) with lesser swimming ability typically have lower survival rates, as they are unable to avoid turbine blades (Schweizer et al. 2012). However, findings on survival of fishes passing through a hydrokinetic turbine from previous research in flumes may not be transferable to Tanana River fishes because of the river's vastly different characteristics including turbidity, fast current, and large turbulence. Therefore, future studies will be needed to describe the realized impacts of hydrokinetic devices on fishes once the devices are placed in the river.

River Debris and Its Impact on Hydrokinetic Devices

River Debris Origins

Any river or river tributary that flows through wooded terrain has the potential to produce and transport woody debris downriver, posing a risk of debris accumulation or impact against infrastructure that is in or on a river. River debris has a variety of shapes, sizes, and types that are generally classified as small, medium, and large debris (Bradley et al. 2005). Small debris consists of leaves, small branches, and bark (Figure 44a), medium debris consists of larger branches and small trees (Figure 44b), and large debris consists of large branches and whole trees (Figure 44c). Small debris enters the river through wind events that blow leaves, grasses, and refuse into the river, and from the abrasion and breakup of bark and branches from trees that fall into the river. Bark is stripped from trees and broken into smaller and smaller pieces as it moves downstream. Small debris can exist on the river's surface; however, a large amount of the small debris eventually becomes waterlogged and sinks beneath the river surface. The small debris shown in Figure 44a was sampled in the lower third of the water column in the Tanana River at Nenana. Ben Beste (AP&T) observed extensive small debris flowing near the riverbed in the Yukon River at Eagle, Alaska, while working on the river bottom (personal communication with J. Johnson). Medium and large debris enter the river system as a result of bank erosion that eventually causes trees to fall into the water (Figure 45). As with small debris, medium and large debris can exist throughout the water column.

a **b** **c**

Figure 44. Small debris (photo credit: Parker Bradley) (a), medium debris (b), and large debris (c) from the Tanana River Test Site at Nenana, Alaska. Photo credit: AHERC.

Figure 45. Tanana River bank.

River Debris Transport

Many river tributaries do not have sufficient flow to transport medium- or large-sized debris downstream except during flood events, which means that the amount of debris in a river generally increases as the flow discharge increases. An increasing river or river tributary discharge causes the water level to rise, picking up stranded debris and moving it downstream. Debris may be stranded and refloated many times during its course downriver as the river level increases and decreases due to rain events or fluctuations in the melt rate of glacier ice, a significant source of water for major rivers in Alaska (Figure 46).

Observations of the amount of debris in the Tanana River as a function of discharge during 2011 (Figure 43) indicated that most debris is flushed as the river discharge increases immediately after breakup and then decreases dramatically after the early discharge maximum that occurs during May. Subsequent discharge increases produced peak debris amounts much smaller than the early season discharge, with the amount of debris in the river decreasing to relatively low levels during July and August even though discharge levels were generally higher during June, July, and August than in May.

a **b**

Figure 46. Stranded Tanana River debris various sizes and shapes (a) and a lower trunk with root ball (b). Photo credit: Jack Schmid. Photos (a) Tanana River May 23, 2010, (b) Yukon River July 7, 2010.

As debris travels downriver, it can float on the surface (Figure 44b and c), in a vertical orientation with its root ball scraping along the riverbed (Figure 47), or as submerged debris (Figure 48). Debris can collect at river bends or channel constrictions, forming entangled masses of logs that, when released by a major flood event, become log islands that pose a major hazard to any hydrokinetic power generating device (HKD) infrastructure in its path (Johnson and Pride 2010; Tyler 2011). One such log island was video recorded at Nenana in August 2008 sweeping away a fish wheel, which is a reasonable analogy to an HKD mounted on a floating platform. Chang and Shen (1979) indicate that the rare occurrence of such large masses of logs may be the result of river turbulence that breaks apart the intertwined logs.

The log island at Nenana appeared to be well consolidated, with logs projecting out of the water. Some of the logs snapped as the log island collided with the outer bank of a bend in the Tanana River before moving off downstream. The log island was not broken apart by the impact against the riverbank or the flow turbulence in the river bend. Some of the logs, however, were left stranded against a pier of a highway bridge located just below where the log island was video recorded, which might indicate that the

log island broke apart to some extent upon impacting the bridge pier. The log island event at Nenana is an extreme example of a high-inertia mass of debris careening from one side of a river to the other, as the debris moves downstream in a meandering river with many bends. The event is a demonstration of inertia on the flow path of debris. Smaller debris (lower inertia) tends to respond rapidly to changes in flow speed and direction, while larger debris (higher inertia) floats across a river's flow lines due to high inertia.

a **b**

Figure 47. Vertically oriented log with its root ball scraping the riverbed as the log moves downstream in the Yukon River. The difference in height above the water between (a) and (b) is due to a change in river bathymetry. Photo credit: Jack Schmid.

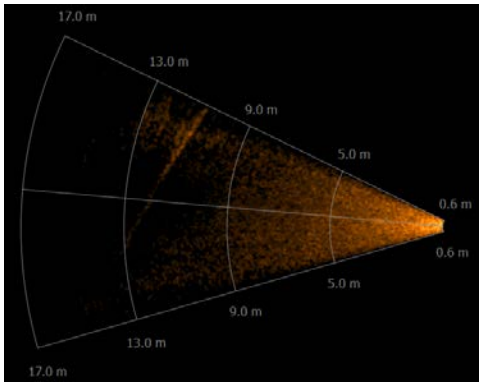

Figure 48. Submerged debris (linear features) in the Tanana River. Speckling in the solar image is due to scattering from suspended sediment particles. Photo credit: AHERC.

In general, floating debris tends to follow the thalweg in straight sections of a river when the river stage is rising, but moves outward toward the riverbanks during periods of a falling river stage. When the river stage is steady, turbulent-induced second-stage current flows often converge at the river surface, resulting in debris that follows the thalweg (Chang and Shen 1979; Lagasse 2010; this study). Large-debris transport downriver can be hindered by a river's width and the radius of curvature of river bends. Debris that is nearly as long as the width of a river is less likely to be transported downriver in one piece. It will either become jammed at a river bend or at some point break into smaller segments, as the force of other

logs piling against the blocking log becomes too great. A flowchart for estimating the potential of a river to produce debris that is transported downriver is shown in Figure 49.

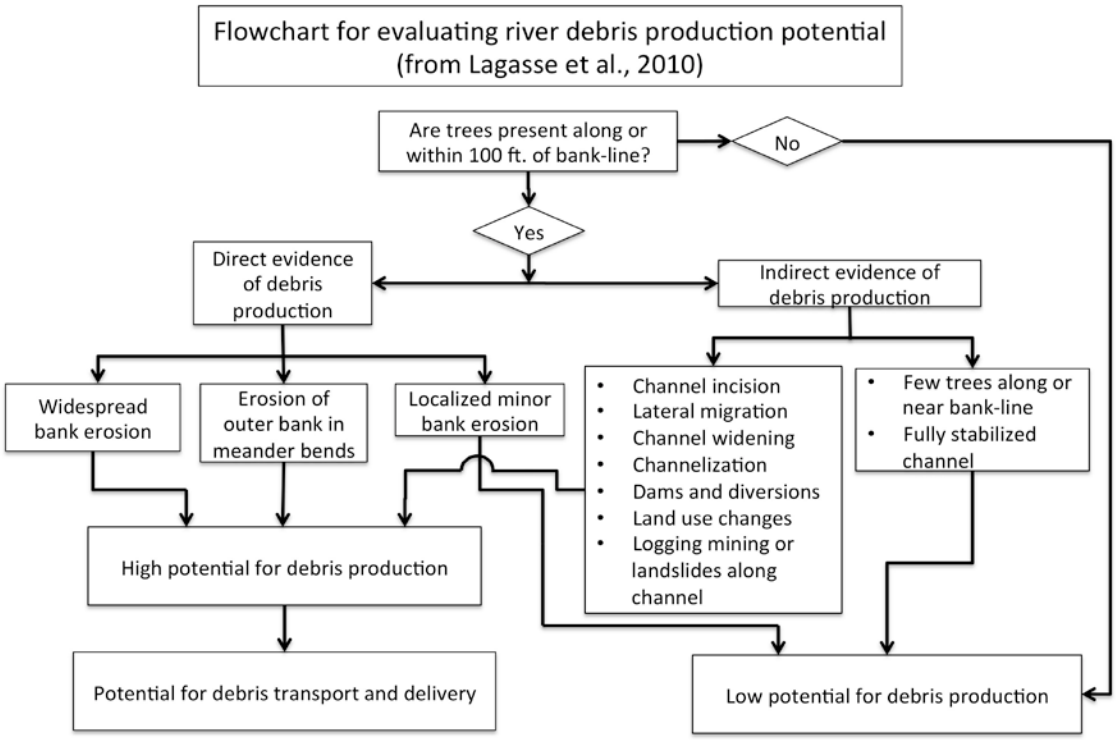

Figure 49. Flowchart for evaluating river debris production potential (from Lagasse 2010).

While not as widespread as surface debris, submerged debris (including neutrally buoyant debris throughout the water column and debris that is at rest or is transported along the riverbed) is common in most rivers in Alaska. The evidence for the existence of submerged debris throughout a river's water column includes the impacts between HKDs at Eagle and Fort Simpson (Tyler 2011), observations of submerged debris in the Tanana River at Nenana, and reports by boaters. At the Tanana River Test Site, submerged debris was pulled up from the riverbed during recovery operations of an anchor chain, and pulled from the chain of a mid-channel mooring buoy in the Tanana River at Nenana (Schmid 2012).

During a period of heavy rain in late September 2012, Tanana River discharge caused near-flood-stage conditions, which produced extensive surface debris (Horn 2012) and submerged debris (J. Holmgren, personal communication to J. Johnson). In locations of high turbulence, subsurface debris was brought up to the river's surface by water boils. Once the debris was expelled from a boil, it sank immediately. These observations imply that, as with surface debris, the amount and size of subsurface debris increase as the discharge of a river increases.

Debris Accumulation

While surface debris accumulation against bridge piers and at water intakes of hydroelectric dams are the most common infrastructure concerns, debris has also been shown to adversely affect HKD operations on the Yukon River and the Mackenzie River (Johnson and Pride 2010; Thompson 2010; Tyler 2011 NUL

2012) (Figure 50). Those HKD operations experienced debris accumulation in front of their floating support platforms and/or suffered impact damage to turbine blades. As a result, the period of operation for the HKDs was limited because of delays required to clear debris from the HKDs or repair damaged components. In addition, the task of clearing debris from HKD floating platforms under dynamic and high-force conditions posed significant personnel safety issues.

a **b**

Figure 50. Debris accumulation on the bow of the 5 kW New Energy EnCurrent turbine barge on the Yukon River at Ruby, Alaska (Pelunis-Messier 2010) (a); debris accumulation in front of a 25 kW New Energy turbine barge on the Yukon River at Eagle, Alaska (photo credit: Alaska Power & Telephone) (b).

Debris accumulation on HKDs suspended from a floating platform generally occurs as individual logs and branches hit the front structure of the floating barge and become wedged into or caught on parts of the barge. Neutrally buoyant debris just beneath the water surface can also catch on parts of a turbine that is deployed from a floating platform (e.g., on the turbine shaft or blades or electrical cabling running from the HKD to shore). At Eagle, a submerged root ball caught on the vertical electrical cable that ran from the pontoon barge to the riverbed. Because of concern that the pull of the snagged cable might result in damage to the barge, the crew cut the cable free from the barge (D. Light, personal communication).

Debris Mitigation Methods

As part of this project, Tyler (2011) reviewed the literature on debris in rivers, its impact on infrastructure, and methods used to mitigate debris on infrastructure and HKDs. We refer the reader to Tyler's report for a general overview of debris and debris mitigation methods (see Appendix A). Here, we present ideas for mitigating surface debris damage to HKDs. The character of subsurface debris is not understood well enough to rationally develop subsurface debris measures (e.g., debris amount as a function of river discharge and location in the water column, debris size range, debris type).

The primary methods that have been attempted or considered (Tyler 2011) for reducing the influence of debris on HKDs include:

1. Using debris diversion booms – Deploying a debris diversion boom immediately in front of a floating HKD platform to divert debris around the HKD.
2. Placing the HKD in a location that has a lower probability of encountering debris.
3. Removing debris manually or mechanically.
4. Designing the HKD to be debris tolerant

5. Furling (to roll up and secure) – Used to remove an HKD from the path of debris either by removing the HKD from the water or out of the debris travel path.
6. Blocking or capturing debris with trash racks.

Debris Diversion Booms

A debris diversion boom consists of two pontoons joined together at one end and separated at the opposite end to form an angle with its apex pointing upstream (Figure 51). The operating principal of a diversion boom is that debris that impacts a boom is redirected sideways along the angle of the pontoons around an HKD by the force of water pushing against the debris. The operators of the three 2010 HKD demonstration projects (Ruby, Eagle, Fort Simpson) indicated that their diversion boom deflected debris, and Ben Beste from AP&T thought that some modification to the boom used at Eagle could greatly improve its performance (Johnson and Pride 2010; Tyler 2011). Ultimately, despite the presence of debris booms, debris still forced each of these demonstration projects to end. At Ruby, debris overwhelmed their debris diversion boom, and at Fort Simpson submerged debris passed under the boom to impact their HKD. The turbine at Eagle also suffered from submerged debris impacts.

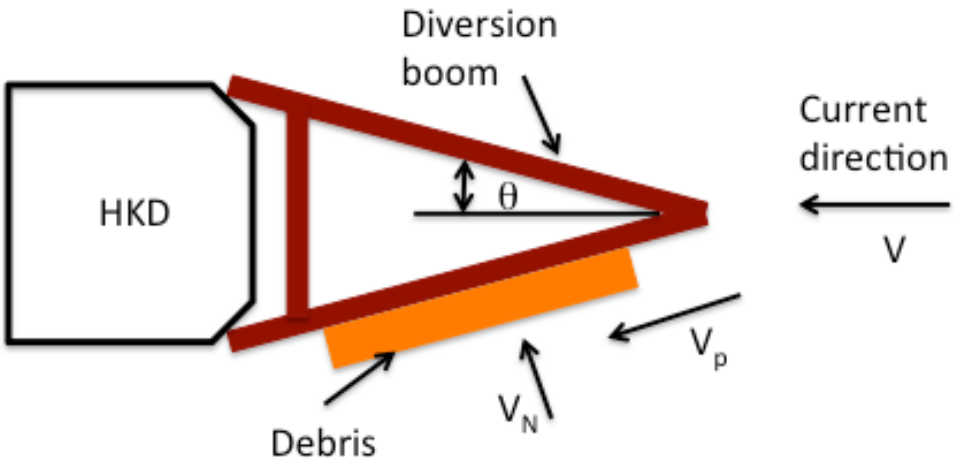

Figure 51. Debris diversion boom protecting an HKD from surface debris.

An examination of the mechanics of diversion boom interaction with the river current and debris provides some qualitative insight into how the performance of a diversion boom is affected by the design of the boom and the method of deployment. In Figure 51, the change in river current velocity (V) around a diversion boom is shown referenced to the geometry of the pontoon, where V_p is water velocity parallel to the pontoon surface, and V_N is water velocity in the normal direction to the pontoon surface where

$$V_p = V \cos\theta \tag{2}$$

and

$$V_N = V \sin\theta \tag{3}$$

where θ is the half angle between the two pontoons (Figure 51).

When debris impacts the diversion boom pontoon (and does not catch on the boom's sharp front end), the debris must be able to slide along the pontoon surface to clear the boom. If the debris object cannot slide along the pontoon surface, then the debris object will become pinned to the debris diversion boom. This is undesirable, as it may result in additional debris collecting on the diversion boom.

To clear the debris object from the diversion boom requires that the force of water pushing on the debris is greater than the frictional resistance of the pontoon surface. The problem can be treated qualitatively by drawing a force balance diagram (Figure 52) and making some simple assumptions about how the forces are related to the river currents.

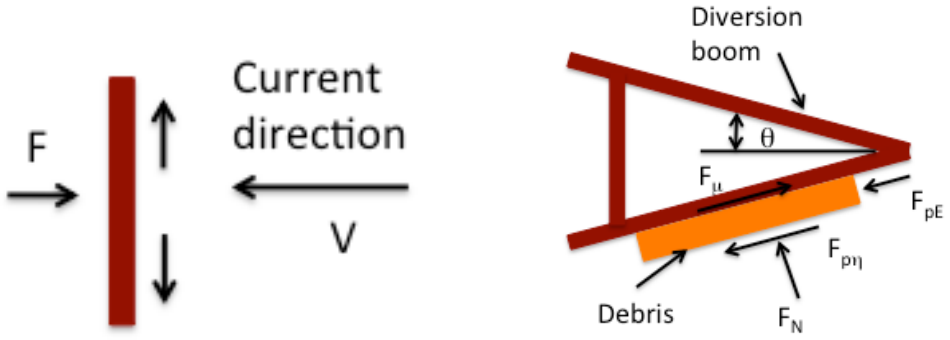

Figure 52. Force required to hold a plate fixed in a current flow, V (a) and the forces acting on a debris object against a debris boom pontoon (b).

The force acting on a fixed flat plate oriented perpendicular to the current is

$$F = \rho V^2 A \tag{4}$$

where ρ is the density of water and A is the area of the plate (Crowe et al. 2009). The force F required to hold the plate fixed is due to the fixed plate causing water velocity, hence its momentum, to decrease to zero as the water flow is redirected laterally across the face of the plate (Figure 52a). Extending this concept to components of the current velocity acting on the debris gives

$$F_{pE} \propto \rho (V \cos\theta)^2 A_E \tag{5}$$

and

$$F_N \propto \rho (V \sin\theta)^2 A_L \tag{6}$$

where A_E is the area of the end of the debris object (e.g., $A_E = \alpha_E \pi r^2$ for a log, where r is the log's radius), and A_L is the area of the log's long direction (e.g., $A_L = \alpha_L 2rL$, where L is the length of the log).

The shear force acting on the debris object due to the boundary layer shear with the water flow is estimated using

$$F_{p\eta} = \eta \frac{V \cos\theta}{y} A_\eta \tag{7}$$

where η is the coefficient of viscosity for water, *y* is the boundary layer thickness from the debris surface to the free flow velocity parallel to the debris surface, and A_η is the half circumference area of the debris object (e.g., $A_\eta = \alpha_\eta\ \pi r^2 L/2$, for a log of length *L*). Only half the circumference area of the debris log is used, since we assume that the flow on the pontoon side of the log is stagnant.

The friction between the debris boom pontoon and the debris object is given by

$$F_\mu = \mu F_N \tag{8}$$

where μ is the coefficient of friction between the debris object and the pontoon surface.

The coefficients $\alpha_{E,}$ $\alpha_{L,}$ and α_η denote the degree of submersion of the debris object in the water. For a completely submerged object, the coefficients equal one and decrease with the amount of the debris object that floats above the waterline.

The force that determines if the debris object slides off the debris boom or is pinned to the pontoon is given by the force balance equation

$$\frac{F_{pE}+F_{p\eta}}{F_\mu} > R. \tag{9}$$

As it is not possible to know all of the relevant parameter values for Equation 9, and we are not so interested in the actual force values as much as we are interested in examining how the force balance equation varies with debris boom geometry, friction, and the debris object—are V, θ, μ, L = βr and *r* = 1; the remaining parameters are set to 1. With these simplifications, the force balance inequality for a round log can be written as

$$Q = \frac{\pi\,\mathrm{V}\cos\theta\left(\mathrm{V}\cos\theta+\frac{\beta}{2}\right)}{2\mu\beta(\mathrm{V}\sin\theta)^2} > R. \tag{10}$$

where *Q* is the ratio of driving forces from the river current that act on a debris object to slide it along the debris diversion boom, to the frictional resistance forces that act on a debris object to resist sliding along the diversion boom. When *Q* exceeds the threshold parameter (*R*), the driving forces are greater than the resistance forces, and debris will slide off the diversion boom. When $Q \leq R$, the resistance forces are greater than the driving forces, and a debris object will be pinned to the diversion boom's pontoon surface.

The results of calculating *Q* as a function of diversion boom half-angle (θ) and current velocity (*V*) with constant coefficient of friction (μ) is shown in Figure 53a.

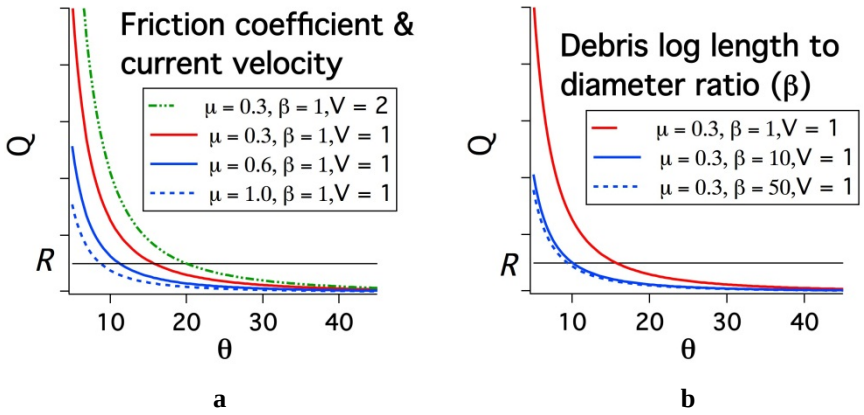

Figure 53. The change in Q as a function of diversion boom half-angle (θ) and current velocity (V) (a) and as a function of boom half-angle and debris log length to diameter ratio (β) (b).

The effect of the debris length ratio (β) is shown in Figure 53b. The threshold parameter (*R*) is shown on the plots for reference, and the scale of the *Q* axis is the same for both Figure 53a and Figure 53b. From the figures, it is apparent that *Q* decreases rapidly as a function of θ for all cases of friction coefficient, current velocity (Figure 53a), and β (Figure 53b), which indicates that decreasing the half-angle of a diversion boom will improve its debris-clearing performance in all situations. The results shown in Figure 53a also indicate that *Q* decreases as the coefficient of friction increases for a given debris diversion boom half-angle. Thus, the smaller the coefficient of friction for the diversion boom surface, the more effective it will be at clearing debris (e.g., a boom made from low-friction plastic will clear debris more effectively that a boom made from rough wood at the same boom half-angle).

In addition to diversion boom design, the type and size of debris and the river current velocity affect the ability of a debris diversion boom to clear debris. As the river current velocity increases, *Q* increases for a given θ (Figure 53a), improving debris-clearing performance. As β (the ratio of log length to its radius) increases, *Q* decreases for a given θ (Figure 53b), resulting in the decreased capacity of a diversion boom to clear debris. These results imply that the probability of debris becoming pinned to the diversion boom increases as river current velocity decreases and debris size increases.

The sharp apex of a diversion boom provides a particular challenge to clearing debris with branches, hard knobs, or a tangled mass of debris, all of which have projections that can catch on the diversion boom's point. Debris that is hung up on the point of a diversion boom provides rough projections that catch additional debris, which can build into a mass of debris that overwhelms the diversion boom unless the debris is removed. A possible way to reduce the probability of debris catching on the point of a diversion boom is to place a debris sweep (a freely rotating cylindrical-shaped diversion object) in front of a diversion boom's apex (Tyler 2011). The radius of curvature of the cylinder must be large enough to prevent debris projections from catching on the cylinder.

Once a debris object contacts a diversion boom, the flow of the river current produces a downstream flow under the debris that produces torque on the debris object, causing it to rotate in a backward direction. (That is, the top of the debris object rotates away from the diversion boom, and the bottom of the debris object rotates toward the diversion boom). The magnitude of the torque action on the debris object

increases with θ, V, and the amount of branches with attached needles or leaves on the debris object. Increasing θ will cause V_N to increase for a given V, and increasing V will result in an increase in V_N. Branches projecting into the river provide additional surface area for the river current to push against. This backward rotation can result in a debris object being submerged under the diversion boom, to resurface on the downstream side of the diversion boom with little effect on its path of flow. Such debris could continue downstream to impact the HDK being protected by the diversion boom.

The obvious solution to reducing the probability that backward-rotating debris will roll under a diversion boom is to ensure that the boom is deep enough that debris cannot rotate under it and/or reduce θ. A deeper diversion boom provides more protection against near-surface submerged debris; however, deeper booms may create additional turbulence that may have an adverse effect on the current flow at the HKD.

The Alaska Hydrokinetic Energy Research Center developed a research debris-diversion platform that incorporates some of the improvements described in this section, such as adjustable θ, a debris sweep, and low friction coatings. Preliminary tests indicate that such modifications can significantly improve the ability of a diversion boom to clear debris (Johnson 2012). Analysis of the test results, including the effect of the diversion boom on current velocities behind the boom, is ongoing, and results will be reported at a later date.

HKD Placement

A common and effective way to mitigate debris problems is to select a location where there is low probability of encountering debris. This might include placing an HKD on the bottom of a river, downstream of the inner edge of a river curve, or behind an impoundment structure that prevents debris from entering a river channel.

Since most debris floats, it may be possible to avoid debris by placing an HKD far below the depth of floating debris. This is an approach used by small-scale turbines in remote areas of the developing world (Tyler 2011). In Alaska, an HKD placed on or near the river bottom may avoid floating debris, but it will not necessarily avoid submerged debris. While the amount of submerged debris and its type and location in the water column are not known, it is well known that submerged debris exists in sufficient amounts to cause problems for HKDs mounted to the river bottom.

The strategy of placing an HKD downstream of the inner edge of a river curve is based on the observation that most floating debris travels down the thalweg and that debris inertia generally forces the debris to the outer edge of a river curve. Debris forced to the outer edge of a river curve often remains toward the outer bank of the curve, even at a distance far enough below the curve where the river current has recovered its velocity and added turbulence. This strategy does have its limits, since some debris will enter at the inner edge of a river curve and remain fairly close to that edge throughout the curve.

Placing an HKD behind a debris impoundment (e.g., lake, dam) is the most effective method to avoid debris problems, as the debris is prevented from entering the river or flow channel by the impoundment structure. A lake provides a large impoundment area for debris to wash up onshore or become waterlogged and settle to the lake bottom. A dam collects all the debris on the upstream side of the dam, to be removed as needed by the dam operators. A debris-detention system consists of posts set into the river in a “V” pointing either downstream or upstream, with spacing between posts set to capture the

smallest desired debris. Debris is periodically removed from the detention system as it fills (Tyler 2011). A debris-detention system is not practical in most rivers in Alaska due to their size and power, and frequent high-water events.

Manual or Mechanical Debris Removal

All HKDs and related infrastructure that are deployed in debris-prone rivers will encounter conditions where debris is likely to accumulate. Well-designed debris diversion systems or other debris mitigation methods will have a plan for how to remove debris either manually or mechanically.

Accumulated debris on the Ruby turbine (Figure 50a) was removed by pulling the lightweight pontoon boat sideways into the current until debris was no longer pressing against the boat (D. Pelunis-Messier, personal communication to J. Johnson). This technique moved the boat out of the path of debris as the force of the current washed the debris off the debris diversion boom. Debris accumulation on the 25 kW turbine barge at Eagle (Figure 50b) had to be removed manually using chainsaws, pikes, and light boats, which created a number of safety issues.

The experiences with debris during the Ruby and Eagle HKD demonstration projects highlight the need to plan methods and technologies that are able to remove debris accumulation safely and effectively when it occurs. This effort would primarily involve developing methods of debris removal that minimize the need for people to operate from a boat, because any mishap in a flowing river can have immediate and severe consequences due to the velocity and power of the river. An extended, railed platform (sometimes referred to as a pulpit or a bow pulpit; http://pulpit.askdefine.com/) that juts out from the bow of an HKD or debris diversion platform can facilitate manual debris removal. This method allows a person to operate from a stable platform above the debris accumulation. The pulpit design can incorporate or complement specialized equipment to facilitate debris removal and enhance operator safety (e.g., a safety harness, grappling hooks, boom crane, saws). A further potentially useful design feature is to have the pulpit stowed when not needed, yet easily and quickly deployable from different locations where debris may need to be removed.

Trash racks

Trash racks are essentially grates (usually constructed from metal) intended to block debris, while allowing water to pass through to a water intake. Some grates are built at an angle to provide the ability to divert debris around the water intake, but they still collect significant amounts of debris, requiring removal by manual or mechanical means (Tyler 2011). For surface-mounted HKDs, a trash rack is not a particularly useful means of dealing with debris problems, because the volume of debris that floats on, or that may be submerged near, the water surface can quickly fill up and overflow a trash rack. As the trash rack fills with debris, the water current behind the trash rack will decrease in velocity and become more turbulent, adversely affecting the performance of any HKD that is immediately behind the trash rack. As the downstream distance between an HKD and debris-filled trash rack increases, the adverse effects of reduced current velocity and increased turbulence caused by a trash rack will decrease.

While not much is known about the volume of submersed debris in rivers as a function of river stage or flooding events, observations indicate that significantly less submerged debris exists in rivers than surface debris under similar river discharge conditions. Depending on the actual volumes of submerged debris in the river, a trash rack system (perhaps combined with some debris diversion capabilities) could be used to

protect a submerged HKD. Some mechanism would need to be in place for determining when debris in the trash rack needed to be removed and disposed of in a manner that would not affect the deployed HKD. This process might involve monitoring the load buildup on the trash rack and having a means of taking the debris to shore or moving the debris downstream around an HKD installation and releasing it. Such an operation might be extremely time-consuming and labor-intensive, unless some novel technologies are developed to make the process easier and more efficient.

Debris-tolerant HKD design

Tyler (2011) describes several HKD blade designs that minimize debris effects by shedding debris or folding back when hit by debris (Anyi et al. 2010; Kirke, interview with Tyler in 2010). None of these concepts is currently in use in Alaska; however, developing a debris-tolerant HKD design could be beneficial for improving the ability of HKDs to operate sustainably.

Summary and Conclusions

Woody debris exists in any river that passes through wooded terrain or that is fed by tributaries that pass through such terrain. The primary exceptions are those rivers that are immediately downstream from a natural or constructed impoundment basin for debris, such as a lake or dam. The probability of encountering debris below an impoundment basin increases with the downstream distance from the basin. For Alaska, and much of the rest of the world, this means that significant amounts of debris travel on, and under, the surface of the majority of rivers and can pose a hazard to HDK deployments and operations.

Demonstration projects of HKDs on the Yukon River at Ruby and Eagle in Alaska and on the Mackenzie River at Fort Simpson in Northwest Territories, Canada, during 2010 were all ended due to debris accumulation on the HKDs or by debris impacts that caused damage or disrupted operations. In each instance, the projects had incorporated debris-diversion boom systems that worked to some degree, but were ultimately unable to prevent debris accumulation or impacts, forcing an end to the projects. These experiences dramatically highlight the need to find technologies and methods that mitigate the effect of debris on hydrokinetic device operations if HKDs are to be a viable way to generate power in Alaska rivers.

Methods and technologies that have been used to mitigate the effects of debris in rivers include:

1. Using debris diversion booms
2. Placing HKDs in locations were debris encounters have low probability of occurrence
3. Using manual or mechanical debris-removal methods
4. Designing debris-tolerant HKDs
5. Furling HKDs (i.e., removing the HKD, either from the water or out of the debris travel path)
6. Blocking or capturing debris with trash racks

Debris diversion booms and manual debris removal have been used in Alaska and Canada in an attempt to reduce the influence of debris on HKDs operating from floating platforms. In each situation where a debris diversion boom was used, HKD operators reported that the boom diverted debris many times. The booms ultimately were unable to handle all the different debris conditions, including submerged debris that went under the diversion boom, debris that rolled under a shallow boom, and debris accumulation on

a diversion boom. The HKD operators at Ruby and Eagle indicated that, with some modifications, a debris diversion boom could be made into an effective debris diversion system. Tests at the TRTS using a research debris diversion platform indicate that adjusting the diversion boom angle and the friction of boom surfaces, and adding a bow sweep (a freely rotating cylinder mounted at the front of the diversion boom) would greatly improve the performance of diversion booms. The tests also indicate that the debris-diversion platform pontoons must be deep enough in the water to prevent debris from being forced under them.

Furling is used for small-scale HKDs in remote areas (not in Alaska), but probably is not practical for large-scale HKD installations. Trash racks are not practical for protecting HKDs mounted on floating platforms in Alaska rivers because of the amount of debris floating on or near the river surface, which would quickly overwhelm a trash rack system. In addition, some means of disposing of the captured debris without damaging an installed HKD would need to be developed. Trash racks may be able to help protect HKDs from debris when the amount of debris in the river is relatively small. For example, when an HKD is submerged, it is exposed to much less debris than when it is located near the river surface.

Current velocity decreases and turbulence increases downstream from debris-diversion boom and trash rack installations. The magnitude of river current velocity reductions or increases in turbulence caused by diversion booms or trash racks is not known, and efforts to determine the effect of diversion booms on current flow are part of ongoing studies at the Alaska Hydrokinetic Energy Research Center. It may be possible to locate HKDs far enough downstream of diversion or capture devices that river current velocities and turbulence magnitudes recover sufficiently to have little effect on HKD operations. A similar problem exists when trying to minimize the turbulence effect of one HKD on another when installing several HKDs in an array.

Conclusions and Implications for In-Stream Hydrokinetic Power Generation

A three-year study (2009–2011) to characterize the Tanana River environment at Nenana, Alaska, was conducted as it relates to the deployment and operation of hydrokinetic power generating devices (HKDs) (Figure 54). An additional goal was to establish the Tanana River Test Site (TRTS) at Nenana to facilitate development and testing of HKD technology under realistic Alaska river conditions. The Ocean Renewable Power Company (ORPC), which holds a Federal Energy Regulatory Commission preliminary permit to operate at the site, initially identified the study site. With ORPC's encouragement, the Alaska Hydrokinetic Energy Research Center of the University of Alaska Fairbanks, Alaska Center for Energy and Power conducted the HKD-related studies of the Tanana River at Nenana.

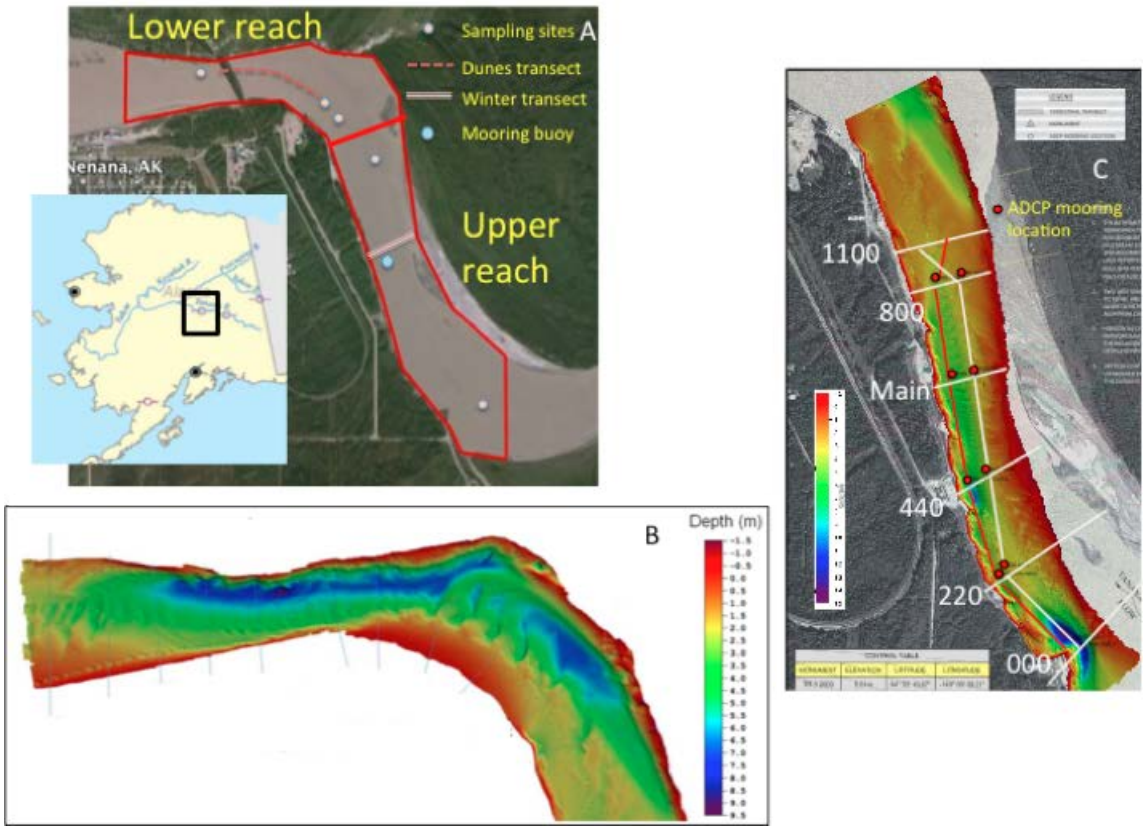

Figure 54. Tanana River Test Site location and sampling station map (A), bathymetry and velocity transect locations for the lower reach (B), and upper reach bathymetry, velocity transect locations, and ADCP mooring locations (C).

An intensive measurement program was conducted to determine river hydro-sedimentological conditions (discharge, current velocity, power density, turbulence, suspended and bed load sediment transport), wintertime conditions (frazil ice and current velocity), baseline fish stocks, and debris prevalence and type. Bathymetry measurements of the TRTS upper reach were made in 2009 and 2010, and bathymetry measurements of the lower reach were made in 2010 (Figure 54). A 2D numerical model (CCHE2D) of both the upper river reach (2010) and the complete river reach (2011) was constructed using TRTS bathymetry and discharge measurements (Figure 55). The model was validated using current velocity measurement data. The model was then used to determine current velocity at every location throughout

the TRTS. A hydrokinetic calculator module (HYDROKAL) was developed to process CCHE2D output to estimate the instantaneous power density, maximum current velocity, and specific discharge in each river cross section. An HKD efficiency factor, used to account for turbine efficiency, allows HKD developers and users the ability to quickly estimate the amount of hydrokinetic energy that can be extracted at a given location in the river.

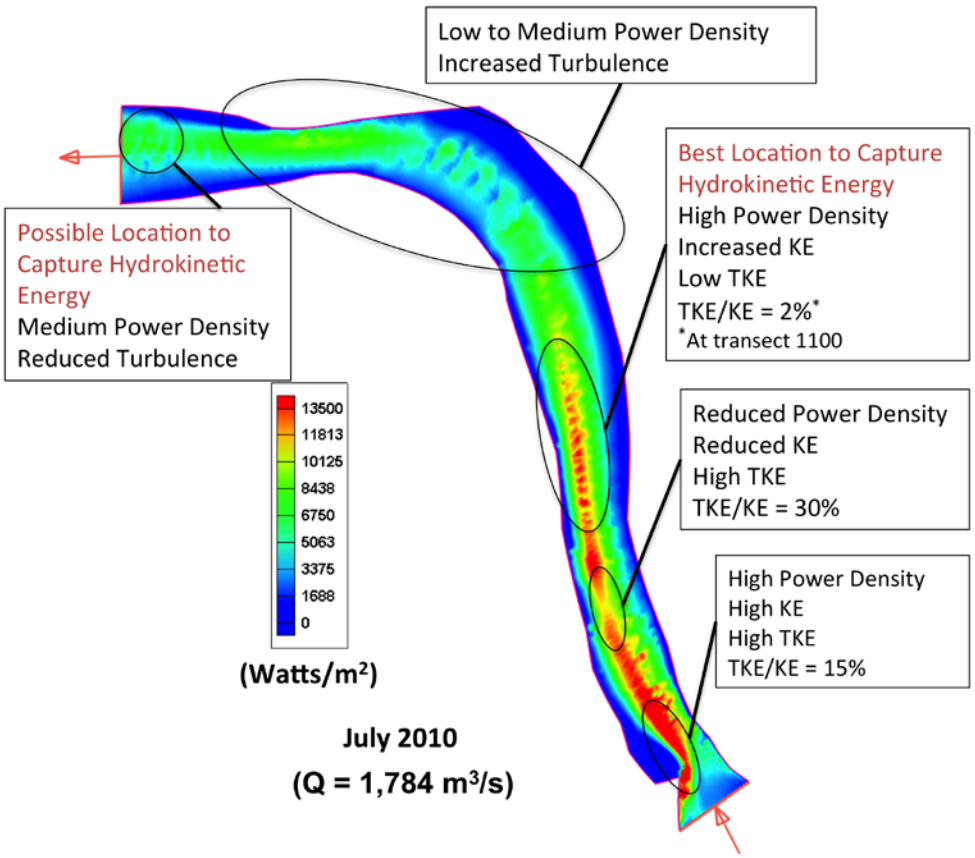

Figure 55. Power density as a function of location in the Tanana River Test Site river reach, with notations about turbulence and placement of HKDs. Figure modified from Duvoy and Toniolo 2012.

River Hydro-Sedimentological Conditions

Maximum measured current velocities at the TRTS ranged between less that 0.5 m/s in winter months to over 2.5 m/s during summer months and over 3 m/s during high-water events. Average monthly discharge ranged from a low of 496 m^3/s to a high of 1702 m^3/s during the open-water season (i.e., May to October), and from a low of 185 m^3/s to a high of 268 m^3/s during the winter months (i.e., November to April). The minimum discharge year during the period of record occurred in 1996, and the maximum average discharge occurred in 1967. During the summer months of July, August, and September, the average discharge was approximately 1423 m^3/s, when considering years 1962 to 2010. In 1996, the discharge was only 1047 m^3/s for the same summer months, while in 1967, the discharge increased to 1940 m^3/s.

River current velocities and discharge are highest in the thalweg in the upper part of the TRTS river reach. Toward the downstream end of the upper reach, current velocity and discharge magnitudes

decrease as the river flow transitions from the left bank to the right bank. The river channel and current flow is unstable in this transition region, as both the location of the river channel and the current flow change with discharge, the existing riverbed configuration, and sediment load. River power density magnitudes are proportional to the cube of the current velocity producing the highest power densities in the thalweg near the upstream end of the upper reach (Figure 55). The magnitude of power density diffuses and becomes unsteady around the bend in the lower river reach. Power densities again concentrate against the right bank downstream from the river bend.

Power densities for August 2009 and July 2010 were 6500 W/m^2 and 13,500 W/m^2, respectively. The power density distribution along the TRTS for the July 2010 estimate is shown in Figure 55. The maximum wintertime power density in 2010 was about 256 W/m^2. The high discharge year (occurring in 1967) peak power density is estimated to be 27,800 W/m^2, the average discharge (based on a 48-year record) peak power density is estimated to be 12,800 W/m^2, and the low discharge year (corresponding to 1996) peak power density is estimated to be 6,800 W/m^2.

Seasonally, discharge and power density begins increasing from the middle to the end of April (when breakup occurs), peaks sometime in July or August, and then decreases to normal winter low-discharge levels in early to mid-October when freeze-up occurs. Seasonal power density can also vary significantly at different locations within the TRTS, as shown in Figure 56 and Figure 57. These results are qualitative estimates only since the same bathymetry was used for the total time period while in actuality the bathymetry can vary significantly as river stage changes with time. Three locations in the upper reach are shown in the power density plot of Figure 56 along with the estimated seasonal power density variation at each location (Figure 57). The highest seasonal power density location is at P2, which is near or just below a bathymetric depression at transect 440. The next highest seasonal power density is at location P1, which is just downstream of the upper river bend. The constricted channel and the depressed bathymetry just above P1 produce highly turbulent flow conditions. The lowest seasonal power density location is at P3, which is just downstream from transect 1100 near the start of the transition of current flow from the left bank to the right bank of the river.

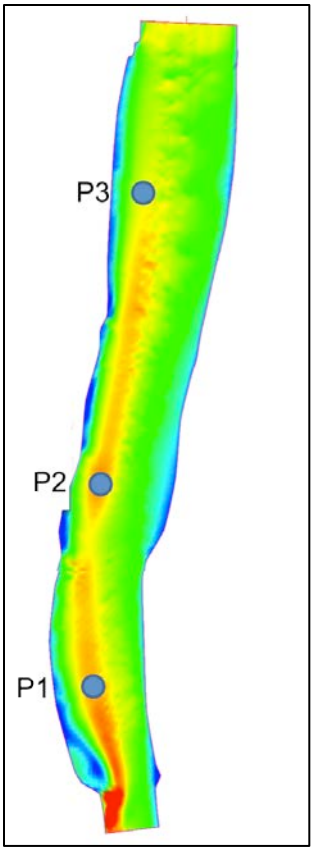

Figure 56. Power density plot for the upper TRTS reach, with the three locations used to estimate seasonal power densities shown in Figure 57.

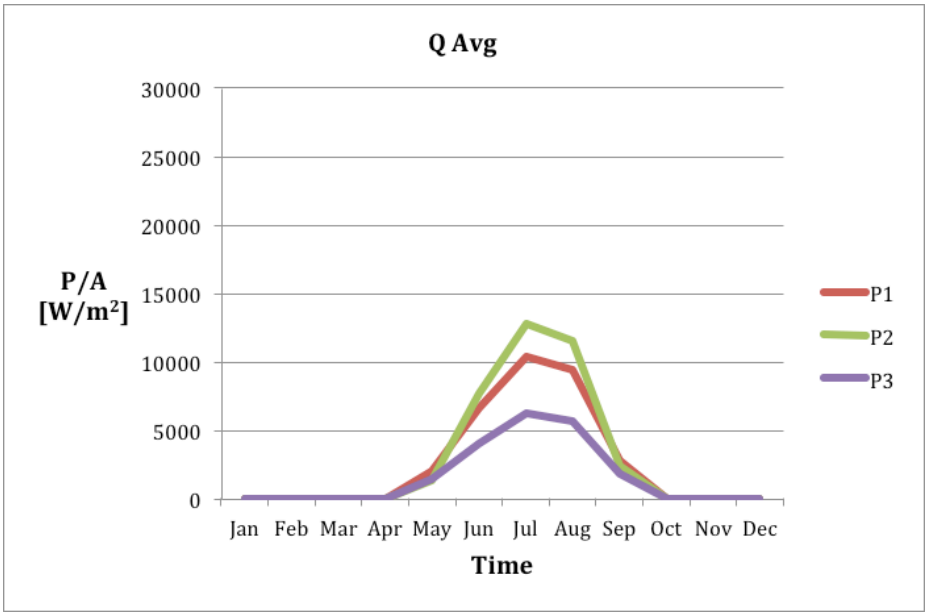

Figure 57. Instantaneous power density in W/m^2 for the three locations shown in Figure 56 for an average discharge year.

Riverbed dunes occur along the river bottom in the transition between the upper and lower reaches of the TRTS as the river enters the lower reach river bend. Average dune wavelengths ranged from 41 to 67 m, and average dune heights ranged from 0.6 to 1.2 m. Small superimposed dunes were found along the riverbed with wavelengths of about 15 m and heights of about 0.3 m. Bed load grain-size distributions ranged from fine sand, to sand and gravel, to medium gravel. Both suspended and bed load sediment concentrations are nonlinear functions of discharge. Suspended sediment concentrations ranged from 0.2 g/l at 500 m^3/s discharge to 2.3 g/l at 1800 m^3/s discharge, and bed load sediment concentrations ranged from around 1 g/l at 500 m^3/s discharge to 16 g/l at 2000 m^3/s discharge.

Turbulence occurs at the TRTS where the river channel geometry changes due to changes in bathymetry or direction. This includes a bathymetric depression and channel constriction around transect 000, where about 9% of the total river kinetic energy is turbulent. A second depression at transect 440 in the upper reach creates turbulence that is about 20% of the total river kinetic energy (Figure 54C). Other high turbulence reaches likely include bathymetric depressions between transects shown in the lower reach (Figure 54B).

The increased turbulence due to bathymetric depressions is exacerbated by flow direction changes due to the river bend just above transect 000 in the upper reach and throughout the river bend that includes transects shown in the lower reach. Relatively low turbulence exists in the constant cross-section straight sections of river from around the Main transect to transect 1100 in the upper reach, where turbulence constitutes only about 2% to 4% of the total energy (Figure 54C).

Current flows are lower in wintertime than during the open-water season due to the lack of available liquid water and the overlying ice cover, with maximum under-ice velocities of from 0.5 to 0.8 m/s, which corresponds to a maximum obtainable power density of 256 W/m^2.

Frazil ice forms at the TRTS beginning in October, when cold air temperatures supercool the water. During freeze-up, frazil ice adheres to objects that it contacts, blocking water intakes and accumulating on isolated structures. Frazil accumulation thickness on isolated objects (e.g., cylinders) reaches a steady-state accumulation profile as the shear forces from water flowing around the frazil limit its thickness. Frazil accumulations on Teflon®, stainless steel, and mild steel of up to 150 mm were observed during freeze-up.

Debris Hazards and Mitigation Approaches

Any river that flows through wooded terrain has the potential to capture and transport woody debris downstream, posing a risk of debris accumulation or impact against infrastructure that is in or on a river. Small river debris consists of leaves, small branches, and bark; medium debris is made up of larger branches and small trees; and large debris consists of large branches and whole trees. Small debris can exist on the river's surface; however, a large amount of the small debris eventually becomes waterlogged and is transported in the lower third of the water column. Medium and large debris enter the river system as a result of bank erosion that eventually causes trees to fall into the water. As with small debris, medium and large debris can become waterlogged. Medium and large debris are transported at any level in the water column.

As debris travels downriver, it can float on the surface, in a vertical orientation with its root ball scraping along the riverbed, or in a submerged state. Debris that collects at river bends or channel constrictions can form entangled masses of logs that, when released by a major flood event, become log islands that can pose a major hazard to HKD infrastructure in its path. One such log island that was video recorded at Nenana in August 2008 swept away a fish wheel, which is a reasonable analogy to an HKD mounted on a floating platform.

Most floating debris follows the thalweg in straight sections of a river when the river stage is rising, but moves toward the riverbanks when the river stage is falling. Large-debris transport downriver can be hindered by a river's width and the radius of curvature of the river bends. Debris whose length approaches the width of a river is less likely to be transported downriver in one piece; it becomes jammed at a river bend or it breaks into smaller segments as the force of other logs piling against the blocking log exceeds its strength. Submerged debris (including neutrally buoyant debris) is common in most rivers in Alaska. Submerged debris has been observed catching on hydrokinetic device electrical cabling in the Yukon River at Eagle, Alaska, and it has been observed riding up the anchor chain of the mid-channel mooring buoy in the Tanana River at Nenana, Alaska. During flood stage conditions, extensive amounts of surface and submerged debris can be transported in the river flow. In locations of high turbulence, subsurface debris can be carried to the river surface by water boils and then expelled, to immediately sink.

In 2010, debris accumulation and impacts were responsible for ending HKD demonstration projects on the Yukon River, Alaska, at Ruby and Eagle and on the Mackenzie River, Northwest Territories, Canada, at Fort Simpson. Deployed debris-diversion boom systems at Ruby and Fort Simpson worked to some degree, but were ultimately unable to prevent debris accumulation or impacts that forced an end to the projects. These experiences illustrate the need to find debris-mitigation technologies if HKDs are to be a viable way to generate power in Alaska's rivers. Existing debris-mitigation methods include:

1. Using debris diversion booms
2. Placing HKDs in locations were debris encounters have a low probability of occurrence
3. Using manual or mechanical debris removal methods
4. Designing HKDs to be debris tolerant.
5. Furling HKDs (i.e., removing the HKD from the water or out of the debris travel path)
6. Blocking or capturing debris with trash racks

Important factors affecting debris-diversion boom performance include the angle between the boom pontoons, pontoon surface friction, current velocity, and the ratio of debris diameter to length. Reducing the separation angle between pontoons and reducing the surface friction of the pontoon surfaces improves the ability of the diversion boom to shed debris. Higher current velocities also improve the ability of a diversion boom to shed debris. Long, narrow logs that impinge the diversion pontoons are generally more difficult to clear than short, thick debris, because forces normal to the debris object increase the frictional resistance of debris against the diversion pontoon causing the debris to become pinned against it. The pinning force increases with log length, while the force parallel to a diversion boom pontoon is a function of the debris cross section. The sweeping force must exceed the resistance force to clear debris from the pontoons.

Fish Baseline Information about Juvenile and Larval Downstream Migration

The goal of the fish study was to provide baseline information about the downstream migration of juvenile and larval fishes in the mainstem of the Tanana River near Nenana, Alaska, to understand spatial and temporal patterns so that times of potential interactions between juvenile and larval fishes and a hydrokinetic turbine could be determined. To achieve this goal, the study objectives were to:

1. characterize the juvenile and larval fishes communities in the mainstem of the Tanana River, including species composition and relative abundance.
2. characterize the spatial and temporal patterns of the downstream juvenile and larval fishes migration and determine environmental associations with migration.

To accomplish these objectives, downstream migrating juvenile and larval fishes were sampled in the river margins and mid-channel of the Tanana River near Nenana. In addition to fish sampling, a suite of environmental variables was collected throughout the sampling season to explore possible associations of these environmental variables with temporal patterns of the downstream migrating juvenile and larval fish.

In the surface waters of the mid-channel, the location where a hydrokinetic device would likely be installed, at least six species were captured, with Chinook/coho salmon and chum salmon being the only commonly captured species, and whitefish, Arctic lamprey, and burbot being very infrequently captured. In the river margins, at least eleven species of fishes were captured, with whitefish being the most abundant, followed by longnose suckers, chum salmon, lake chub, larval lamprey, burbot, Arctic grayling, Chinook/coho salmon, slimy sculpin, Arctic lamprey, adult Alaskan brook lamprey, and northern pike. In both the mid-channel and margins, most of the captured fishes were relatively small juveniles (<10 cm), including age-1 Chinook/coho and age-0 chum salmon smolts that were migrating to the Bering Sea.

Several species/taxa of fishes displayed temporal trends in abundance in the Tanana River. Longnose sucker abundance had a small peak in late May; whitefish abundance peaked in late June. Other species of fish displayed increasing or decreasing trends in catches throughout the sampling season, such as chum and Chinook/coho salmon, both of which generally decreased in abundance, and lake chub, which increased in abundance. In contrast to the species that exhibited seasonal patterns in catches, the remaining species did not display temporal patterns in catches.

The seasonal patterns in catches of some fish species were associated with environmental variables. When abundance of woody debris increased, longnose sucker abundance increased while whitefish abundance decreased. When water temperature increased, catches of chum salmon, whitefish, longnose suckers, and lake chub all decreased. When turbidity decreased, catches of whitefish and longnose suckers both decreased. Finally, catches of chum salmon, whitefish, Chinook/coho salmon, and longnose suckers were all positively correlated to increasing river discharge.

Current State of Knowledge and Recommendations for Fisheries Studies

The realized impacts of hydrokinetic devices on fishes in Alaska are unknown at this time because no observational or modeling studies have been conducted on common fish species in Alaska. Results from studies conducted elsewhere suggest that realized impacts of hydrokinetic devices on fishes are likely related to the species and size of fish passing through a spinning turbine. To date, four studies have been

conducted in which fish were forced to pass through a spinning turbine. Of these three studies, only one was conducted in an actual free-flowing river. This study, which was conducted in 2009 at the Hastings, Minnesota, Mississippi Lock and Dam No. 2 Hydroelectric Project, monitored the survival and injury of several freshwater fish species, including representatives from the perch, sunfish, sucker, catfish, and temperate bass families, that passed through a HGE (Hydro Green Energy) hydroelectric turbine (Normandeau Associates 2009). Of fish that passed through the turbine, the survival estimate for those between 114 and 710 mm in size was 99%, and no blade-strike injuries were observed. Additionally, the turbine design appeared to eliminate the possibility of pressure-related injuries, as there was no operational head or sudden pressure changes. Based on the results of this study and the turbine design, the authors concluded that the HGE hydrokinetic unit "has little if any considerable impact on the fish populations in the vicinity of the Mississippi Lock and Dam No. 2 Hydroelectric project." (Normandeau Associates 2009, page ES-2).

Three additional studies on the impacts of hydrokinetic turbines on fishes have been conducted in laboratory flumes. The first study, which was conducted at Alden Research Laboratory, Inc., observed injury and survival rates as well as behavioral reactions and avoidance of two species of fish—rainbow trout and largemouth bass—that were exposed to two hydrokinetic turbines (Lucid spherical turbine and Welka UPG) in a flume (EPRI 2011). For fish that passed through the turbine at two different approach velocities (1.5 and 2.1 m/s), survival rates were greater than 98% for those fish that ranged from 125 to 250 mm in size. Injury rates as measured by de-scaling of turbine-exposed fish were also low (0.0 to 4.5%). Video observations of the fishes showed active avoidance of turbine passage by a large proportion of fish despite being released in close proximity (25 cm) to the leading edge of the turbine blade sweep. When released farther from the turbine, few if any of the fish passed through the spinning device.

The second study, which was conducted at Conte Anadromous Fish Research Laboratory, observed injury and survival rates as well as behavioral reactions and avoidance of two different species of fish—Atlantic salmon and American shad—that were exposed to EnCurrent turbines in a flume (referenced in EPRI 2011). A final report for this study has not been published, but preliminary results indicate that no Atlantic salmon smolts (size unknown) were killed or visibly injured by passing through the spinning turbine (EPRI 2010). Similarly, there was no clear evidence of strike injuries on American shad that had passed through the spinning turbine. However, mortality of American shad was observed in individuals that passed through the turbine as well as control individuals that did not pass through the turbine. Statistical analyses are not available to determine whether the mortality of turbine-exposed individuals was significantly different from control individuals. In behavioral observations, the turbine appeared to represent a swimming barrier for adult American shad trying to move upstream in the flume.

The third flume study, which was conducted at Oak Ridge National Laboratory, observed how several species of fish larvae and juveniles, including members of the perch, sunfish, minnow, and temperate bass families, encountered different blade profiles of hydrokinetic devices at different approach velocities, and how such encounters influenced survivorship (Schweizer et al. 2012). Importantly, this is the only study that has examined larval and juvenile fishes as small as 4 mm. Relatively high mortality of individuals resulted in an unbalanced study design that prevented statistical analyses and quantitative conclusions, but some general qualitative trends emerged. The presence of a spinning turbine blade in the path of drifting larval and juvenile fishes increased mortality rates when compared with control fishes that did not experience a spinning turbine blade. The mortality rate of experimental fishes appeared to be inversely

related to the development of the fish (size, age, and life stage) and the current velocity of the water. Mortality also appeared to be related to the shape of the leading edge of the turbine blade.

These observational results from in-river and flume studies indicate that for larger individuals of several fish families (>150 mm), downstream passage through hydrokinetic devices does not cause a direct threat of injury or death. However, spinning turbines may impede upstream migration of adult fishes such as American shad, and may cause deleterious effects on several species of small larval and juvenile fishes (<100 mm). Because the effects of hydrokinetic turbines on fishes appear to be related to the size and species of fish, as well as to water velocity and several engineering aspects of the turbine, there are no general rules governing the outcome of fish-turbine interactions. As such, outcomes of fish-turbine interactions from previous experiments may not necessarily apply to similar interactions involving different turbines and sizes and species of fishes in different riverine environments. Therefore, it is necessary to conduct studies on fish-turbine interactions for each deployment of a hydrokinetic device.

Specifically in Alaska, the river environment and fish community are completely different from those in previous laboratory experiments. The largest and most powerful rivers in Alaska are relatively fast and glacially turbid, and the fish community in these rivers contains small larvae and juveniles from several species whose behavior around a turbine has not been observed. These fish are particularly important because they support culturally and economically valuable subsistence, sport, and commercial fisheries (Bradley 2012). Because of the distinctive characteristics of Alaska rivers and the importance of fishes in them, fish-turbine interaction studies need to be conducted for hydrokinetic deployments in Alaska.

Implications for Hydrokinetic Energy Production Devices

The goal of HKD developers and users is to generate electricity from the hydrokinetic power of river currents economically (i.e., to make a profit for developers and utilities and provide power to consumers at an affordable cost). The interaction of HKDs with the river environment, which is the focus of this study, is one of the factors that can affect HKD power generation economics (other factors might include HKD development capital costs, the operating constraints of a given HKD, and the economics of the power market). Interactions between an HKD and a river's environment that affect the economics of an HKD include the following:

1. The power density and turbulence of a river's current, which determine the available extractable energy and the shear forces that create fatigue stresses in HKD infrastructure.
2. Suspended and bed load sediment concentrations, which can affect the rate of abrasion on HKD components and the erosion and deposition of sediment around riverbed-mounted HKD infrastructure.
3. Surface and subsurface woody debris that can accumulate on, or damage, HKD infrastructure.
4. Downstream migrating juvenile and larval fish and upstream migrating adult anadromous fish of commercial and cultural value. Concern about ensuring that fish stocks are not harmed by HKDs affects the degree of agency oversight and regulation, which add costs and delay timelines for HKD projects.

Selecting the best site for an HKD installation requires a characterization survey of the river to determine river power density and turbulence as a function of location and river discharge over as long a period of

record as possible. This information is needed to determine where the combination of high specific power density and low turbulence occurs that optimizes HKD power extraction efficiency. Selection of the best site for HKD installation also requires determining the river's suspended and bed load sediment concentrations as a function of discharge. In earlier river characterizations, the focus was only on determining power density. In some cases, the average power density across a river cross section was used. The results of this study indicate that it is important to determine the specific power density of the river, since the current flow is not the same everywhere in the river. It is also important to measure the river turbulence as a function of location and discharge. Turbulence both reduces the effectiveness of an HKD in converting a river's kinetic energy to electricity and increases shear loading on an HKD. Turbulence increases with discharge, and during high-water events, it can create sufficient vertical and horizontal flows such that submerged debris can be carried vertically and laterally as well as downstream (submerged root balls have been observed rising to a river's surface in a river boil and then sinking once the boil dissipates).

Most HKD site investigations include a multi-beam sonar bathymetric survey to determine riverbed conditions to aid in planning HKD installations. In the Tanana River, small-scale debris flowing in the lower third of the water column appears to have interfered with sonar returns, resulting in higher than normal uncertainties in bathymetry (a second bathymetry was done in a following year because of this problem). Small-scale debris flowing in the lower part of a river's water column probably exists in most large rivers that flow through timbered terrain (extensive small-scale debris was observed in the Yukon River at Eagle). The presence and amount of small-scale debris can be estimated by physical sampling at different depths in the water column.

With bathymetry, it becomes possible to conduct 2D and 3D hydrodynamic modeling to examine the flow and power density character of a river as a function of location rather than using current velocity transect measurements alone. If a river carries a high sediment load, then two bathymetries within the same open-water season along with suspended and bed load sediment concentration ratings curves are needed to calibrate the sediment transport model parameters, allowing for a complete analysis of the hydro-sedimentological character of the river. Such model characterization can provide information about changes in bathymetry as a function of discharge and, for 3D models, a quantitative estimation of turbulence. Models may also allow the inclusion of HKD modules to evaluate their influence on the river flow.

While the amount and type of debris may vary, most rivers carry woody debris to some extent, and HKD developers and users need to incorporate debris-mitigation strategies if they are to avoid disruptions to their operations. Such strategies may involve placing HKDs in channeled waterways behind dams or other structures that prevent debris from entering the water channel. Other mitigation methods may include designing HKDs to be debris tolerant or easily repaired when damaged or incorporating a detect-and-protect scheme of debris mitigation that is only deployed when debris is present (for locations with low probability of debris occurrence). Work on debris-deflection technology at the Tanana River Test Site has demonstrated that surface debris can be deflected in most situations with properly designed and deployed systems. However, no single debris-mitigation system will work for the variety of HKDs being developed, and much work remains to be done to find practical debris-mitigation systems that are suitable for HKDs.

Alaska regulators responsible for balancing the risks and benefits both to HKD project proponents and to public trust fish resources need to know the potential for, and magnitudes of, interactions between fish and any proposed HKD device. Until the permitting agencies have developed sufficient information to establish specific guidelines for HKD operations, there will be a need to gather device-specific information on the potential mechanisms for interactions (strike, pressure change, etc.) of the device with fish, site-specific information on which fish species and life stages may be present and susceptible to such interactions, and information about whether or not fish in fact interact with the device in a way harmful to them. Establishment of test bed sites and the sharing of engineering characteristics can be important ways to spread the risks and costs of acquiring the needed information. Each new evaluation and deployment adds to the knowledge base, but HKD proponents can expect a cautious approach to continue for the next few years (J. Durst – Alaska Dept. of Fish and Game, personal communication).

Recommendations

1. Focus research and development related to HKD interactions with Alaska's river/ocean environments at a center for hydrokinetic energy research and development (such as exists in Europe). The center would provide facilities for testing, consulting services for HKD developers and users, and information on lessons learned from their work and the work of others. The center would have a test site and mobile test-and-measurement capability for use at the test site or for transport to other sites for conducting specialized studies

   From observations of HKD demonstration projects in Alaska, it is apparent that individual developers struggle repeatedly to solve problems that are common to all HKD developers and users (e.g., debris, turbulence, model simulation, measurement technique development).

2. Conduct measurements of two bathymetries, current velocity, and turbulence in a single open-water season to support development and testing of 2D and 3D hydro-sedimentological models. These measurements would verify the usefulness of such models to evaluate river conditions (current, power density, turbulence, sediment transport) for HKD deployments as a function of location in a river reach, seasonally in a given year and over the period of record for discharge measurements.

3. Develop methods to detect and characterize debris, model debris/HKD infrastructure interactions, and develop technology and methods to mitigate debris-flow problems with HKDs. This recommendation also includes determining the influence of debris-mitigation methods on HKD performance. Modeling debris interaction with HKD devices requires combining 3D hydrodynamic modeling capability with 3D discrete element method simulations of debris under hydrodynamic forcing.

4. Conduct collaborative studies that include HKD developers/users and relevant agencies to provide information about HKD/fish interactions in Alaska. The lack of information about the impact of HKDs on Alaska's fish stocks has resulted in agencies (e.g., Alaska Dept. of Fish and Game) requiring studies that provide information to help them establish known procedures for HKD operators, such that the agencies have certainty in planning.

5. Conduct direct testing of HKD systems, measuring data to develop models of HKD economics to help developers and users assess economics. Such models should include physical factors to

allow assessments of the economics of present HKD state-of-the-art technology and that can be adjusted as the state of the art improves (e.g., debris-mitigation technology).

6. Conduct turbulence studies to better understand how turbulence magnitude changes in a river as a function of river discharge, to predict its effect on HKDs and to examine its role in debris-transport pathways. These studies would be facilitated by modeling efforts described in Recommendation 2.

References

Achord, S.R., Zabel, W., and Sanford, B.P. (2007). Migration timing, growth, and estimated parr-to-smolt survival rates of wild Snake River spring-summer Chinook salmon from the Salmon River basin, Idaho, to the lower Snake River. *Transactions of the American Fisheries Society*, 136: 142–154.

AEA (Alaska Energy Authority) (2011). Renewable Energy Atlas of Alaska, 29 pp.

AEA (Alaska Energy Authority) (2012). Alaska Energy Statistics CY 2011 – Preliminary, Institute of Social and Economic Research, University of Alaska Anchorage.

Akaike, H. (1973). Information theory and an extension of the maximum likelihood principle. *In:* Petrov, B.N., and Csaki, F. (Eds.), Proceedings of the 2nd International Symposium on Information Theory, pp. 267–281. Budapest: Akademiai Kiado.

Alt, K.T. (1987). Review of Sheefish (*Stenodus leucichthys*) Studies in Alaska. Fishery Manuscript No. 3. Alaska Department of Fish and Game, Division of Sport Fish, Juneau, AK.

Anyi, M., Kirke, B., and Ali, S. (2010). Remote community electrification in Sarawak, Malaysia. *Renewable Energy*, 35(7): 1609−1613.

Ashton, G. (1986). River and Lake Ice Engineering. Water Resources Publication.

Bedard, R.J., Privisic, M., and Polagye, B.L. (2009). Marine energy: How much development potential is there? RenewableEnergyWorld.com. Retrieved from http://www.renewableenergyworld.com/rea/news/print/article/2009/04/marine-energy-how-much-development-potential-is-yhere

Borba, B.M. (2007). Test Fish Wheel Project Using Video Monitoring Techniques, Tanana River, 2003. Fishery Data Series No. 07-55. Alaska Department of Fish and Game, Divisions of Sport Fish and Commercial Fisheries.

Bradford, M.J., Duncan, J., and Jang, J.W. (2008). Downstream migration of juvenile salmon and other fishes in the upper Yukon River. *Arctic*, 61: 255–264.

Bradley, J., Richards, D., and Bahner, C. (2005). Debris Control Structures – Evaluation and Countermeasures. Salem, OR: U.S. Department of Transportation: Federal Highway Administration.

Bradley, P.T. (2012). Characterizing the fish community in turbid Alaskan rivers to assess potential interactions with hydrokinetic devices. M.S. Thesis, University of Alaska Fairbanks.

Bradley, P.T., and Seitz, A.C. (2011). Characterization of the Juvenile Fish Community in the Middle Tanana River Near Nenana, Alaska. Alaska Department of Fish and Game Fisheries Resource Permit #SF2011-145 Completion Report.

Breeser, S.W., Stearns, F.D., Smith, M.W., West, R.L., and Reynolds, J.B. (1988). Observations of movements and habitat preferences of burbot in an Alaskan glacial river system. *Transactions of the American Fisheries Society*, 117: 506–509.

Brown, R.J., Bickford, N., and Severin, K. (2007). Otolith trace element chemistry as an indicator of anadromy in the Yukon River drainage coregonine fishes. *Transactions of the American Fisheries Society,* 136: 678–690.

Burkholder, A., and Bernard, D.R. (1994). Movements and Distribution of Radio-Tagged Northern Pike in Minto Flats. Alaska Department of Fish and Game, Fisheries Manuscript No 94-1, Anchorage, AK, USA.

Burril, S.E., Zimmerman, C.E., Finn, J.E., and Gillikin, D. (2009). Abundance, timing of migration, and egg-to-smolt survival of juvenile chum salmon, Kwethluk River, Alaska. U.S. Department of the Interior, Project 619.

Cada, G., Ahlgrimm, J., Bahleda, M., Bigford, T., Stavrakas, S.D., Hall, D., Moursund, R., and Sale, M. (2007). Potential impacts of hydrokinetic and wave energy conversion technologies on aquatic environments. *Fisheries*, 32: 174–181.

Cappiello, T.A., and Bromaghin, J.F. (1997). Mark-recapture abundance estimate of fall-run chum salmon in the Upper Tanana River, Alaska, 1995. *Alaska Fisheries Research Bulletin*, 4: 12–35.

Chang, F.F., and Shen, H.W. (1979). Debris Problems in the River Environment. Federal Highway Administration.

Couch, S.J., and Bryden, I.G. (2004). The impact of energy extraction on tidal flow development. Presented at 3rd International Conference on Marine Renewable Energy, Blyth, 2004, available from http://www.oreg.ca/docs/ImpactTidalEnergyExtraction.pdf.

Craig, P.C., and Wells, J. (1976). Life history notes for a population of slimy sculpin (*Cottus cognatus*) in an Alaskan Arctic stream. *Journal of the Fisheries Research Board of Canada,* 33: 1639–1642.

Crowe, C., Elger, D., Williams, B., and Roberson, J. (2009). *Engineering Fluid Mechanics*, 9th ed. John Wiley & Sons.

Dahlberg, M.L., and Phinney, D.E. (1967). The use of adipose fin pigmentation for distinguishing between juvenile Chinook and coho salmon in Alaska. *Journal of the Fisheries Research Board of Canada,* 24: 209–210.

Daly, S.F. (1991). Frazil ice blockage of intake trash racks. Cold Regions Research and Engineering. Hanover, NH, U.S. Army Corps of Engineers. Cold Regions Technical Digest 91-1, 14 pp.

Dauble, D.D., Page, T.L., and Hanf, R.W. (1989). Spatial distribution of juvenile salmonids in the Hanford Reach, Columbia River. *Fishery Bulletin*, 87: 775–790.

Daum, D.W., and Osborne, B.M. (1998). Use of fixed-location, split-beam sonar to describe temporal and spatial patterns of adult fall chum salmon migration in the Chandalar River, Alaska. *North American Journal Fisheries Management,* 18: 477–486.

Daum, D.W., and Flannery, B.G. (2011). Canadian-origin Chinook salmon rearing in non-natal U.S. tributary streams of the Yukon River, Alaska. *Transactions of the American Fisheries Society*, 140: 207–220.

Durst, J.D. (2001). Fish Habitats and Use in the Tanana River Floodplain Near Big Delta, Alaska, 1999-2000. Technical Report No. 01-05. Alaska Department of Fish and Game, Habitat and Restoration Division.

Duvoy, P., and Toniolo, H. (2012). HYDROKAL: A Module for In-stream Hydrokinetic Resource Assessment. *Computers & Geosciences*, 39 (February): 171–181. doi:10.1016/j.cageo.2011.06.016.

EPRI (Electric Power Research Institute) (2010). Assessment of the Environmental Effects of Hydrokinetic Turbines on Fish: Desktop and Laboratory Flume Studies. Quarterly Technical Progress Report No. 4.

EPRI (Electric Power Research Institute) (2011). Evaluation of Fish Injury and Mortality Associated with Hydrokinetic Turbines. Palo Alto, CA. Report #1024569.

Evenson, M.J. (2002). Optimal Production of Chinook Salmon from the Chena and Salcha Rivers. Fishery Manuscript Series No. 02-01. Alaska Department of Fish and Game, Division of Sport Fish.

Francisco, K. (1977). Second Interim Report of the Commercial Fish Technical Evaluation Study. Special Report No. 9, Joint State/Federal Fish and Wildlife Advisory Team, Alaska Department of Fish and Game.

Gissberg, J.G., and Benning, D.S. (1965). Yukon Foundation Studies Summary Report, 1965. U.S. Department of Interior, Fish and Wildlife Service, Anchorage, AK.

Gregory, R.S., and Levings, C.D. (1998). Turbidity reduces predation on migrating juvenile Pacific salmon. *Transactions of the American Fisheries Society*, 127: 275–285.

Hastie, T.J., and Tibshirani, R.J. (1990). *Generalized Additive Models.* London: Chapman & Hall.

Hemming, C.R., and Morris, W.A. (1999). Fish Habitat Investigations in the Tanana River Watershed, 1997. Technical Report No. 99-01. Alaska Department of Fish and Game, Habitat and Restoration Division.

Hau, E. (2006). *Wind Turbines: Fundamentals, Technologies, Application, Economics*. Birkhäuser, 783 pp.

Hicks, F. (2009). An overview of river ice problems: CRIPE07 guest editorial. *Cold Regions Science and Technology*, 55: 175–185.

Horn, C. (2012). Nenana River @ Nenana, Alaska Sep. 22, 2012. http://www.youtube.com /watch?NR=1&feature=endscreen&v=qPjCw5Ts7kg.

Johnson, J.B. (2012, unpublished). Quarterly Progress Report to the Denali Commission - Eagle Hydrokinetic Project - Eagle Hydro - INE - Debris - Anchoring, University of Alaska - Fairbanks**:** 9 pp.

Johnson, J.B., and Pride, D.M. (2010). River, Tidal, and Ocean Current Hydrokinetic Energy Technologies: Status and Future Opportunities in Alaska. Fairbanks, Alaska Center for Energy and Power, 32 pp.

Johnson, J.B., Toniolo, H., and Seitz, A.C.(2011). The Alaskan way. *International Water Power & Dam Construction*, 63(7): 4. www.waterpowermagazine.com, http://www.uaf.edu/files/acep/038_041wp0711_z.pdf

Khan, M., Iqbal, M., and Quaicoe, J. (2008). River current energy conversion systems: Progress, prospects and challenges. *Renewable and Sustainable Energy Reviews*, 12(8): 2177–2193.

Khan, M.J., Bhuyan, G., Iqbal, M.T., and Quaicoe, J.E. (2009). Hydrokinetic energy conversion systems and assessment of horizontal and vertical axis turbines for river and tidal applications: A technology status review. *Applied Energy*, 86: 1823–1835. www.elsevier.com/locate/apenergy

Kirillova, E.A., Kirillov, P.I., Kucheryavyy, A.V., and Pavlov, D.S. (2011). Downstream migration in ammocoetes of the Arctic Lamprey *Lethenteron camtschaticum* in some Kamchatka Rivers. *Journal of Ichthyology*, 51: 1117–1125.

Koenig, M. (2002). Life histories and distributions of Copper River fishes. *In*: Mount, J.F., Moyle, P., and Yarnell, S. (Eds.), Glacial and periglacial process as hydrogeomorphic and ecological drivers in high-latitude watersheds. UC Davis Geology Department, Davis, CA, USA.

Lagasse, P.C. (2010). Effects of Debris on Bridge Pier Scour (NCHRP Report 653, Project 24-26). Washington, DC: National Cooperative Highway Research Program, Transportation Research Board, National Academy of Sciences, ISSN: 0077-5614, ISBN: 978-0-309-11834-7, 115 pp. http://onlinepubs.trb.org/onlinepubs/nchrp/nchrp_rpt_653.pdf

Langley, D.E. (2006). Calculation of Scour Depth at the Parks Highway Bridge on the Tanana River at Nenana, Alaska, Using One- and Two-Dimensional Hydraulic Models. U. S. Geological Survey Scientific Report 2006-5023**,** 19 pp. http://pubs.usgs.gov/sir/2006/5023/index.html.

Lucas, M.C., and Baras, E. (2001). *Migration of Freshwater Fishes*. Oxford, UK: Blackwell Science.

Mains, E.M., and Smith, J.M. (1964). The distribution size, time and current references of seaward migrant chinook salmon in the Columbia and Snake rivers. Washington State Department of Fish. Fisheries Research Papers 2: 5–43.

McPhail, J.D., and Paragamian, V.L. (2000). Burbot biology and life history. *Fisheries Management Section of the American Fisheries Society*, 128: 10–23.

Mecklenburg, C.W., Mecklenburg, T.A., and Thorsteinson, L.K. (2002). *Fishes of Alaska*. Bethesda, MD: American Fisheries Society.

Mecum, R.D. (1984). Habitat utilization by fishes in the Tanana River near Fairbanks, AK. M.S. Thesis, University of Alaska Fairbanks.

Miller, G., Franceschi, J., Lese, W., and Rico, J. (1986). The Allocation of Kinetic Hydro Energy Conversion Systems (KHECS) in USA Drainage Basins: Regional Resource and Potential Power. NYUDAS 86-151, Final Report, August, 54 pp.

Muhlfield, C.C., Bennett, D.H., Steinhorst, R.K., Marotz, B., and Boyer, M. (2008). Using bioenergetics modeling to estimate consumption of native juvenile salmonids by nonnative northern pike in the upper Flathead River system, Montana. *North American Journal of Fisheries Management*, 28: 636–648.

Normandeau Associates, Inc. (2009). An estimation of survival and injury of fish passed through the Hydro Green Energy hydrokinetic system, and a characterization of fish entrainment potential at the Mississippi lock and dam no. 2 hydroelectric project (P-4306) Hastings, Minnesota. Prepared for Hydro Green Energy, LLC, Drumore, PA, USA

NUL (Northland Utilities Limited) (2012). Information Request, NTPC GRA 2012/13 and 2013/14: 11–13. http://www.ntpc.com/documents/NTPC%202012_14%20IR%20Response%20-%20NUL,%20June%208,%202012.pdf

Oberg, K.A., Rehmann, C.R., and Nystrom, E.A. (2002). Measurement of turbulence with acoustic Doppler current profilers – Sources of error and laboratory results. *In:* Hydraulic Measurements and Experimental Methods 2002, 1–10. American Society of Civil Engineers.

Osterkamp, T.E., and Gosink, J.P. (1983). Frazil ice formation and ice cover development in Interior Alaska streams. *Cold Regions Science and Technology*, 8: 43–56.

Ott, A.G., Winters, J.F., and Townsend, A.H. (1998). Juvenile Fish Use of Selected Habitats in the Tanana River near Fairbanks (preliminary report). Tech Rep No. 97-1, Alaska Department of Fish and Game, Habitat and Restoration Division, Juneau, Alaska.

Pearse, G.A. (1974). A study of a typical spring fed stream of interior Alaska. Alaska Department of Fish and Game. Federal Aid in Fish Restoration, 1973–1975, Project F-9-6(15)G-III-G.

Pelunis-Messier, D. (2010). YRITWC Ruby Hydro_Sinking Turbine July 6 2010. Youtube.com, Uploaded July 8, 2010. http://www.youtube.com/watch?v=57OA3svudvY

Peterson, B.D. (1997). Estimation of abundance and mortality of emigrating chum salmon and Chinook salmon in the Chena River, Alaska. M.S. Thesis, Alaska Cooperative Fish and Wildlife Research Unit, University of Alaska Fairbanks.

Pierce, G.S. (1977). Spawning migration and population structure of longnose sucker (*Catostomus catostomus*) in Alaska. M.S. Thesis, University of Idaho, Moscow, Idaho.

Polagye, B., and Previsic, M. (2006). System level design, performance, cost and economic assessment – Knik Arm Alaska tidal in-stream power plant. EPRI-TP-006 Alaska, June 10, 2006, 128 pp.

Previsic, M. (2008). System Level Design, Performance, Cost and Economic Assessment – Alaska River In-stream Power Plants. EPRI-RP-006 Alaska, October, 99 pp.

Previsic, M., and Bedard, R. (2008). River In-stream Energy Conversion (RISEC) Characterization of Alaska Sites. EPRI-RP-003-Alaska, 74 pp. http://oceanenergy.epri.com/attachments/risec/reports/Alaska_RISEC_Final_Feasibility_Study_Report_10-31-08.pdf

Ransom, B.H., Johnston, S.V., and Steig, T.W. (1998). Review on monitoring adult salmonid (*Oncorhynchus* and *Salmo* spp.) escapement using fixed-location split-beam hydroacoustics. *Fisheries Research*, 35: 33–42.

Roberge, M., Hume, J.M.B., Minns, C.K., and Slaney, T. (2002). Life History Characteristics of Freshwater Fishes Occurring in British Columbia and the Yukon, with Major Emphasis on Stream Habitat Characteristics. Canadian Manuscripts and Reports on Fisheries and Aquatic Sciences 2611, xiv + 248 pp.

Schaefer, V. (1950). The formation of frazil and anchor ice in cold water. *Transactions, American Geophysical Union*, 31(6): 885. doi:10.1029/TR031i006p00885.

Schmid, J. (2012). Nenana debris – July 2012. www.youtube.com/watch?v=94-d5mKl9og.

Schweizer P.E., Cada, G.F., and Bevelhimer, M.S. (2012). Laboratory Experiments on the Effects of Blade Strike from Hydrokinetic Energy Technologies on Larval and Juvenile Freshwater Fishes. Oak Ridge National Laboratory, Report #ORNL/TM-2012/108.

Scott, W.B., and Crossman, E.J. (1973). *Freshwater Fishes of Canada*. Fisheries Research Board of Canada, Ottawa, Bulletin 184.

Seitz, A.C., Moerlein, K., Evans, M.D., and Rosenberger, A.E. (2011). Ecology of fishes in a high-latitude, turbid river with implications for the impacts of hydrokinetic devices. *Reviews in Fish Biology and Fisheries*, 21: 481–496.

Shestakov, A.V. (1991). Preliminary data on the dynamics of the downstream migration of coregonid larvae in the Anadyr River. *Journal of Ichthyology*, 31: 65–74.

Sutton, T.M., and Bowen, S.H. (1994). Significance of organic detritus in the diet of larval lampreys in the Great Lakes Basin. *Canadian Journal of Fisheries and Aquatic Sciences*, 51: 2380–2387.

TerraSond (2008). Late Fall Reconnaissance Survey for Hydroelectric Turbine Sites. *Appendix_Data_Files\Terrasond_2008*

Thompson, R. (2010, December 16). Lessons Learned from Turbine Project. *Northern News Service: Deh Cho Drum*, pp. 3–4.

Todd, G.L. (1994). A lightweight, inclined-plane trap for sampling salmon smolts in rivers. *Alaska Fishery Research Bulletin*, 1: 168–175.

Todd, I.S. (1966). A technique for the enumeration of chum salmon fry in the Fraser River, British Columbia. *The Canadian Fish Culturist*, 38: 3–35.

Toniolo, H. (2012). Hydrokinetic assessment of the Kvichak River near Igiugig, Alaska, using a two-dimensional hydrodynamic model. *Energy and Power Engineering*, 4(6): 422–431. doi:10.4236/epe.2012.46056.

Toniolo, H. (2013). Bed forms and sediment characteristics along the thalweg on the Tanana River near Nenana, Alaska, USA. *Journal of Natural Resources*, 4: 20–30. doi: 10.4236/nr.2013.41003

Toniolo, H., Duvoy, P., Vanlesberg, S., and Johnson, J. (2010). Modelling and field measurements in support of the hydrokinetic resource assessment for the Tanana River at Nenana, Alaska. Proceedings of the Institution of Mechanical Engineers, Part A: *Journal of Power and Energy*, 224(8) (December 1): 1127–1139. doi:10.1243/09576509JPE1017.

Tyler, R.N. (2011). River Debris: Causes, Impacts, and Mitigation Techniques. Fairbanks, Alaska Center for Energy and Power, 33 pp. http://www.uaf.edu/files/acep/2011_4_13_AHERC-River-Debris-Report.pdf

Tyler, R.W. (1979). Method of sampling seaward migrations of juvenile salmon. *The Progressive Fish-Culturist*, 41: 78–81.

USEIA (2012). State Electricity Profiles 2010. Washington, DC: U.S. Energy Information Administration, 317 pp.

Venables, W.N., and Dichmont, C.M. (2004). GLMs, GAMs, and GLMMs: An overview of theory for applications in fisheries research. *Fisheries Research*, 70: 319–337.

Vladykov, V.D., and Kott, E. (1978). A new nonparasitic species of the Holarctic lamprey genus Lethenteron Creaser and Hubbs, 1922, (*Petromyzontidae*) from northwestern North America with notes on other species of the same genus. Biological Papers of the University of Alaska, Number 19.

Walsh, C., Fochesatto, J., and Toniolo, H. (2012). The importance of flow and turbulence characteristics for hydrokinetic energy development on the Tanana River at Nenana, Alaska. Proceedings of the Institution of Mechanical Engineers, Part A: *Journal of Power and Energy*, 226(2) (March 1): 283–299. doi:10.1177/0957650911424025.

West, R.L., Smith, M.W., Barber, W.E., Reynolds, J.B., and Hop, H. (1992). Autumn migration and overwintering of Arctic grayling in coastal streams of the Arctic National Wildlife Refuge. *Transactions of the American Fisheries Society*, 121: 709–715.

Whalen, K.G., Parrish, D.L., and McCormick, S.D. (1999). Migration timing of Atlantic salmon smolts relative to environmental and physiological factors. *Transactions of the American Fisheries Society*, 128: 289–301.

Wilson, M., Saylor, B., Szymoniak, N., Colt, S., and Fay, G. (2008). Components of Delivered Fuel Prices in Alaska. Prepared for the Alaska Energy Authority, Anchorage: University of Alaska Anchorage, Institute of Social and Economic Research.

Wolter, C., and Sukhodolov, A. (2008). Random displacement versus habitat choice of fish larvae in rivers. *River Research and Applications*, 24: 661–672.

Woodard, C. (2012). Maine tidal turbine goes online, first in North America. *Portland Press Herald.* Portland: 1. http://www.pressherald.com/news/ORPC-turbine-off-Eastport-is-the-first-to-do-so-in-North-America.html.

Zhang, Y. (2006). CCHE-GUI – Graphical Users Interface for NCCHE Model User's Manual – Version 3.0. National Center for Computational Hydroscience and Engineering, Technical Report No. NCCHE-TR-2006-2. October.

Appendices

Appendix A – Papers Derived from Study

Modelling and field measurements in support of the hydrokinetic resource assessment for the Tanana river at Nenana, Alaska

H Toniolo[1]*, P Duvoy[1], S Vanlesberg[2], and J Johnson[3]
[1]Department of Civil and Environmental Engineering, University of Alaska Fairbanks, Fairbanks, Alaska, USA
[2]School of Water Resources, University of Littoral, Santa Fe, Argentina
[3]Intitute of Northern Engineering, University of Alaska Fairbanks, Fairbanks, Alaska, USA

The manuscript was received on 8 April 2010 and was accepted after revision for publication on 26 July 2010.

DOI: 10.1243/09576509JPE1017

Abstract: A comprehensive methodology to assess the hydrokinetic potential of a reach of the Tanana river near Nenana, Alaska, is developed to help determine the suitability of the reach for installing and operating hydrokinetic electric turbines. The methodology utilizes field measurements and two-dimensional model simulations to define the discharge, velocity, power density, turbulence, and Froude number throughout the river reach. Thalweg stability is assessed using the maximum cross-sectional velocity, specific discharge, and turbulence. The thalweg was determined to be stable, for the current river condition, from the upstream end of the reach to about 800 m downstream. From 800 m to the end of the reach, at 1100 m, river hydrodynamics indicate an unstable thalweg shifting towards the right bank. The thalweg instability is associated with the transition between upstream and downstream river bends, which may migrate with river stage, bed load, existing bed conditions, and other factors. The flow is subcritical with an average Froude number of 0.30 along the thalweg. Averaged measured velocities along the thalweg are about 1.5 m/s. The average value for instantaneous power density is approximately 4500 W/m^2 at the period of measurement (late August). Study results indicate that hydraulic conditions in the river reach may be suitable for turbine operations above the 800 m location with the exception of a possible eddy located around the 400 m location.

Keywords: stream, resource assessment, numerical modelling, power density, turbulence

1 INTRODUCTION

The need to reduce dependence on fossil fuels and to reduce greenhouse gas emissions is creating an ever-increasing interest in utilizing renewable energy resources, including the kinetic energy from the currents in large rivers using in-stream hydrokinetic power turbines. Alaska, with 40 per cent of the US's hydrokinetic river energy [1] and over 300 rural villages located near large rivers that are not connected to a regional electrical grid has a particular interest in taking advantage of in-stream hydrokinetic turbine generation of electrical power [2–4]. Rural Alaskan communities are particularly affected by energy costs, paying more than three times the US average, a hardship compounded by per capita incomes less than 75 per cent of the US average [5]. Energy costs consumed about 10 per cent of the total income in rural villages in 2000 [6], and that percentage continues to increase.

Understanding the hydraulic characteristics of a specific reach of river under consideration as a possible location for one or more hydrokinetic turbines is a necessary first step to determine the base-line river dynamics and to plan turbine installations. Since river dynamics respond immediately to objects placed in the current, it is important to know a river's base-line character to assess changes in river dynamics that result from the installation and operation of a turbine.

The suitability of a specific reach of river for the installation and operation of in-stream hydrokinetic turbines (singly or in arrays) depends on river dynamics, bathymetry, and the stability of

*Corresponding author: Department of Civil and Environmental Engineering, University of Alaska Fairbanks, PO Box 755900, Fairbanks, AK 99775-5900, USA.
email: hatoniolo@alaska.edu

Computers & Geosciences 39 (2012) 171–181

Contents lists available at ScienceDirect

Computers & Geosciences

journal homepage: www.elsevier.com/locate/cageo

HYDROKAL: A module for in-stream hydrokinetic resource assessment

Paul Duvoy*, Horacio Toniolo

Department of Civil and Environmental Engineering, University of Alaska Fairbanks, Fairbanks, AK, USA

ARTICLE INFO

Article history:
Received 19 December 2010
Received in revised form
18 June 2011
Accepted 20 June 2011
Available online 21 July 2011

Keywords:
Stream
Resource assessment
Instantaneous power density
Numerical modelling

ABSTRACT

A new tool for hydrokinetic energy potential assessment in rivers—HYDROKAL, which stands for a "hydrokinetic calculator"—is presented. This tool was developed in the Fortran 90 programming language as an external module for the CCHE2D application, an existing two-dimensional hydrodynamic numerical model developed at the National Center for Computational Hydroscience and Engineering, University of Mississippi. Velocity outputs generated by the CCHE2D model are used by HYDROKAL to compute the instantaneous power density, an essential element in calculating the hydrokinetic power of a river reach. The tool includes a user-defined efficiency factor to account for turbine efficiency, which is fundamental for estimating the energy that could be harvested from the river. For each river cross section along the computational domain, maximum velocity and specific discharge are identified to assist in estimating the stability of the river reach and, thus, the feasibility of installing an in-stream turbine. A Python script was also developed to export the results from HYDROKAL to CCHE2D. HYDROKAL is applied to a reach of the Tanana River at Nenana, Alaska, USA.

1. Introduction

The feasibility of extracting river energy using hydrokinetic devices is drawing national and international attention due to higher fuel costs, growing demand for electric energy, and increased focus on renewable energy resources.

Conventional hydroelectric systems use reservoirs to create an artificial water head to extract the potential energy of passing water through a turbine. In contrast, a river current device takes water kinetic energy to generate electricity without changing the water level. The same principle of kinetic energy conversion is applied in the tidal (marine) environment and wind (Khan et al., 2008). Thus, the footprint created by hydrokinetic turbines is small compared to that of manmade reservoirs.

On the many challenges faced by researchers working on hydrokinetic energy extraction, the first question to address is if there are enough resources to extract energy in a cost-effective manner (Khan et al., 2008). This question can be investigated using field measurements, numerical modeling, or a combination of both. This work focuses on the quantification of the power density function in rivers using numerical modeling combined with field measurements. Computational hydrodynamic and sediment transport models generally require numerical solutions of at least the following governing differential equations: continuity, momentum, and sediment conservation (Papanicolaou et al., 2008). Since flow and sediment transport in natural rivers are biphase three-dimensional phenomena, their simulation is more accurately accomplished using three-dimensional models. However, three-dimensional modeling is computationally expensive. Thus, simplified models (one- and two-dimensional) are usually applied to solve engineering problems. One-dimensional models are useful for short- and long-term modeling of flow and sediment transport processes of an entire river reach (Wu, 2007). Hydrodynamic processes in one-dimensional models must be expressed in terms of cross-sectional properties. Furthermore, one-dimensional models are limited by the fact that they cannot resolve local details of flow and mobile-bed dynamics (Spasojevic and Holly, 2008).

Two- and three-dimensional models are frequently used for detailed analysis of morphodynamic processes in a particular subreach subject to complex flow conditions such as bends and hydraulic structures (Wu, 2007). Three-dimensional models require extensive use of central processing unit (CPU) time. This demand can be lessened if the hydrostatic pressure assumption replaces the vertical momentum equation and if a true unsteady calculation per time step is used instead of a single accurate steady-state solution (Spasojevic and Holly, 2008). In general, open-channel flows in nature can be treated like shallow water problems, because the effect of vertical motions is generally insignificant. Thus, a depth-integrated two-dimensional model is usually acceptable for studying open-channel hydraulics with reasonable accuracy and efficiency (Jia and Wang, 1999).

This work focuses on the development of a new hydrokinetic calculator module (HYDROKAL) to estimate the instantaneous power density function in a river reach, as well as the location of maximum velocity and maximum specific discharge in each river cross section. The tool also includes a user-defined efficiency factor to account for

*Corresponding author. Fax: +1 907 474 6087.
E-mail address: poduvoy@alaska.edu (P. Duvoy).

0098-3004/$ - see front matter © 2011 Elsevier Ltd. All rights reserved.
doi:10.1016/j.cageo.2011.06.016

The importance of flow and turbulence characteristics for hydrokinetic energy development on the Tanana River at Nenana, Alaska

C Walsh[1], **J Fochesatto**[2], and **H Toniolo**[1]*
[1]Department of Civil and Environmental Engineering, University of Alaska Fairbanks, Fairbanks, Alaska, USA
[2]Department of Atmospheric Sciences, University of Alaska Fairbanks, Fairbanks, Alaska, USA

The manuscript was received on 22 April 2011 and was accepted after revision for publication on 30 August 2011.

DOI: 10.1177/0957650911424025

Abstract: The site selection for the installation of hydrokinetic devices along a river reach is an issue of fundamental importance. While it is acknowledged that multiple factors such as accessibility, navigation, safety, and hydraulics, among many others, must be considered in the final decision, this article focuses on the influence of river morphology on turbulence flow parameters. Specifically, continuous high-resolution velocity measurements from a hydrokinetic resource assessment on the Tanana River near Nenana in the interior of Alaska are analysed to estimate, kinetic energy (KE), turbulent kinetic energy (TKE) as well as KE partition at particular locations. To accomplish these tasks, two different methods used to rotate the coordinate systems into the main flow direction are correlated and compared in order to extract the turbulent parameters from the main flow. The coordinate system methods include the streamline coordinate rotation and the extraction of statistical fluctuations from the average flow. The streamline coordinate rotation method is chosen to extract the TKE in temporal series. The calculated TKE was up to 30 per cent of the total flow KE in measurements located in pools and dissipated downstream, beyond the highly turbulent locations of bathymetric depressions and river bends. The overall KE increased over a bed free of major macro-obstacles and reduced depth, where the TKE fraction accounted for only 2 per cent of the total KE. The visualizations of the KE and TKE are compared with the river morphology, leading to identification of helical flow, flow separation, and turbulent flow structures along the river bend and in pools to help the decision-making process in hydrokinetic planning.

Keywords: turbulence, kinetic energy, helical flow, detachment, vortex tube development

1 INTRODUCTION

Much analysis is done in engineering and hydraulic work with the average velocity values from acoustic Doppler current profiler (ADCP) measurements. However, useful flow information on small-scale turbulent flow structures is not retained when the data are not fully detailed in space and time. Fluctuations in velocity magnitude, velocity direction, associated kinetic energy (KE), and turbulent kinetic energy (TKE) are not fully visualized when average values are considered. Thus, it is important to include the temporal analysis and the energy distribution of flow measurements when designing river structures and location of hydrokinetic turbines. If the infrastructure is not designed to withstand the fluctuating river energy, the hydraulic structures and river turbines may not perform as designed.

Dynamic perturbations such as eddies occurring in a timescale from seconds to minutes can easily be observed on the free water surface in natural (stream) and artificial (flume) settings. These fluctuations provide insight to the macro-turbulence

*Corresponding author: Department of Civil and Environmental Engineering, University of Alaska Fairbanks, PO Box 755900, Fairbanks, AK 99775-5900, USA.
email: hatoniolo@alaska.edu

River Debris:

Causes, Impacts, and Mitigation Techniques

Ryan N. Tyler

Prepared for Ocean Renewable Power Company
By the Alaska Center for Energy and Power, April 13, 2011

ACEP
Alaska Center for Energy and Power

Rev Fish Biol Fisheries
DOI 10.1007/s11160-011-9200-3

REVIEWS

Ecology of fishes in a high-latitude, turbid river with implications for the impacts of hydrokinetic devices

Andrew C. Seitz · Katie Moerlein · Mark D. Evans · Amanda E. Rosenberger

Received: 3 August 2010 / Accepted: 19 January 2011

Abstract Hydrokinetic devices generate electricity by capturing kinetic energy from flowing water as it moves across or through a rotor, without impounding or diverting the water source. The Tanana River in Alaska, a turbid glacial system, has been selected as a pilot location to evaluate the effects of such a device on fish communities that are highly valued by subsistence, sport, and commercial users. The basic ecology and habitat use of fishes in turbid glacial systems are poorly understood; therefore it is necessary to study the species composition of the fish community and the spatial and temporal patterns of mainstem river use by these fishes to evaluate impacts of a hydrokinetic device. In this document, we provide an overview of existing knowledge of fish ecology in the Tanana River and impacts of hydrokinetic devices on fishes in other river systems. Seventeen fish species are known to inhabit the Tanana River and several may utilize the deepest and fastest section of the channel, the probable deployment location for the hydrokinetic device, as a seasonal migration corridor. Previous studies in clearwater river systems indicate that mortality and injury rates from turbine passage are low. However, the results from these studies may not apply to the Tanana River because of its distinctive physical properties. To rectify this shortcoming, a conceptual framework for a comprehensive fish ecology study is recommended to determine the impacts of hydrokinetic devices on fishes in turbid, glacial rivers.

Keywords Hydrokinetics · Tanana river · Turbine · Glacial river · Salmonid · Smolts

A. C. Seitz (✉) · K. Moerlein · M. D. Evans · A. E. Rosenberger
School of Fisheries and Ocean Sciences, University of Alaska Fairbanks, PO Box 757220, Fairbanks, AK 99775-7220, USA
e-mail: acseitz@alaska.edu

Published online: 12 February 2011

Introduction

In-stream hydrokinetic devices generate electricity by capturing kinetic energy from flowing water as it moves across or through a rotor, without impounding or diverting the water source (Cada et al. 2007). These devices may aid in alleviating the high cost (>US$1 per kW h) of diesel-generated electricity in remote communities near large rivers. For example, Alaska has many villages located along large, turbid glacial rivers and most of them are not connected to the main electrical grid supplying power to the state's large cities. Hydrokinetic turbine projects are either being developed or considered for many of these rural communities. Development projects are actively under construction at Eagle and Ruby, both on the Yukon River, while feasibility studies are being conducted for the communities of Whitestone and Nenana on the Tanana River and Igiugig on the Kvichak River (Previsic et al. 2008). Other

Characterization of the juvenile fish community in the middle Tanana River near Nenana, AK

November 2011

Parker T. Bradley
Andrew C. Seitz
School of Fisheries and Ocean Sciences
University of Alaska Fairbanks
P.O. Box 757220
Fairbanks, AK 99775-7220
(907) 474-5254
ptbradley@alaska.edu
acseitz@alaska.edu

Project conducted under State of Alaska Fish Resource Permit #SF2011-145

Appendix B – AHERC Equipment and Operation Notes

1. Boat and General Equipment

The research boat (Figure B-1) is a trailerable 6 m × 1.8 m (20 ft × 6 ft) riveted aluminum jon boat powered by a 30 hp outboard motor with a 25.4 cm diameter × 20 cm pitch (10 in. × 8 in.) prop.

Figure B-1. Research boat on trailer with mounted ADCP & GPS.

The boat is operated from a side-mounted steering and control console. The lightweight flat-bottom hull form minimizes the effect of turbulence on the motion of the boat, making a relatively stable instrument platform. The low-pitch prop improves control at low speed, enhancing the ability to maintain a stationary position in the channel or make accurate survey transects. A removable canvas top with side curtains protects operators and equipment from inclement weather. For general navigation and operation, the boat is equipped with a 200 kHz Humminbird model 161 Combo fathometer/GPS.

The boat electrical system is a 100 AH 12 V lead-acid battery, charged by the outboard motor alternator. A separate 12 AH 12 V gel cell battery provides power to the scientific equipment. The separate battery system can be used as a stand-alone battery or connected to the boat's electrical system through an isolation diode. The isolation diode reduces the episodic power fluctuations caused by starting the motor, while still enabling the scientific equipment battery to be charged by the boat charging system. Modular aluminum rail fittings are fixed amidships on the port and starboard gunwales to accommodate a 6 cm (2.4 in.) aluminum tube that spans the width of the boat for mounting sonar equipment. The tube is fixed with setscrews to allow easy rotation of equipment out of the water. By using both gunwales as mounting points, the spanning 2 in. tube adds stiffness to the lightweight hull that otherwise would be subject to excessive twisting if the sonar equipment were fastened to only one side. A second equipment-mounting frame is place on the forward part of the boat. This frame is a welded aluminum box tube 5 cm × 5 cm (2 in. × 2 in.) secured to the port and starboard gunwales with a center 7.6 cm × 7.6 cm (3 in. × 3 in.) aluminum box tube and extending to the bow to support a precision sounding reel for lowering equipment off of the bow.

1.1 Anchor and Mooring Buoy

In spring 2011, a mid-channel mooring system was deployed in the Tanana River. The system, which initially supported baseline fish studies at the river test sight, was designed to allow it to be a mooring site for a hydrokinetic generating device and to accommodate a debris load if necessary. The system consists of a 1500 kg (3300 lb) Flipper Delta® high holding power anchor with 55 m (180 ft) of 22 mm (7/8 in.) stud link anchor chain with a floating mooring buoy at the water surface. The approximate position is 64.560393° N, 149.065306° W via the Novatel RTK.

1.2 Positioning

1.2.1 Boat General Navigation GPS

The Humminbird, model 161 Combo, fathometer/GPS on the boat provided general navigation information and a means to easily record positions of sampling or transect events. The GPS function employs WAAS (Wide Area Augmentation System) corrections that yield typical position accuracies of less than 3 m (9.9 ft) (www.humminbird.com).

1.2.2 Handheld GPS

Two handheld GPS receivers were used for general position documentation, typically for positions on the riverbank or on the ice cover. The first was a Garmin eTrex (model 295, 2006), and the second was a Garmin eTrex Legend H (2010). Both units could store positions in memory, and both units could employ WAAS corrections that yield typical position accuracies of less than 3 m (9.9 ft) (www8.garmin.com). The WAAS is operated by the Federal Aviation Administration and is one of a number of satellite-based augmentation systems (SBAS) used throughout the world.

1.2.3 RTK/GPS System

A Real Time Kinematic (RTK)/GPS system provided precision position information for the Acoustic Doppler Current Profiler (ADCP) and other sonar systems. The system is comprised of a Novatel SMART-V1G base station antenna, Novatel SMART-V1 rover, and 900 mHz radio modems for communication between the base and rover receivers. Novatel GPS receivers use a single-frequency (L1) carrier phase positioning system that yields 20 cm position accuracy; the position update rate is 5 Hz. The base station RTK receiver was mounted on a tripod over one of two survey monuments on the riverbank; the position of the mark was programmed into the base receiver, expediting field setup. The two survey monuments used as reference points were both set by TerraSond, as described in Table B-1.

Table B-1. TerraSond Survey monuments (from TerraSond Ltd. 2010)

TerraSond Survey Monuments			
Label	Latitude	Longitude	Vertical WGS84 ellipsoid (m)
NTR-01 2008	64° 33′ 32.26538″	149° 03′ 57.00281″	119.370
TR-2 2009	64° 33′ 50.50195″	149° 04′ 10.67873″	118.951

The rover RTK antenna was located directly above the ADCP or on the steering console when used with other sonar equipment. The RTK baseline, the distance between the base and rover, at the Nenana test site was always less than 1 km, so any position error due to baseline length was negligible. The output of the rover included the NMEA data sentences of “gga” (GPS fix data) and “vtg” (track made good and ground speed). The “vtg” information allows the ADCP to perform Doppler measurements of water velocities without the need for any differential correction. The GPS receiver speed and direction

reported in the “vtg” sentence is valid even when conditions are present that affect the fix precision (Mueller and Wagner 2009)

During the 2010 and 2011 seasons, the radio modems used were Data-Linc model SRM 6000. The Data-Linc modems, which were not weatherproof, were housed in plastic toolboxes to protect them from the elements. Weatherproof Zlinx modems model ZXT9-RM were purchased for the 2012 season. The weatherproof Zlinx modems eliminated the necessity of taking steps to protect the vulnerable Data-Linc modems. The power and serial data connections were hard-wired into the Zlinx modems, reducing the number of connections to be made during field setup. The antenna for the RTK rover modem was a 3 dB gain “rubber duck” type antenna fixed directly to the modem that was mounted on the steering console of the boat. During the 2010 and early part of the 2011 season, the Data-Linc base station radio modem used a 3 dB “rubber duck” type antenna. The Data-Linc radio modem in its protective box was placed on the ground on the riverbank; thus, the antenna was close to the ground where the transmitted signal could possibly be adversely affected by low foliage in the vicinity. Periodically during field operations, the RTK system seemed to give anomalous position information, so in July 2011, the radio-mounted 3 dB antenna was replaced with a 6 dB tripod-mounted antenna to avoid the problem of poor received signal strength at the rover radio modem. When the Data-Linc modems were replaced with the Zlinx modems, the base modem was tripod-mounted and again used a 3 dB “rubber duck” type antenna that was fixed to the tripod-mounted modem. The Zlinx modems had easily viewed RF signal strength indicators, and the received signal strength at the rover radio modem was always satisfactory. All subsequent operations continued with the use of the 3 dB antennas on the base and rover radio modems.

A 100 AH lead-acid battery supplied 12 V DC power for the RTK base system and radio modem at the riverbank site, and the 12 V DC scientific equipment battery on the boat supplied 12 V DC power for the RTK rover and radio modem.

2. Hydro Acoustic Equipment

2.1 ADCP

The ADCP used was a 1200 kHz Teledyne RDI Workhorse Rio Grande. The mounting hardware for the downward-looking ADCP was 6 cm (2.4 in.) aluminum tubing fixed with commercial railing hardware to the gunwales of the research boat. The system allowed for an adjustable transducer depth and easy rotation of the ADCP out of the water. The mounting hardware allowed positioning of the rover RTK receiver directly over the ADCP. The ADCP operating power was the same 12 V equipment battery that powered the RTK system. The user interface with the ADCP was via a laptop PC running WinRiver II. The ADCP WinRiver II operating software accepted the position and velocity information from the RTK/GPS system.

2.1.1 ADCP Operations

Establishing the RTK base station at one of the fixed survey monuments on the riverbank preceded ADCP operations. The boat-mounted ADCP system and PC was interfaced with the RTK/GPS rover. An ADCP check and compass calibration were performed at the beginning of each day’s ADCP operation. Start and end points of the ADCP transect were positions stored in the memory of the boat general-navigation GPS. After initial transects were performed, physical features on the riverbank were also used as visual references for starting and ending transects. The end-point locations of transects are reported in Table B-2.

Table B-2. ADCP transect end-point locations

		N Latitude (dd.ddddd)	W Longitude (dd.ddddd)
Upriver transect	River Right	64.55787	149.06105
Upriver transect	River Left	64.55680	149.06348
Middle transect	River Right	64.56143	149.06328
Middle transect	River Left	64.56097	149.06675
Downriver transect	River Right	64.56455	149.06993
Downriver transect	River Left	64.56355	149.06527
Mid-channel transect	Upstream	64.56645	149.07100
Mid-channel transect	Downstream	64.56692	149.08393
Below AKRR	River Right	64.56756	149.08130
Below AKRR	River Left	64.56645	149.08147

On June 24, 2010, the RTK base station located at survey monument NTR-01 was erroneously programmed with a position that was approximately 95 km (59 mi) east of the actual position. The ADCP/RTK operation appeared normal, and the error was not noticed during ADCP operations. The differences between the programmed position and the actual position are reported in Table B-3.

Table B-3. RTK base programming error at survey monument NTR-01

	N Latitude (dd.dddddd)	W Longitude (dd.dddddd)
Programmed position	64.555380	147.059518
Actual position	64.558962	149.065834
Position offset	0.003582	2.006316

A quality check of a representative transect was performed to determine the effect of the offset position information in the transect data. The start and end points of each transect were known from field notes and the stored position information in the general navigation GPS receiver. Data from a representative transect were adjusted with the position offset, which resulted in the transect information aligning with the known transect, as determined from field notes. The boat velocity information that was needed to make Doppler measurements of water velocity was determined to be valid from the “vtg” information contained in the WinRiver II data files (Mueller and Wagner 2009).

On August 10, 2010, the RTK/GPS rover had no RTK fixes because of communication problems; all of the rover data did have WAAS corrections applied. The lack of RTK fixes caused the absolute position accuracy to be reduced from 20 cm to 60 cm (http://www.novatel.com) with no degradation of velocity information in the “vtg” data (Mueller and Wagner 2009).

The ADCP transects of 2010 were repeated in 2011 after the installation of a mid-channel anchor and buoy system used to support fish studies. In 2012, a larger buoy was installed at the mooring station, and periodically a research debris-diversion platform was moored. Additionally, more closely spaced ADCP transects were performed to document the effects of the buoy and platform on the river.

2.2 Imaging Sonar – BlueView

A BlueView imaging sonar, model P900-2250-45-G-MKS, was acquired in June 2012. The device has a 45° field of view, operates at 900 kHz or 2250 kHz, and can operate at both frequencies simultaneously. The sonar was deployed using a BlueView model BV3100 pan and tilt system fixed to the 6 cm (2.4 in.) aluminum tube mounting system on the research boat. The BlueView sonar is accessed through a laptop PC running BlueView ProViewer software that controls the sonar/pan and tilt function, displays sonar images, and records sonar images. The recorded sonar images contain relative azimuth information, and when the Novatel GPS/RTK system information is input into the PC, the ProViewer adds a position stamp to the recorded image. The BlueView images are analogous to a video recording with a practical range in the Tanana River of 30 m (99 ft).

The BlueView sonar head on the pan and tilt system can be positioned up to 110 cm (43.3 in.) below the surface of the water. Keeping the sonar head well below the surface of the water reduces the angle between the sonar beam and the bottom, resulting in a better sonar image.

With the sonar deployed, boat speed is limited to little more than the speed of the river current because of the long moment arm of the underwater part of the sonar mount and the flexibility of the mount. To reduce transit times between operation sites, the sonar mount can rotate the sonar head out of the water. The 120V AC power for the BlueView system was provided by a 1 kW gasoline generator.

3. Sediment Sampling

3.1 Sediment Sampling Equipment

Sediment sampling was deployed from the research boat using a manually operated sounding reel secured to the frame on the forward part of the boat. The sounding reel is a Rickly model B-56M with 43.9 m (144 ft) of 0.25 cm (0.10 in.) steel cable. The cable is led forward from the reel over a pivoting nose piece that extends beyond the bow of the boat. When the equipment on the cable is lifted, the nose piece lifts, allowing the sediment sampling equipment to be worked on. Originally, Rickly model 4600 boat equipment was used as a frame to support the reel and nose piece, but it proved prone to excessive flexing, so a new framework of aluminum box tubing was commissioned for use beginning in spring 2010.

Sampling locations were stored as waypoints in the boat's GPS to ensure return to the same locations for each sampling event.

3.2 Bedload Sampling

Bedload sampling was performed with a Rickly model 8055 47.4 kg (105 lb) Helley-Smith bedload sampler using a Rickly style #1 sample bag. The sampling operation consisted of using the reel to manually lower the sampler to the bottom of the river for a given length of time and then retrieve it. Location, time of sample, and bottom time were recorded in a field notebook.

3.3 Suspended Sediment Sampling

Suspended sediment sampling was performed using a 40.8 kg (90 lb) Rickly model D77 depth-integrating sampler that accommodates 3-liter sample bottles and a nozzle cape with a 7.9 mm (5/16 in.) orifice. A sample was retrieved by lowering and retrieving the sampler at a constant rate. If the sample bottle was approximately 0.5 to 0.9 full, the sample was considered acceptable. If there was too little sample in the bottle, sampling was repeated at a slower rate. If there was too much sample in the bottle, sampling

was repeated at a faster rate. In deeper water, tape over the orifice was sometimes used to reduce the flow rate of water into the sampler.

4. River Stage

A river stage gauging station was set up on the riverbank near the middle of the reach of the Tanana River Test Site, approximately 64.5620° N 149.0675° W. The station consisted of a Campbell Scientific CR1000 logger and two Campbell Scientific CS450 pressure transducers. The logger was powered with a 100 AH gel cell lead-acid battery; the battery capacity was sufficient to power the data logger for a complete ice-free season without additional charging. The data logger and battery were housed in a locked steel box weighing about 90 kg (198 lb) that was secured to the bank with a Duckbill® earth anchor to reduce the probability that the box would be moved. The pressure transducers, which were placed in the water shortly after ice-out and removed prior to freeze-up, were located near the riverbank on the downriver side of a rock stream barb. A pair of transducers was used to provide evidence of movement of one or both transducers. If the transducers remain undisturbed, the pressure difference between the two should remain constant throughout the season. The data logger has the capacity to accommodate data for an entire season, but data were downloaded periodically through the season to monitor the system and to note any data anomalies that would indicate problems. A manual measurement of river stage, measuring the elevation distance between the river surface and a reference mark on the upland part of the riverbank, was performed periodically by using a level and surveyor's rod.

The data logger was programmed to record 15-minute averages of pressures sampled at a rate of 1/sec. The program also recorded the supply battery voltage and temperatures at the transducers at 15-minute intervals.

5. Winter Measurements

5.1 Electronic Velocity Meter

A Marsh-McBirney model 2000 Flo-Mate portable flow meter was used to measure under-ice current velocities. The flow meter sensor is the electromagnetic type that produces a magnetic field and infers velocity by measuring the voltage induced in a conductor, the flowing water, which is passing through the field. The published range of the flow meter is -0.15 m/sec to +6 m/sec (-0.5 to +19.9 ft/sec). The velocity output was kept in what Marsh-McBirney described as a time-constant filtering mode, with the time constant set at 2 seconds. This time-constant mode is in contrast to using a fixed-point averaging mode that would average the velocities over a defined amount of time before reporting.

The velocity sensor was fixed to a Rickly wading rod, also referred to as an ice rod, approximately 25 cm (10 in.) from the bottom of the rod. A measurement was made by inserting the ice rod with sensor into a 25 cm (10 in.) hole in the ice made with a gasoline-powered auger. The orientation of the sensor was monitored by means of locking pliers clamped to the upper end of the ice rod and used as a "tell-tale." Velocity measurements were made at nominal 0.5 m intervals between the river bottom and the underside of the ice cover. Velocity measurements were manually recorded in a field notebook. The locations of the winter velocity measurements are reported in Table B-4

Table B-4. Location of winter transect ice hole locations using Garmin eTrex handheld GPS on 4/15/2009

Identifier (Garmin waypoint memory)	April 2009 field notebook notation #	December 2009 to April 2010 field notebook notation #	Latitude (N) dd.ddddd	Longitude (W) dd.ddddd	Interval between holes as measured via tape (ft)
NEN-0 (river bank)			64.56100	149.06694	
NEN-1	1	1	64.56103	149.06661	20
NEN-2	2		64.56106	149.06655	20
NEN-3	3	2	64.56109	149.06644	20
NEN-4	4		64.56111	149.06632	20
NEN-5	5	3	64.56113	149.0662	20
NEN-6	6		64.56115	149.06609	20
NEN-7	7	4	64.56117	149.06597	20
NEN-8	8		64.56119	149.06585	20
NEN-9	9	5	64.56120	149.06573	20
NEN-10	10		64.56125	149.0656	20
NEN-11	11	6	64.56126	149.06551	20
NEN-12	12		64.56122	149.0653	20
NEN-13	13	7	64.56134	149.06518	40
NEN-14	14	8	64.56138	149.06493	40
NEN-15	15	9	64.56142	149.06471	40
NEN-16	16	10	64.56147	149.06441	40
NEN-17	17	11	64.56150	149.06422	40
NEN-18	18	12	64.56155	149.06399	40
NEN-19	19	13	64.56162	149.06339	40

Note: After drilling twelve measurement holes at 6.1 m (20 ft) intervals, the spacing requirements were reassessed and 12.2 m (40 ft) intervals were subsequently used. Actual measurements were performed at 12.2 m (40 ft) intervals

5.2 Frazil Ice Sampling

Frazil ice formation investigations were performed in late fall 2009 and 2010 during freeze-up. Two platforms were used for collecting frazil ice samples formed on test materials: the 6 m research jon boat and the frazil ice growth test platform.

5.2.1 Frazil Ice Sampling Equipment – 2009

For frazil sampling in 2009, we employed the 6 m (20 ft) jon boat, which we also used for the open-water season research. The boat was moored perpendicular to the riverbank, with the bow on the outer edge of the shore-fast ice that was forming on the bank. This position allowed the stern to be in moving water approximately 9 m from the bank edge.

As pictured in Figure B-2, a light steel frame, 152 cm × 20 cm (60 in. × 8 in.), holding sample wafers was suspended from the starboard (downriver) side of the boat in the river current. The top of the frame was approximately 60 cm (23.5 in.) below the water surface. This depth was well below the bottom of

the support boat that was approximately 10 cm (4 in.) below the water's surface. The frame was suspended horizontally so that all samples were at the same water depth. The sample wafers were thin squares of aluminum, steel, and high-density molecular-weight polyethylene. The wafers were 10.2 mm × 10.2 mm (4 in. × 4 in.) square; the steel and aluminum wafers were approximately 1 mm (0.045 in.) thick; and the polyethylene wafers were approximately 3 mm (0.12 in.) thick. The wafers were suspended in the frame using 4 lb test, 0.2 mm (0.008 in.) diameter, monofilament fishing line.

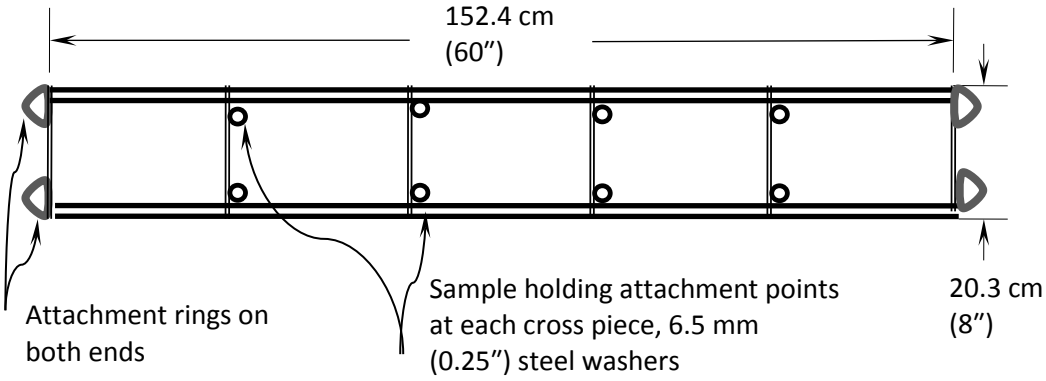

long sides are 1.9 cm (0.75") square steel channel
short cross pieces are 1.3 cm (0.5") square steel channel
short cross pieces are on 30 cm (12") centers

Figure B-2. Frazil frame (drawing not to scale).

Frazil accumulation was measured by mass. The scale used was a Sartorius model GE812 gold scale with a capacity of 810 grams and a resolution of 0.01 gram. To support the weighing process, a weigh station on a table was set up in a winter tent that had an oil heater. Electric power for lighting and instrumentation was provided by a 1 kW gasoline generator.

5.2.2 Frazil Ice Sampling Equipment – 2010

The frazil investigation in 2010 was performed from an assembly composed of two 3 m × 1.2 m (10 ft × 4 ft) Lowe model 1032 aluminum jon boats fastened together with and supporting a 2.4 m × 2.4 m (8 ft × 8 ft) platform framework of 13 mm (1/2 in.) plywood and 38 mm × 89 mm (1.5 in. × 3.5 in.) framing lumber (Figure B-3). The separation between the two boat hulls was approximately 1.5 m (59 in.).

The platform, which was moored to the riverbank using a line to the upstream bank, was held off of the bank and the shore-fast ice with a 4.9 m × 0.61 m (16 ft × 2 ft) plank that was also used for researcher access to the platform. A 4.9 m (16 ft) long by 10 cm × 15 cm (4" × 6") spruce timber was fastened to the bow of the outboard boat and to the upstream riverbank to deflect ice floating downriver.

Samples for accumulating frazil were placed in a wood frame on the aft and downstream end of the platform (Figure B-4). The frame was hinged to allow insertion, removal, and examination of the samples on the platform deck.

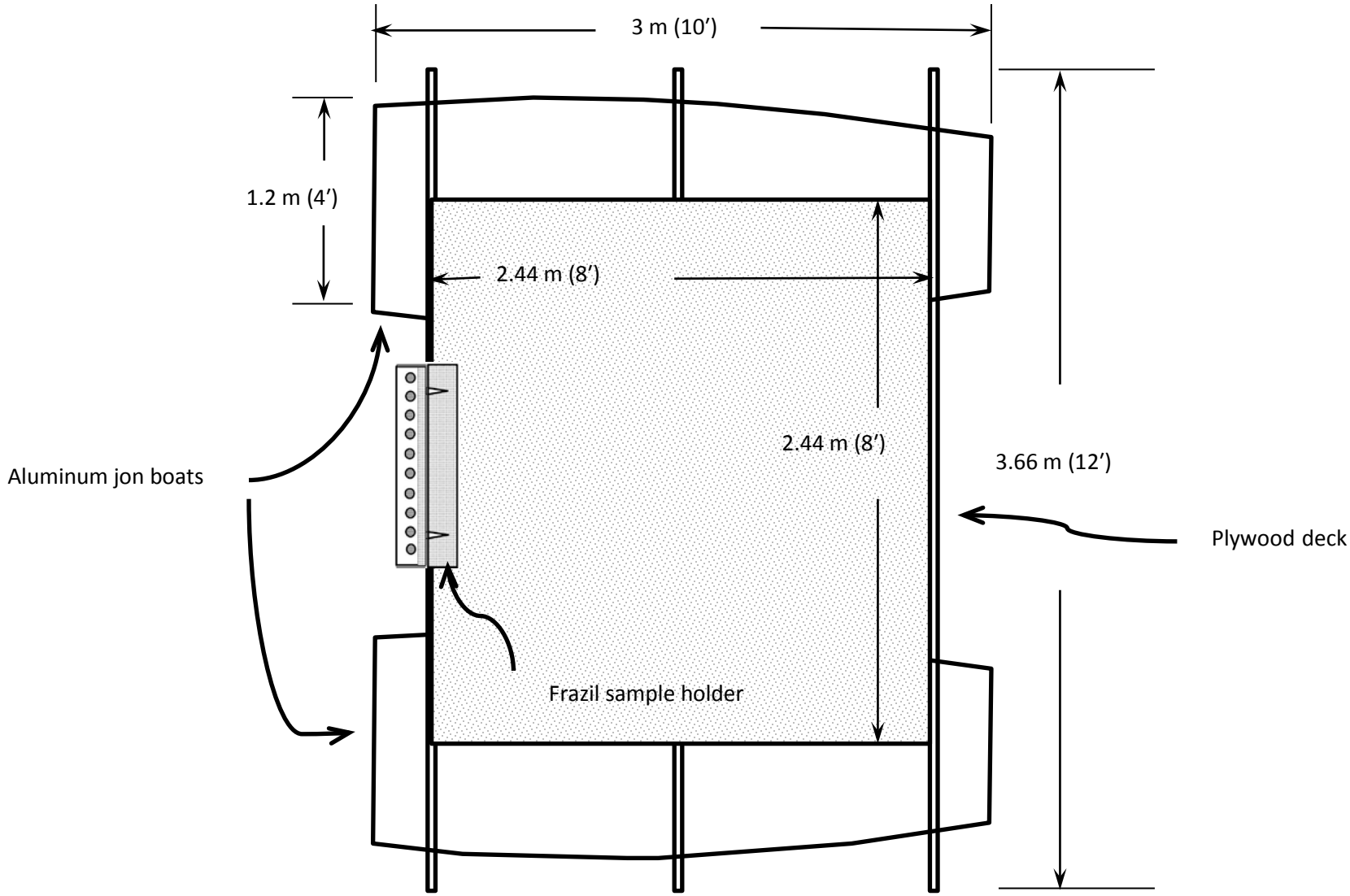

Figure B-3. Floating platform for frazil sampling (plan view) (drawing not to scale).

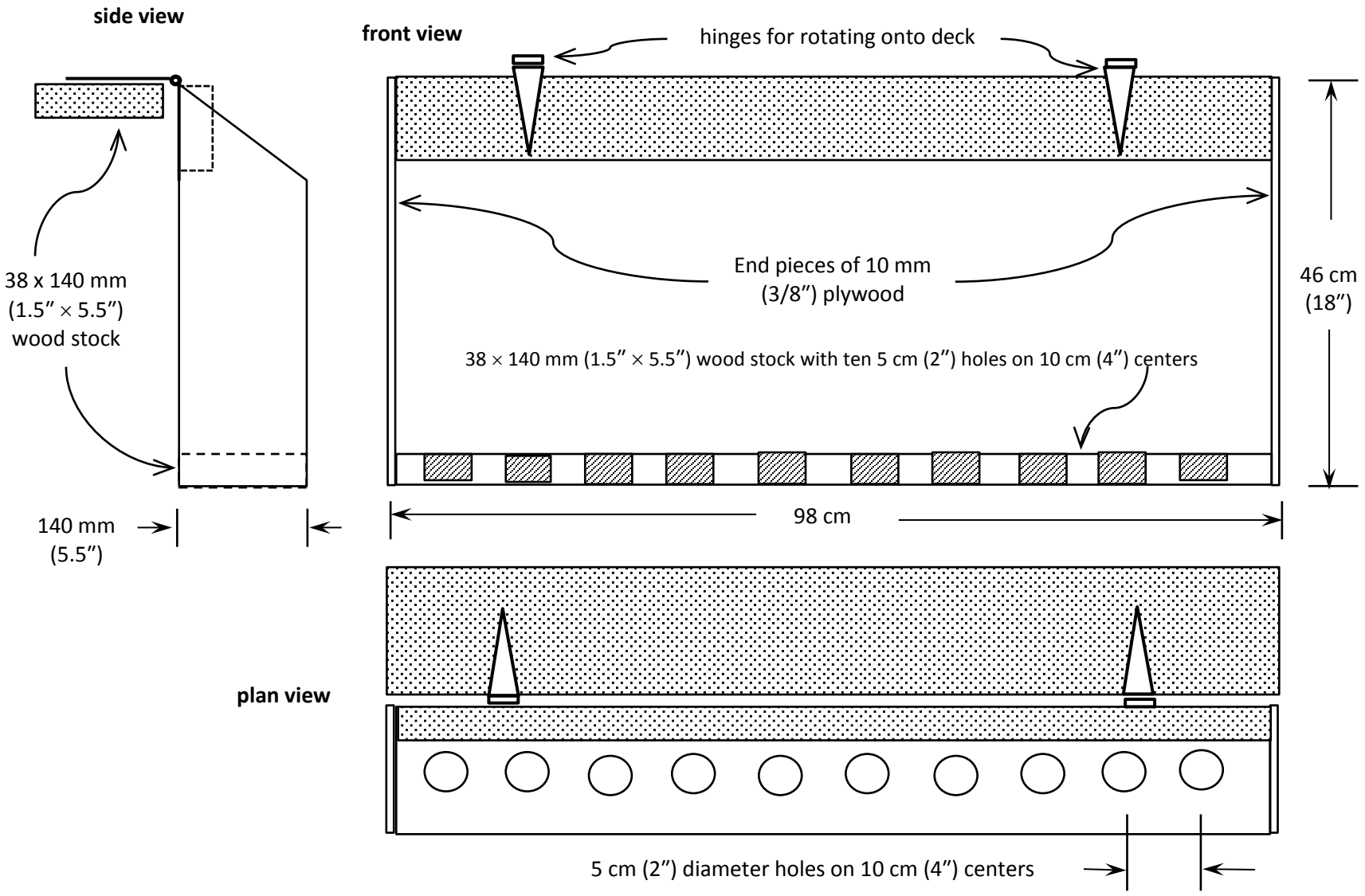

Figure B-4. Hinged sample, holding frame for attachment to deck of floating frazil platform (drawing not to scale).

The material samples (Figure B-5) were composed of a 50 cm (20 in.) cylinder of tubing stock 25 mm (1 in.) in diameter fastened by means of urethane expanding foam in a section of ABS plastic pipe of 38 mm (1.5 in.) diameter. At the upper end of the plastic pipe, a stop collar was fixed to allow the sample holder to nest in the wood frame. After placement in the wood frame, a piece of wood stock was placed over the sample holder to act as a "keeper" so that the holders would remain in place when they were lowered into the water. To reduce the probability of heat flow to the cold air above the water surface, the sample tubing stock was short so that when the sample holder was deployed in the water, the end of the tubing stock remained approximately 37 cm (14.5 in.) below the water surface. Sample materials used were 316 stainless steel, mild steel, Teflon®, ABS, aluminum, and acrylic.

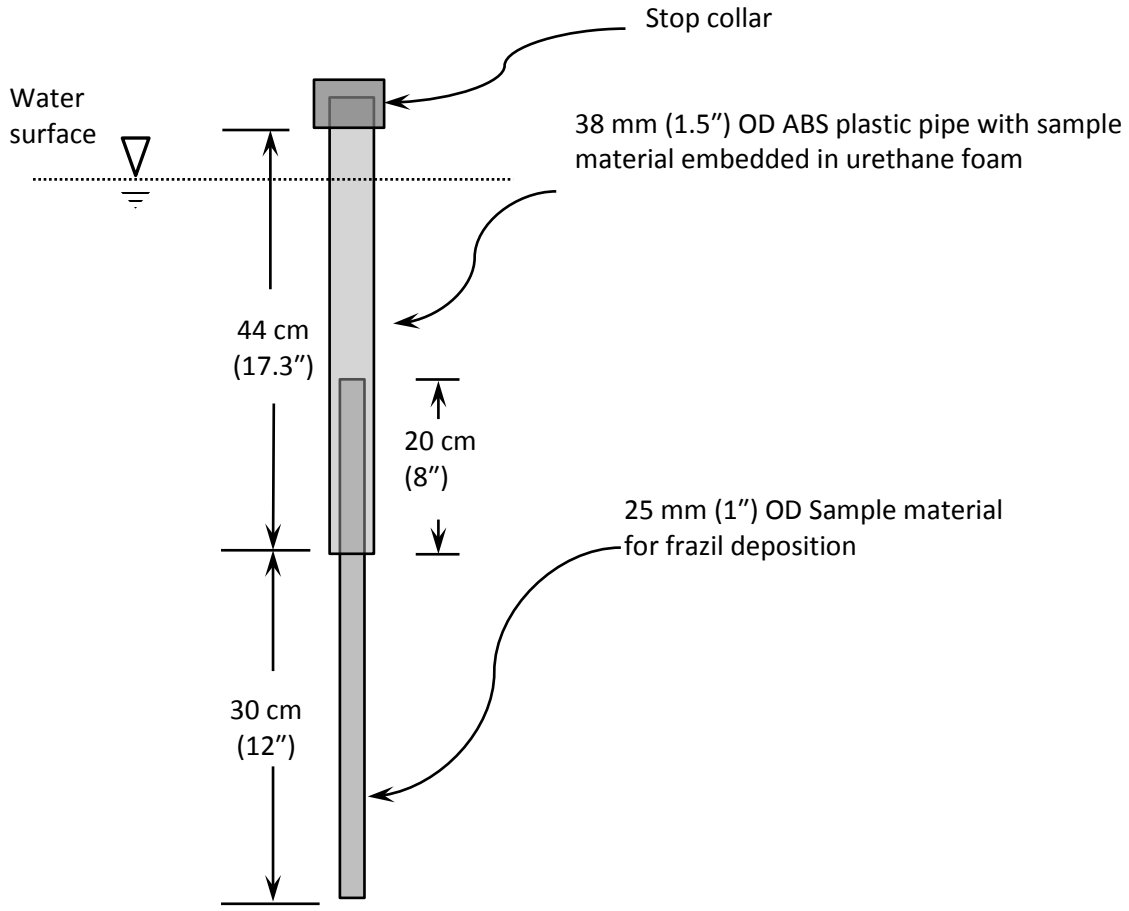

Figure B-5. Frazil collection material sample configuration (drawing not to scale).

5.2.3 Frazil Ice Sampling Observations – 2010

The frazil ice investigation on October 21 and 22, 2010, included observations of frazil depositions on a set of three samples deployed from the downstream end of the floating sampling platform, observations of depositions on a 25 mm (1 in.) OD mild steel pipe, and current velocities near the sampling platform. The convention for describing frazil growth on the cylindrical samples is shown in Figure B-6. The three measurements of frazil deposition on samples are described as follows:

- Thickness of deposition on the forward or upstream-facing surface – L_f
- Thickness of deposition on the rear or downstream-facing surface – L_r
- Thickness of deposition on the side – L_w

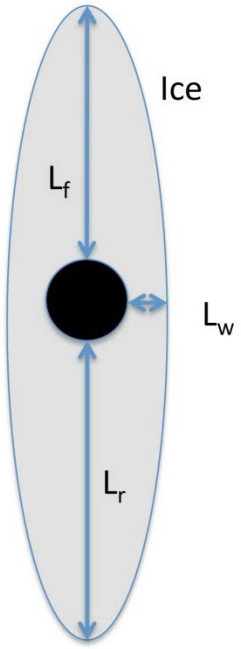

Figure B-6. Schematic of frazil ice growth on cylinders of different materials. Refer to Figure B-5 for experiment setup and Table B-5 for frazil accumulation dimension with time.

The observations of deposition on the set of three samples are reported in Table B-5, and the observations of deposition on the mild steel pipe are reported in Table B-6. Figure B-7 is a photo of the sampling platform at 10 A.M. on 10/22/2010 as deployed and just prior to sample examination. The mild steel sample pipe is visible at the aft corner of the platform with approximately 1.5 m (5 ft) of the pipe exposed above the deck.

Table B-5. Frazil ice accumulation on cylinders of different materials

Top of sample (at junction of sample and ABS holder)	Growth time (hr:min)	Air temp (°C)	Teflon® Deposited frazil thickness (mm)			316 Stainless Steel Deposited frazil thickness (mm)			Mild Steel Deposited frazil thickness (mm)		
10/21/10 9:45 PM	start		L_f	L_r	L_w	L_f	L_r	L_w	L_f	L_r	L_w
10/22/10 3:00 AM	5:15	-11	none	none	none	n/d	n/d	n/d	35	20	25
10/22/10 10:25 AM	12:40		76	52	42	55	45	29	95	72	95
Middle of sample											
10/21/10 9:45 PM	start		L_f	L_r	L_w	L_f	L_r	L_w	L_f	L_r	L_w
10/22/10 3:00 AM	5:15	-11	none	none	none	none	none	none	none	none	none
10/22/10 10:25 AM	12:40		lost	lost	lost	66	46	35	66	53	25
Lower end of sample											
10/21/10 9:45 PM	start		L_f	L_r	L_w	L_f	L_r	L_w	L_f	L_r	L_w
10/22/10 3:00 AM	5:15	-11	none	none	none	35	n/d	25	35	20	25
10/22/10 10:25 AM	12:40		lost	lost	lost	90	47	43	150	150	150

Notes: Refer to Figure B-5 for a description of the frazil collection material sample configuration
"none" means the sample was observed and no deposition was noted
"n/d" means no data, no observation was recorded
"lost" indicates that a large part of the frazil deposited on the Teflon® sample broke off and fell into the river before a measurement could be made

Table B-6. Frazil ice accumulation on 25 mm OD mild steel pipe

Start: 10/21/2010 9:45 PM	10/22/10 3:00 AM			10/22/10 10:25 AM		
Distance from bottom (cm) [water surface at 210 cm]	L_f (cm)	L_r (cm)	L_w (cm)	L_f (cm)	L_r (cm)	L_w (cm)
120		30	no data			
108	30		no data			
100				64	63	75
70				60	70	72
66		30	no data			
60	25		no data			
50				55	56	75
44		25	no data			
30	25		no data	52	54	70
20		10	no data			
14	20		no data			
12		20				
10				50	40	50
6		0	no data			

Note: No accumulation from 121 cm to surface

Figure B-7. Frazil ice growth platform deployed on Tanana River near Fairbanks showing vertical mild steel pipe on aft corner; river current is flowing from left to right. This image depicts the scene at 10 A.M. on 10/22/2010, just prior to removing the frazil samples in the frame on the aft end of the platform.

Table B-7 reports the velocities of the river current in the water column observed from the platform.

Table B-7. Velocities during frazil sampling

Location	Sensor depth below surface (cm)	Velocity (m/sec) 10/21/2010 10 PM	Velocity (m/sec) 10/22/2010 12 PM
Aft of platform, inboard of outer hull	10	0.24	
	30	0.38	0.18
	80	0.30	0.27
	130	0.43	0.35
	190	0.30	0.33
Outboard of outer hull	10	0.53	
	30	0.02	0.25
	80	0.36	0.53
	130	0.37	0.55
	180	0.14	0.4
	200	0.11	0.34
2 meters outboard of outer hull	30		0.6

References

Mueller, D.S., and Wagner, C.R. (2009). Measuring discharge with acoustic Doppler current profilers from moving boat: U.S. Geological Survey Techniques and Methods 3A–22, 49 pp. (available online at http://pubs.water.usgs.gov/tm3a22).

TerraSond Ltd (2010). Hydrokinetic Power Conversion Project Physical Characterization Survey. May 1, 2010, pp. 1–3 and 1–5.

www8.garmin.com/aboutGPS/waas.html.What is WAAS?

www.humminbird.com, Model 161 GPS Chartplotter Operation Manual, 2006, Humminbird, Eufala, AL USA.

www.novatel.com, Novatel OM-20000093 Rev 10 OEMV Family Installation and Operation User Manual.

Appendix C – Project Data in Electronic Form

http://www.uaf.edu/files/acep/2013_8_8_HKD_report_appendix_data_files.zip